FACULTY OF ENGINEERING AND ARCHITECTURE

Development of Low-Cost and Low-Power Wearable Sensor Nodes Based on Bluetooth Low Energy

Nick De Raeve

Doctoral dissertation submitted to obtain the academic degree of
Doctor of Electronics and ICT Engineering Technology

Supervisors
Prof. Jo Verhaevert, PhD - Prof. Patrick Van Torre, PhD
Department of Information Technology
Faculty of Engineering and Architecture, Ghent University

October 2022

GHENT UNIVERSITY

ISBN 978-94-6355-637-8
NUR 959, 958
Wettelijk depot: D/2022/10.500/78

Members of the Examination Board

Chair

Prof. Em. Daniël De Zutter, PhD, Ghent University

Other members entitled to vote

Prof. Luca Catarinucci, PhD, Università del Salento, Italy
Prof. Sam Lemey, PhD, Ghent University
Prof. Hendrik Rogier, PhD, Ghent University
Prof. Nobby Stevens, PhD, KU Leuven

Supervisors

Prof. Jo Verhaevert, PhD, Ghent University
Prof. Patrick Van Torre, PhD, Ghent University

Dankwoord

Had je mij 12 jaar geleden verteld dat ik deze tekst ging schrijven, had ik u gewoon uitgelachen! Met het idee om elektricien te worden en nadien onze winkel over te nemen had ik nooit gedacht om nu af te studeren als dokter. De eerste kennismaking met EN-, OF- en NIET-poorten in het eerste middelbaar heeft ervoor gezorgd dat het originele plan heel snel begon te wankelen. De overgang van elektriciteit-elektronica was niet gemakkelijk. Zoals velen weten had ik het niet gemakkelijk met de wiskunde en met chemie I. Maar doorzetting, motivatie en ondersteuning van vrienden en familie heeft hiervoor gezorgd. Daarom zou ik enkele mensen in het licht willen zetten.

Om te beginnen zou ik mijn promotoren Jo Verhaevert en Patrick Van Torre willen bedanken. Jo, bedankt voor de nauwe samenwerking en de verschillende mogelijkheden (projecten) dat je mij hebt gegeven. De samenwerking voor het opleidingsonderdeel elektronica heeft mij veel bijgeleerd. Dit was een mooie afwisseling tussen de lange dagen van programmeren, simuleren en tekenen aan PCBs. Patrick, bedankt voor de samenwerking en de vele praktische feedback. De babbels en wijsheden die je gedeeld hebt aan de koffiemachine of over de chat zullen mij voor eeuwig bijblijven. Verder wil ik jullie beide bedanken voor het vele nalezen van de verschillende papers en verslagen. Bedanken voor de feedback op de verschillende presentaties en de kalmerende babbels wanneer ik uitdagende leesverslagen ontvangen had.

Furthermore, I would like to thank the members of the examination board. Prof. Luca Catarinucci, prof. Nobby Stevens, prof. Hendrik Rogier, prof. Sam Lemey and prof. em. Daniël De Zutter. Thank you for evaluating my work and providing me with your valuable remarks, this increased the readability and comprehensibility of the complete work.

Verder zou ik Hendrik Rogier willen bedanken voor zijn feedback en academische raad die ik de voorbije jaren heb gekregen. U feedback was soms moordend voor mijn papers, maar resulteerde steeds in prachtige teksten. Bedankt hiervoor! Next we have Adnan Shahid. Thank you for the collaboration on the fall detection paper. It was very pleasant working together with you. It's a pity we could not collaborate on more projects. Vervolgens is er Sam Lemey. Sam, je bent een top kerel! Steeds joviaal, vriendelijk,

paraat om te helpen of om dingen te bespreken werk gerelateerd of niet. Ik hoop dat iedereen beseft wat een meerwaarde je bent voor deze groep. Volgende in de rij is Matthias de Schepper. De man die zijn volk leert programmeren, ontwerpen, solderen en voornamelijk debuggen. We zijn met enkele weken verschil gestart aan de UGent, maar werkten bijna vanaf het begin samen. Ik kan de uren niet noemen dat we samen hebben zitten solderen, programmeren, verhuizen of brainstormen over hoe bepaalde zaken aan te pakken in het labo. Later werden deze brainstorms aangevuld door Dimitri Van Cauwelaert. Eerst was ik zijn student en later zijn collega. Desalniettemin, zoals we Dimitri graag hebben als hoogleraar is het een nog betere collega. Altijd paraat voor een leuke babbel, staat u bij met raad en daad en geniet even hard van een drankje NA de werkuren als ik. *"You can take a man from his roots, but you can never take the Oilsjters blood out of the man"*. Heren, bedankt om de lange labo dagen op te vrolijken en te ondersteunen waar nodig. En dan, the one and only, Stefaan Lambrecht. Ik heb vier jaar naast u labo mogen geven en heb hier hartelijk van genoten. Het was leerrijk om te luisteren naar uw jaren aan ervaring als hoogleraar, sportman en ondernemer. Finaal zou ik de spotlight willen zetten op de vrouw die ons iedere dag opnieuw een net bureau en proper labo bezorgt. Sabrina, bedankt! Het waren aangename babbels die we 's ochtends hadden.

And then, office 210.031 better known as *"the cool office"*. First of all, we have Olivier Caytan. I have never met a person who knows so much about the world wars, likes to talk about politics and has such an enormous passion for his Mazda RX7. Nevertheless, I have enjoyed all of these conversations and I still dream of the moments when we both were laughing at Quinten's expense the few times he was in the office. Secondly, we have Kamil Yavuz Kapusuz also known as *"our Turkish Delight"*. On my first day, they told me you were a handsome, very muscled playboy. When you returned from your conference, I saw they didn't lie. All jokes a side, you are an extremely smart person, a person with an enormous work ethic, but most of all a very kind person that I enjoyed talking to on our early morning sips. I think it is time to do another barbecue, no? From all the colleagues that left us, I would like to express my gratitude to Thomas Deckmyn, also known as *"Uncle Harley"* and currently CEO and founder of Koboi consulting. At the beginning, there was nothing. But at the end there was a friendship, shared passion for alcohol and good food. Let's see what the future will bring! And then, my brother from another mother, my fingerbud, the ying to my yang, Quinten Van den Brande also known as *"Uncle Scooter"*. Our story started several years ago when we were students at Ghent University. I still remember how you were trying to get my notes from classes that started at 8:15 in the morning. Nevertheless, from that point on, I felt a certain sympathy for you that is still there to this day. Having us together results in a very fun time for us, but maybe less fun for our queens. To

the people that read this book, I would like to point out that our dynamic duo are the president and vice-president of the Sons of Maxwell motorcycle gang.

To the colleagues that are currently still present in the office, I would like to thank you for the fun moments during and after office hours. A special thank you to the best office representative we've ever had, Samuel Rimbaut. The way you are guiding our office is previously unseen . You have a strong hand on the managing of all the important topics concerning the office and your rule with an iron fist. I hope from the bottom of my heart that the rest can enjoy this ruling for many years. Secondly, I would like to address Jelle Jocqué. We crossed each others paths briefly, but I enjoyed the work and private talks we had. I enjoy you hands on approach to you research and teaching. Good luck with all the future research. Thirdly, there is Nicolas Claus. Even though you are from Dendermonde, I enjoy working together with you on different research topics and master theses. Sharing a passion for cocktails makes the working together even more fun. Alcohol brings people together! Then there are Seppe Brandt, Igor Lima de Paula and Laura Van Messem. The conversations we had about home (office) grown vegetables and herbs, freshly made salads, small parties or drinking a glass of wine at the end of the week. All those activities were fun and I would like to thank you for those. Victor and Bram, you guys are new in the office, we did not talk that much, but I wish you the best and lots of papers. Ps: always listen to your masters Olivier, Kamil and our ruler S. Rimbaut.

In the other office I would like to thank everybody for the many fun lunches over the past years. I would especially like to show my gratitude to Thomas Ameloot and Duygu Kan. I was lucky to follow the courses on antennas & propagations and EMC together with you guys. This made studying for the exams much more pleasant. Martijn Huynen, I have never met a guy who knows so much tidbits and facts. Nevertheless, thank you for your advise and knowledge over the past 5 years and especially the day before my internal defence. And then there is Alessandro Felaco also known as *"Uncle Spaghetti"*. You arrived as a quiet student and became a fun and loud colleague and eventually a friend. The few times we were together in the office were always fun and resulted in a lot of laughs (for us anyways). Finally, we have the young ones: Gert-Jan, Emile, Jul, Dries, Pieter, Arno, Maxim and Joryan. I wish you all the best of luck in your future endeavors and lots of publications. Joryan, I expect an invitation to try your home distillation projects, preferably the safe ones.

En dan zijn we aangekomen bij de niet academici. Om te beginnen zou ik mijn ouders willen bedanken. Het is dankzij jullie dat ik heb kunnen studeren en dat ik later de kans heb gekregen om mijn doctoraat te behalen. Ik heb geen idee hoe ik mijn dankbaarheid kan uiten, maar duizend maal dank. Verder hebben we een belangrijk persoon. Ons verhaal start

meer dan 10 jaar geleden, maar de vriendschap is er alleen maar sterker op geworden. Nadine, bedankt om er te zijn en te luisteren naar mijn gezaag wanneer ik uitdagende leesverslagen ontving. Bedankt om met mij mijn toekomst te bespreken en vijf jaar geleden mij de duw te geven die ik nodig had om te starten aan mijn doctoraat. Thank you bestie! Speciaal bedankje voor Thomas Verstringe om mij gedurende deze jaren te vergezellen naar verschillende whisky en rum tastings en de bijhorende comedy avonden. Deze waren een mooie afwisseling tijdens de lange dagen achter een bureau. Finaal heb ik dan nog de bende uit de Wholly Spirits winkel te bedanken. De laatste jaren is dit uitgegroeid naar een soort van tweede thuis waar ik op regelmatige basis eens stoom kon aflaten over de academische wereld of enkele studenten. Maar telkens vergezeld door een lekkere spirit. Bart, Sofie, Wouter, Georgina, Mario VB, Lieven, Mario H, Cindy, Guy en Daisy, bedankt en we drinken er zeker ene op! Verder wil ik nog een woordje richten naar mijn voormalige leerkrachten en collega's van Richtpunt campus Zottegem. Bedankt voor de opleiding, bedankt voor de leerrijke lesopdracht en bedankt om mee te werken aan mijn onderzoek.

Om af te sluiten zou ik een heel belangrijk iemand willen bedanken. Sommige kennen haar als Delyse Utetiwabo, voor mij staat ze gekend als *"Icyuki"*. We hebben elkaar pas leren kennen in de laatste maanden van mijn doctoraat, maar dan nog heb je mij met de juiste raad en daad bijgestaan. Kon ik verschillende topics met je aftoetsen, je was er om mij te kalmeren, je was er om met me te vieren en je was er om te overtuigen wanneer ik twijfelde. Baby, bedankt om er te zijn wanneer ik je nodig had schat. Ndagukunda!

Herzele, oktober 2022
Nick De Raeve

What the result of these investigations will be, the future will tell. But whatever they may be, and to whatever this principle may lead, I shall be sufficiently recompensed if later it will be admitted that I have contributed a share, however small, to the advancement of science.

– Nikola Tesla, 1888

Contents

Dankwoord **i**

Samenvatting **xi**

Summary **xv**

List of Abbreviations **xix**

List of Publications **xxv**

1 Introduction **1**
1.1 Context . . . 1
1.2 Motivation . . . 2
1.3 State of the art . . . 5
1.3.1 Blind spot detection . . . 7
1.3.2 Fall detection . . . 8
1.3.3 Train integrity . . . 9
1.4 Own Contribution . . . 10
1.5 Outline . . . 10
References . . . 12

2 Bluetooth-Low-Energy-Based Detection and Warning System for Vulnerable Road Users in the Blind Spot of Vehicles **19**
2.1 Introduction & related work . . . 20
2.2 Design . . . 21
2.2.1 Hardware implementation . . . 22
2.2.2 Software . . . 24
2.2.2.1 Wearable . . . 24
2.2.2.2 Detection and central node . . . 28
2.2.3 Filtering . . . 30
2.3 Measurements . . . 31
2.3.1 Measurement setup . . . 32
2.3.1.1 Static RSSI measurement . . . 32
2.3.1.2 Dynamic RSSI measurement . . . 33
2.3.2 Threshold filtering . . . 34
2.3.3 Weighted average filter with sliding window . . . 35

2.3.4 Optimized algorithm . . . 37
2.4 Real-life Measurements . . . 38
2.4.1 General test . . . 38
2.4.2 Large group of people . . . 39
2.4.3 Verification measurement . . . 41
2.5 Conclusion . . . 41
References . . . 43

3 Bluetooth-Low-Energy Based Fall Detection and Warning System for Elderly People in Nursing Homes 47
3.1 Introduction . . . 48
3.2 Related Work . . . 49
3.3 Design . . . 51
3.3.1 Hardware design . . . 53
3.3.2 Algorithm design and filtering procedure . . . 55
3.3.3 Convolutional Neural Network Design . . . 59
3.4 Measurement and Analysis . . . 60
3.4.1 Measurement setup . . . 60
3.4.2 Fall . . . 61
3.4.3 Validation with open-source dataset . . . 63
3.5 Power management . . . 68
3.6 Conclusion . . . 70
3.7 Funding Statement . . . 71
References . . . 72

4 Bluetooth Low Energy based Power Efficient WSN for Industrial IoT Train Integrity Monitoring 83
4.1 Introduction . . . 84
4.2 Measurement Setup . . . 85
4.2.1 Used hardware . . . 85
4.2.2 Acceleration measurement setup . . . 86
4.2.3 RF measurement setup . . . 87
4.3 Measurements & Discussion . . . 89
4.3.1 Acceleration measurements . . . 89
4.3.1.1 Wagon stopped . . . 89
4.3.1.2 Is the train moving? . . . 90
4.3.1.3 Air brakes . . . 91
4.3.2 RF Measurement . . . 92
4.3.2.1 Reference measurements . . . 92
4.3.2.2 Real-life measurements . . . 93
4.3.2.3 Brakes . . . 96
4.4 Conclusion . . . 98
References . . . 100

5 Conclusion & Future Work 103

A Wearable Bluetooth Low Energy Based Miniaturized Detection Node for Blind Spot Detection and Warning System on Vehicles 109
A.1 Introduction . . . 110
A.2 Design . . . 110
A.2.1 Printed Circuit Board . . . 113
A.2.2 Miniaturized BLE antenna . . . 113
A.3 Simulations & discussion . . . 115
A.3.1 Matching network . . . 115
A.3.2 Folded Shorted-Patch antenna results . . . 117
A.4 Conclusion . . . 119
A.5 Future work . . . 119
References . . . 121

B Fall Detection and Warning System for Nursing Homes based on Bluetooth Low Energy 123
B.1 Introduction . . . 124
B.2 Design . . . 125
B.2.1 Design requirements . . . 125
B.2.2 System design . . . 125
B.2.3 Communication steps . . . 126
B.2.4 PCB Design . . . 127
B.3 Measurement & Discussion . . . 129
B.3.1 Range Measurement . . . 129
B.3.2 Latency Measurement . . . 131
B.4 Conclusion . . . 132
B.5 Future Work . . . 132
References . . . 134

Samenvatting

Wearables en smart devices hebben steeds meer invloed op ons dagelijks leven. Van intelligente wekkers in de ochtend tot ultramoderne wondbewaking, al deze sensoren spelen een zeer belangrijke rol in onze dagelijkse beslissingen. Sportliefhebbers gebruiken fitnesstrackers om hun resultaten dagelijks te verbeteren, terwijl medische professionals deze sensoren gebruiken om het genezingsproces van hun patiënt te volgen of, in het ergste geval, het zorgpersoneel te waarschuwen wanneer de toestand van hun patiënt verergert. De meeste van deze Internet of Things (IoT)-applicaties werken met een goedkope, energiezuinige sensor die deel uitmaakt van een draadloos sensornetwerk (Engels: Wireless Sensor Network (WSN)). Om al deze sensoren aan te sluiten, is een energiezuinig, betaalbaar communicatieprotocol (Engels: Communication Protocol (CP)) vereist met een behoorlijke datadoorvoer en een beperkte vertraging. De literatuur biedt voldoende oplossingen, maar de meeste hebben een aantal nadelen. Dit proefschrift richt zich op het gebruik van Bluetooth Low Energy (BLE) als voornaamste CP voor drie uiteenlopende onderwerpen waar een WSN wordt gebruikt.

Hoofdstuk 2 beschrijft het eerste onderwerp dat betrekking heeft op dodehoekdetectie bij vrachtwagens. Jaarlijks gebeuren er op de Belgische wegen meerdere dodelijke ongevallen door de dodehoekproblematiek. Een van de belangrijkste oorzaken van deze ongevallen is het gebrek aan communicatie tussen vrachtwagenchauffeurs en zwakke weggebruikers (Engels: vulnerable road users (VRUs)). Dit, in combinatie met de toenemende werkdruk van vrachtwagenchauffeurs, vergroot de kans op dodelijke ongevallen nog meer. De literatuur biedt meerdere oplossingen om deze ongevallen te voorkomen. Van radar tot camera gebaseerde systemen gecombineerd met eenvoudige voorwaarden of met een machine learning (ML) algoritme. Al deze systemen hebben verschillende voor- en nadelen. Toch worden ze nog steeds niet geïnstalleerd op echte vrachtwagens vanwege de kosten, de moeilijke installatie of het lage detectiepercentage. Daarom richt Hoofdstuk 2 zich op de ontwikkeling van een goedkoop en energiezuinig dodehoekdetectie- en waarschuwingssysteem voor voertuigen. Dit systeem bestaat uit vijf detectienodes (Engels: Detection Nodes (DNs)) die aan de linkerkant van de vrachtwagen en oplegger zijn gemonteerd. Deze adverteren voortdurend hun aanwezigheid en communiceren met de centrale node (Engels: Central Node (CN)) in de cabine van de vrachtwagen. De VRU draagt een onopvallende wearable met daarin enkele LEDs, een vibratiemotor en

een luide zoemer. Wanneer ze in de buurt van de vrachtwagen komen, ontvangen ze deze advertentiepakketten en een energiezuinig, zelfontwikkeld, op voorwaarden gebaseerd algoritme, dat gebruik maakt van ontvangen signaal sterkte indicator (Engels: Received Signal Strength Indicator (RSSI))-waarden, zal voorspellen of de VRU te dicht bij de vrachtwagen staat. Als dit het geval is, wordt er een alarm ingesteld en worden de LEDs, trilmotor en zoemer geactiveerd. Tegelijkertijd wordt het alarm doorgestuurd naar de CN in de cabine van de vrachtwagenchauffeur. Zo worden VRU en vrachtwagenchauffeur gewaarschuwd voor een mogelijk dodehoekongeval en delen ze dezelfde verantwoordelijkheid. Met beperkte non-verbale communicatie kunnen beide partijen de nodige maatregelen nemen voor een veilig vervolg van hun reis. In dit hoofdstuk wordt nader ingegaan op de ontwikkeling van de hardware voor de verschillende nodes, maar ook op voorwaarden gebaseerd algoritme. Op basis van simulaties werd het algoritme gedefinieerd en getest in real-life metingen.

Het volgende onderwerp beschrijft een valdetectiesysteem voor ouderen en is te vinden in Hoofdstuk 3. De literatuur biedt meerdere oplossingen aan op basis van camera, radar of trillingen gemeten via wearables of smart devices. Sommige van deze metingen worden gecontroleerd door een op voorwaarden gebaseerd algoritme of maken gebruik van een ML-algoritme dat is geïmplementeerd op een smart device of in een cloudtoepassing. Hoofdstuk 3 stelt een onopvallende wearable voor die oudere mensen om hun middel kunnen dragen en waarschuwt een verzorger wanneer een val wordt gedetecteerd. Het maakt gebruik van een kleine, energiezuinige accelerometer die continu de bewegingen van ouderen scant. Op basis van een energiezuinig, op voorwaarden gebaseerd, algoritme wordt een waarschuwing ingesteld wanneer een val wordt gedetecteerd. Dit hoofdstuk behandelt de uitgevoerde simulaties om de verschillende drempels in dit zelfontwikkelde algoritme te bepalen. Vervolgens is een convolutional neural network (CNN) algoritme ontwikkeld om het op voorwaarden gebaseerde algoritme mee te vergelijken. Dit is gebaseerd op drie open-source databases met accelerometer data van 85 mensen die 18 835 algemene dagelijkse levensverrichtingen (Engels: activities of daily livings (ADLs)) of valactiviteiten uitvoeren. Na een uitgebreide training, testen en validatie van beide algoritmen werden vergelijkbare resultaten behaald. Tot slot is er een energieanalyse voor de wearable gemaakt op basis van een realistisch scenario van een bejaarde. Dit resulteerde in een zeer energiezuinig systeem, terwijl toch een hoge detectiegraad werd behaald in vergelijking met andere oplossingen die in de literatuur worden voorgesteld.

Het derde en laatste onderwerp betreft integriteit van treinen (Engels: Train Integrity (TI)) in Hoofdstuk 4. Jaarlijks wordt er door bedrijven veel geld geïnvesteerd om handmatig de staat van locomotieven en treinwagons te controleren. Het inzetten van een WSN rond deze locomotieven of treinwagons, zal de jaarlijkse kosten aanzienlijk verlagen. De literatuur biedt beperkte oplossingen, variërend van elementaire WSNs tot sensoren met

geïntegreerde energiewinningstechnieken (Engels: energy harvester (EH)). Hoofdstuk 4 stelt enkele manieren voor om metingen met een WSN energiezuinig en betrouwbaar te maken. De eerste metingen zijn gebaseerd op de trillingen gemeten aan verschillende treinwagons. Een accelerometer is bevestigd aan een treinwagon en meet continu de versnellingen bij starten, rijden en stoppen. Op basis van deze metingen zijn enkele ingebouwde interrupts gebruikt om te detecteren of de trein rijdt of stilstaat. Op deze manier kan de WSNs gewekt of in slaapstand gezet worden. Vervolgens worden enkele radiofrequente metingen (Engels: Radio Frequency (RF)) voorgesteld. Twee verschillende planair geïnverteerde F-antennes (Engels: planar inverted-F antennas (PIFAs)) worden op vooraf gedefinieerde plekken op een treinwagon geplaatst. Een Tx-node verzendt 300 advertentiepakketten op verschillende Tx-niveaus, variërend van 0 dBm tot 10 dBm in stappen van 1 dBm. De Rx-node wordt op verschillende posities rondom de treinwagon geplaatst en zal continu naar deze advertentiepakketten scannen. De resultaten van deze metingen worden geïllustreerd en besproken.

Appendix A richt zich op de miniaturisering van de DN, voorgesteld in Hoofdstuk 2, zodat deze in het zijlicht van de vrachtwagen of oplegger past. Eerst wordt de ontwikkeling van de meerlaagse printplaat (Engels: Printed Circuit Board (PCB)) uitgewerkt. Er werd een Grounded Co-Planar Waveguide (GCPW) gebruikt om de RF transceiver impedantie af te stemmen op de SubMiniature version A (SMA)-connector, wat resulteerde in een kleine, universele DN. Er werd een SMA-connector gebruikt om verschillende antennetopologieën te testen. Deze bijlage stelt ook een geminiaturiseerde PIFA voor. Eerst wordt het enkele antenne element gesimuleerd, gevolgd door de antenne die op verschillende posities en verschillende oriëntaties op een trailer is gemonteerd.

Terwijl in Hoofdstuk 3 een wearable werd voorgesteld die detecteert wanneer een bejaarde is gevallen, beschrijft Appendix B de rest van het systeem. Het complete systeem bestaat uit vier verschillende soorten nodes. De eerste node is de wearable voor de patiënt die eerder werd voorgesteld. De volgende is de DN, deze is op een centrale positie in de kamer gemonteerd en scant continue op alarmpakketten die door de wearable van de patiënt worden verzonden. Bij ontvangst voegt deze node de benodigde gegevens zoals kamernummer, verdieping of locatie van waaruit de waarschuwing is verzonden toe, en stuurt deze naar de netwerknode (Engels: Network Nodes (NNs)) in de gang. Het doel van deze NNs is om de dichtstbijzijnde verzorgers node (Engels: Caretaker Node (CTN)) te zoeken en het waarschuwingspakket te verzenden. De CTN is voorzien van een LCD-display en laat de verzorger weten welke patiënt is gevallen, maar ook waar de val heeft plaatsgevonden. Dit hoofdstuk stelt de ontwikkelde hardware en software voor van de DN, NN en CTN. Tenslotte worden enkele metingen voorgesteld die aantonen dat deze proof-of-concept werkt.

Summary

Wearables and smart devices have become increasingly influential in our daily lives. Ranging from intelligent alarm clocks in the morning to state-of-the-art wound monitoring, all these sensors play a very important role in our day-to-day decisions. Sports enthusiasts use fitness trackers to improve their results on a daily basis, while medical professionals use these sensors to monitor their patient's healing process or, in a worst case scenario, alert the healthcare staff when the patient's conditions are bad. Most of these Internet of Things (IoT) applications rely on a low-cost, low-power sensor that is part of a Wireless Sensor Network (WSN). To connect all these sensors, a low-power, low-cost and low-latency Communication Protocol (CP) with a decent data throughput is required. Literature provides sufficient solutions, but most of these have several disadvantages. This dissertation focuses on the use of Bluetooth Low Energy (BLE) as main CP for three divergent topics where a WSN is enrolled.

Chapter 2 describes the first topic concerning blind spot detection for vehicles. Annually, several lethal accidents occur on Belgian roads due to blind spot accidents. One of the main causes for these accidents is the lack of communication between truck drivers and vulnerable road users (VRUs). This in combination with the increasing workload of truck drivers, increases the possibility of lethal accidents even more. Literature provides multiple solutions to prevent these accidents from happening, focusing on solutions ranging from radar-based to camera-based systems combined with a rule-based or machine learning (ML) algorithm. All of these systems have different advantages and disadvantages. Nevertheless, they still do not get installed on real-life trucks, due to cost, difficult implementation or low detection rate. Therefore, Chapter 2 focuses on the development of a low-cost and low-power blind spot detection and warning system for vehicles. This system consists of five Detection Nodes (DNs) that are mounted along the left side of the truck and trailer. These will continuously advertise their presence and communicate with the Central Node (CN) inside the truck cabin. The VRU is wearing an unobtrusive wearable containing some LEDs, vibration motor and loud buzzer. When they come in the vicinity of the truck, they will receive these advertisement packages. A low-power self-developed rule-based algorithm, utilizing Received Signal Strength Indicator (RSSI) values, will then predict if the VRU is too close to the truck. If so, an alert is set and the LEDs, vibration motor and buzzer are activated. At the same

time, the alert is transferred to the CN inside the cabin of the truck driver. In this way VRU and truck driver are alerted for a potential blind spot accident and share the same responsibility. With some small non-verbal communication, both parties can take the required measures. In this chapter, we will take a closer look at the development of the hardware for the different nodes, but also at the rule-based algorithm. Based on simulations, the algorithm was defined and tested in a real-life measurements.

The next topic describes a fall detection system for the elderly, described in detail in Chapter 3. Literature provides multiple solutions based on camera, radar or vibrations measured via wearables or smart devices. Some of these measurements are monitored by a basic rule-based algorithm or utilize a ML algorithm implemented on a smart device or cloud application. Chapter 3 proposes an unobtrusive wearable that elderly people can wear around their waist and that alerts a caretaker when a fall is detected. It utilizes a small, low-power accelerometer that continuously scans the movement of the elderly. Based on a low-power rule-based algorithm, an alert is set when an elderly falls. This chapter provides the required simulation for the different thresholds in this self-developed algorithm. Next, a convolutional neural network (CNN) algorithm was developed to compare the rule-based algorithm with. Validation is performed based on three free open-source databases containing accelerometer data of 85 people performing 18 835 activities of daily livings (ADLs) or fall activities. After an extensive training, testing and validation of both algorithms, comparable results were achieved. Finally, a power analysis for the wearable was made based on a realistic scenario of an elderly. This resulted in a highly power-efficient system, while still achieving a high detection rate compared to other solutions proposed in literature.

Third and final topic concerns Train Integrity (TI) in Chapter 4. Annually, much money is invested by companies to manually check the condition of locomotives and train wagons. Employing a WSN around these locomotives or train wagons, will reduce the annual cost significantly. Literature, provides limited solutions, ranging from basic WSNs to sensors with integrated energy harvester (EH) techniques. Chapter 4 proposes some measures to make measurements with a WSN energy efficient with reliable communication. A first technique is based on the vibrations measured on different train wagons. An accelerometer is attached to a train wagon and measures continuously the acceleration due to starting, moving and stopping. Based on these measurements, some built-in interrupts were utilized to detect if the train is moving or standing still. In this way, the WSNs can be put to sleep or woken up. Next, some Radio Frequency (RF) measurements are proposed. Two different planar inverted-F antennas (PIFAs) are placed on predefined spots on a train wagon. A TX node sends 300 advertisement packages at different Tx levels, ranging from 0 dBm to 10 dBm in steps of 1 dBm. The Rx node is placed on different positions around the train wagon and continuously scans for these advertisement packages. The

results of these measurements are illustrated and discussed.

Appendix A focuses on the miniaturization of the DN, proposed in Chapter 2, to make it fit inside the sidelight of the truck or trailer. First, the development of the multilayer Printed Circuit Board (PCB) is elaborated. A Grounded Co-Planar Waveguide (GCPW) was utilized to match the RF transceiver impedance to the SubMiniature version A (SMA) connector, resulting in a small, universal DN. An SMA connector was utilized to test different antenna topologies. This appendix also proposes a miniaturized PIFA. First, the single antenna element is simulated, followed by the antenna mounted on a trailer at different positions and different orientations.

While in Chapter 3, a wearable was proposed that detects when an elderly has fallen, Appendix B proposes the rest of the system. The complete systems consists of four different types of nodes. The first node is the patient wearable that was proposed previously. Next is the DN, this one is mounted in a central position of the room and will continuously scan for alert packages sent by the patient wearable. On receiving, this node adds the necessary data such as room number, floor number or location from where the alert was sent from and transmits it to the Network Nodes (NNs) in the hallway. The purpose of these NNs is to look for the closest Caretaker Node (CTN) and send the alert package. The CTN is equipped with an LCD-display and informs the caretaker which patient has fallen, but also where the fall occurred. This chapter proposes the developed hardware and software for the DN, NN and CTN. Finally, some measurements are proposed that demonstrate this proof-of-concept works.

List of Abbreviations

A

ABS	Acrylonitrile Butadiene Styrene
ACK	Acknowledgment
ADL	activities of daily living
AFH	Adaptive frequency-hopping spread spectrum
AoA	Angle of Arrival
AoD	Angle of Departure
API	Application Programming Interface
ARM	Advanced RISC Machines
ARP	Average Received Power

B

BLE	Bluetooth Low Energy

C

CN	Central Node
CNN	convolutional neural network
CTN	Caretaker Node
CP	Communication Protocol

D

DN Detection Node

DSP Digital Signal Processing

E

EDR Enhanced Data Rate

EH energy harvester

F

FIFO first in first out

G

GATT Generic Attribute

GCPW Grounded Co-Planar Waveguide

GPRS General Packet Radio Service

GSM Global System for Mobile Communications

I

IEEE Institute of Electrical and Electronics Engineers

IoT Internet of Things

L

LCD Liquid Crystal Display

LoRa Long Range

LoS Line-of-Sight

LSB Least Significant Bit

M

MCU microcontroller

MEMS micro-electro-mechanical systems

MGS micro generator system

ML machine learning

N

NFC Near-Field Communication

NN Network Node

P

PC personal computer

PCB Printed Circuit Board

PIFA planar inverted-F antenna

PLA polylactic acid

PRR Package Receive Rate

PSU Power Supply Unit

R

RAM Random Access Memory
RF Radio Frequency
RFID Radio-frequency identification
RNN Recurrent Neural Network
RSSI Received Signal Strength Indicator

S

SiLabs Silicon Laboratories
SIG Special Interest Group
SMA SubMiniature version A
SMV Signal Magnitude Vector
SN Sensor Node
SoC System-on-Chip
SPI Serial Peripheral Interface
SVM support vector machine
SWD Serial Wire Debug

T

TI Train Integrity

U

UWB ultra-wideband

V

VRU vulnerable road user

W

WCP Wireless Communication Protocol
Wi-Fi Wireless Fidelity
WHO World Health Organization
WPAN Wireless Personal Area Network
WSN Wireless Sensor Network

X

XML eXtensible Markup Language

List of Publications

Articles in International Journals

- **Nick De Raeve**, Matthias de Schepper, Jo Verhaevert, Patrick Van Torre, and Hendrik Rogier, "A Bluetooth-Low-Energy-Based Detection and Warning System for Vulnerable Road Users in the Blind Spot of Vehicles," *MDPI Sensors*, vol. 20, no. 9, p. 2727, May 2020, doi: 10.3390/s20092727.

- **Nick De Raeve**, Adnan Shahid, Matthias de Schepper, Eli De Poorter, Ingrid Moerman, Jo Verhaevert, Patrick Van Torre, Hendrik Rogier, "Bluetooth-Low-Energy-Based Fall Detection and Warning System for Elderly People in Nursing Homes", *Hindawi Journal of Sensors*, vol. 2022, Article ID 9930681, 14 pages, 2022. https://doi.org/10.1155/2022/9930681

Articles in Conference Proceedings

- **Nick De Raeve**, Quinten van den Brande, Matthias de Schepper, Jo Verhaevert, Patrick Van Torre and Hendrik Rogier, "Wearable Bluetooth Low Energy Based Miniaturized Detection Node for Blind Spot Detection and Warning System on Vehicles," *2021 6th International Conference on Smart and Sustainable Technologies (SpliTech)*, 2021, pp. 1-5, doi: 10.23919/SpliTech52315.2021.9566348.

- **Nick De Raeve**, Jo Verhaevert, Patrick Van Torre, Frederick Ronse and Hendrik Rogier, "BLE-based Power Efficient WSN for Industrial IoT Train Integrity Monitoring," *2022 7th International Conference on Smart and Sustainable Technologies (SpliTech)*, 2022, pp. 1-6.

- **Nick De Raeve**, Cédric Nzamuye, Nicolas Claus, Jo Verhaevert, Patrick Van Torre and Hendrik Rogier, "Fall Detection and Warning System for Nursing Homes based on BLE," *2022 7th International Conference on Smart and Sustainable Technologies (SpliTech)*, 2022, pp. 1-5.

1 Introduction

Wearable devices are here to stay, and they'll only get more sophisticated and effective as they evolve. Until now, most of us have made our health and fitness decisions based on what we think we know about ourselves. Advancements in technology - wearables and otherwise - will eventually take much of the guess work out of healthy living.

– Michael Dell, 2015

⋆ ⋆ ⋆

1.1 Context

Just like Michael Dell quoted in 2015, wearables are woven into our daily lives and have a massive influence on our day-to-day decisions. From an intelligent alarm clock that tracks your sleep pattern, to an intelligent water bottle that reminds you to drink during the day. From getting up in the morning till going to sleep at night, wearables are sending their data to a smartphone or another smart device. These devices have known a huge increase in sales and daily usability since the development of the first Bluetooth headset in 2002 [1, 2]. The estimation is that by 2028 the sale of wearable technology will be USD 118.16 billion, resulting in a 13.8 % increase from 2021 to 2028, according to a study conducted by Grand View Research, Inc. [3]. This rapid increase in sales is mainly due to a rapid

growing need of smart devices in the healthcare and fitness community in combination with a rising income per family.

Current fitness users make decisions based on data retrieved from their heart rate monitor, movement monitor and food tracker. In healthcare, the increase in wearables sale and usage is enormous. Ample research is performed in the development of different biomaterials and sensors [4] to monitor dedicated parameters of the human body. Examples range from the well-known heart rate monitor with integrated temperature sensor, to state-of-the-art sensors for wound, blood pressure and/or breath monitoring. All these sensors capture data with a high efficiency and accuracy, which are then transferred to any kind of smart device.

This dissertation presents research on the development of sensor nodes based on Bluetooth Low Energy (BLE). This research is subdivided into three topics. First, we take a closer look at blind spot detection of vulnerable road user (VRU) around trucks. The problem is analysed and a prototype with custom developed hardware and software is proposed, followed by an extensive simulation and real-life measurement campaign. Second, fall detection of an elderly in nursing homes is discussed. An unobtrusive, low-power wearable is developed that is worn around the waist and detects when an elderly person has fallen. Extensive simulations were performed to determine the best suited parameters for the self-developed rule-based algorithm. Afterwards, a comparative study was performed with a convolutional neural network (CNN) algorithm based on three open-source datasets. Third and final topic handles on the development of a energy efficient Wireless Sensor Network (WSN) for locomotives and train wagons. A thorough measurement campaign was executed to find a suitable antenna topology and the vibrations of the locomotives and train wagons were analysed. In this way, reliable and an energy efficient communication is ensured.

1.2 Motivation

With the ever-growing need for food and supplies delivered by and towards shipping companies, there is a significant increase in trucks on highways and secondary roads. This increase resulted in 92 lethal accidents on the Belgian Roads [5, 6] caused by trucks in 2021. Approximately 20 % of these accidents are due to the blind spot around a truck [7]. Most of the accidents are caused due to inattention of the driver or pedestrian [8], and a lack of communication between them. The inattention can be caused by distraction and monotonous driving. In current times, the distraction is mostly caused by social media, news alerts and other text messages on smartphones. Furthermore, due to the increasing workload among truck

drivers, driving and relaxing times are not always respected, resulting in tired drivers and raised work pressure. Road accidents are not only due to truck drivers. Most pedestrians and cyclists are wearing headphones. Thereby they pay less attention towards their surroundings and may fail to see a potential accident or respect the traffic rules. When combining this with jaywalking, it is nearly impossible for the truck driver to prevent an accident from happening. The challenge of this topic is to make the pedestrian and the truck driver communicate with each other and hence prevent a possible accident. This can be done via a low-cost wearable for the pedestrian and a straightforward WSN mounted in the truck.

When we move our attention from the roadusers to the elderly people, we come to the conclusion that a wearable is also useful in this field. According to [9], 37.3 million severe falls occur globally on an annually base that require medical attention. Of these millions of falls, 684 000 have a fatal ending, which makes falling the second leading cause of unintentional injury deaths [9]. Statistically, elderly above 60 year suffer the largest number of these fatal falls [10]. This puts much pressure on the nursing personnel that has to manually check if and elderly person has fallen or not. Making the elderly wear a small wearable that will detect a fall and alarm the nursing personnel will lower the work pressure and limit the lethal accidents.

In a final part of the research, the experience with wearable nodes was employed to develop small autonomous nodes for monitoring Train Integrity (TI). Annually, companies invest massive amounts in the maintenance of locomotive and train wagons. A large portion of this budget is spent on manual labour, where technicians check the condition of these locomotives and train wagons before they decide to bring them in for maintenance. Therefore, a WSN is deployed around a locomotive and train wagon in combination with several sensors. To transfer the data efficiently, some design requirements [11] are listed. Some very important requirements are the energy efficiency of the nodes and intelligent communication between them. When nodes send several data packages, the power consumption is high and the communication channels are always in use. Furthermore, it is challenging due to the large amount of metal that will influence the performance of the antenna and communication channel.

Since wearables are worn, they must comply with some basic design requirements. These requirements can be split up into three properties [12, 13]. First, you have the physical property. The most important here is being unobtrusive and comfortable. If wearing it is too much of a burden on the person, it will affect the functioning and usability of the wearable. Second, there is the cognitive property. The wearable should be intuitive and easy to use. This means that the wearable has a limited amount of

inputs, and the ones that are available should have a simple and easy use. Third and final is the emotional property. The wearable has to respect the privacy of the user data and a fashionable design will increase the sale.

Taking previously mentioned design requirements of the wearables into account in combination with the challenges described earlier, some requirements for the Communication Protocol (CP) can be derived. Current wearables need a Wireless Communication Protocol (WCP) that is low-power, low-cost and has a low latency. Energy-efficient operation is a very important factor, since wearables have to be unobtrusive. This results in a small design and even smaller battery size with limited battery capacity. The WCP has to be scalable and easy integrable in other smart devices. In this way, the data collected from all different sensors can be visualized on a smartphone and no extra smart devices have to be added. A scalable WCP will not limit the amount of connected sensors. Finally, the WCP needs to be able to cover a decent range, since it has to cover the human body to a full room in a hospital or a complete locomotive and train wagon.

Current literature provides multiple wireless solutions to connect all these smart devices with each other or to the cloud. Most commonly known is Wireless Fidelity (Wi-Fi) [14]. Wi-Fi was developed by the Institute of Electrical and Electronics Engineers (IEEE) 802.11-standard [15] which aim is a high data. It offers IP support, is easily accessible and does not hinder the mobility of the user. Furthermore, there are no compatibility problems between different Wi-Fi versions. Nevertheless, it is not energy-efficient and it is less scalable for large WSN, since the amount of connected nodes is limited. Finally, Wi-Fi has a limited range. In most cases, it is used in a residential environment where no large distances have to be covered.

Other WCP are Z-Wave [16] and ZigBee [17], which are known as a low-power wireless technology designed for use in residential areas or industrial Internet of Things (IoT) applications [18], respectively. Z-Wave is built on the IEEE 802.11-standard, the aim is to have a reliable, low-latency transmission of small data packets for control and sensor applications. It utilizes full mesh networking and operates in the sub-1 GHz. ZigBee is build on IEEE 802.15.4-standard [19], which is best suited for Wireless Personal Area Networks (WPANs) with a need for low-power and low-bandwidth communication based on a small, low-power digital radio. Besides the sub-1 GHz, it also utilizes the 2.4 GHz band. A large disadvantage of these WCPs is the lack of support by other commonly used smart devices and the low communication throughput.

Finally, there is Bluetooth Low Energy (BLE). This WCP is developed to be used for all types of WSN. Low-cost and low-power combined in small microcontroller (MCU) were three of the main pillars for the developers of

Bluetooth. Owing to these pillars, BLE is enrolled in almost every smart device on the market. A brief history outline of Bluetooth is depicted in the following section. This describes the different updates that were executed to make Bluetooth and later BLE a perfect match for WSN.

1.3 State of the art

Bluetooth [20] is created to comply with all the previously summarized design requirements. In 1994 Ericsson started the development of a cheap wireless communication platform to transfer small portions of data between mobile devices. By 1997, the first working solution is presented, followed by the Bluetooth Special Interest Group (SIG) which was launched by IBM, Ericsson, Nokia, Toshiba and Intel as the founding signatories in 1998. The name Bluetooth is proposed by Jim Kardach from Intel, who linked the Swedish technology to the 10th-centrury Danish King Harald Bluetooth.

In 2002 the Bluetooth 1.1 version is released and ratified as the IEEE 802.15.1 – 2002 standard. This version solved multiple errors of the 1.0 version and Received Signal Strength Indicator (RSSI) is added. Later on, this was updated to 1.2, 2.0, 2.1 and 3.0. During these updates, multiple features such as Adaptive frequency-hopping spread spectrum (AFH) and Enhanced Data Rate (EDR) were added to further improve Bluetooth. In 2011, Bluetooth SIG released Bluetooth 4.0 called Bluetooth Smart. This version includes Classic Bluetooth, Bluetooth High Speed (Bluetooth 3.0) and BLE, as can be seen in Figure 1.1.

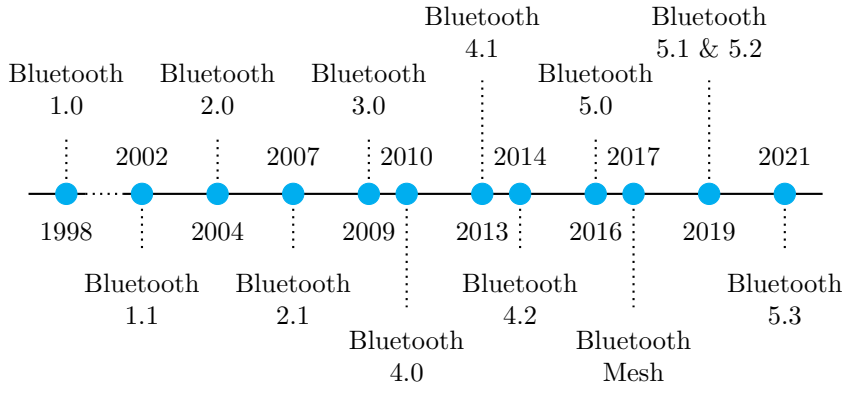

Figure 1.1: Timeline of the different Bluetooth versions.

BLE [21] is a subset of Bluetooth 4.0 with an entirely new protocol stack. Instead of 79 channels, BLE has only 40 channels of 2 MHz. Three of these channels are used for advertising while, the others are used for data transmission. In combination with the AFH, there is less interference between channels of two coupled devices, while advertising or sending data. Furthermore, BLE carries power efficiency as a top priority. To achieve this, the PHY and link layer [22–25] as well as the packet format from the basic Bluetooth version were redesigned to act as a transmitter (master) or a receiver (slave). Since only a short burst of data needs to be transmitted, there is no need for full duplex communication. When the standard was updated to version 4.1, the role of master and slave was made switchable on a device. This way, a so-called "mesh" feature could be achieved by continuously switching between roles, but keeping a point-to-point connection. Version 4.2 [26] allowed a master to connect with more than one slave at the same time, this is a first step towards one-to-many communication and even closer to a full mesh network. Finally, the payload was increased from 27 byte to 251 byte, while keeping the same packet format. This results in a throughput increase of a factor 2.6.

In 2016, Bluetooth 5.0 [27] was introduced with the aim to overcome all limitations of the previous versions. By using some data channels as advertisement channels, the advertisement payload was increased by 8 times. By doubling the modulation rate, an increase of data rate was achieved. This improvement lowered the power consumption and shortened the occupancy of air time. In 2019, Bluetooth 5.1 [28] was introduced. The most important contribution is the direction-finding feature. The addition of Angle of Departure (AoD) and Angle of Arrival (AoA) [29, 30] improves the usability of BLE in indoor localization and industrial IoT. Unfortunately, due to unstable and protected Application Programming Interface (API) functions, these features were not further examined. Furthermore, using an antenna array of minimum four antennas is not always convenient. Figure 1.1 illustrates the timeline of all the different Bluetooth versions.

All of these BLE versions are based on a point-to-point or star-based network topology, with a smart device as a central node. But in current IoT applications, the need for a full Mesh network becomes important. Furthermore, Bluetooth had to find an answer to the full mesh solution of Zigbee and Z-Wave to overcome this rivalry. Therefore, in 2017 Bluetooth SIG released Bluetooth Mesh [31–34]. The Mesh utilizes several features like profile types [31] for the nodes within a network, a publish and subscribe mechanism and relationships between nodes/groups, as can be seen in Figure 1.2. Via these features, the network becomes energy-efficient [35], easy scalable and is able to communicate with other devices that support BLE

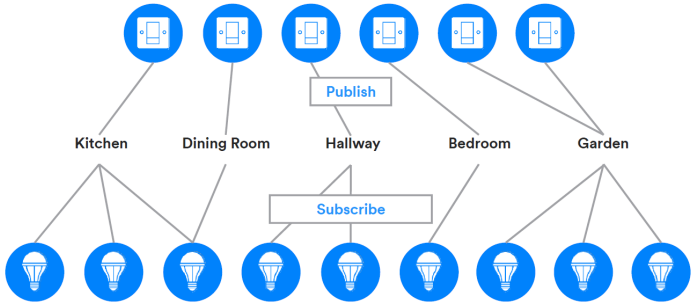

Figure 1.2: Graphical representation of a mesh network [31].

but not the Mesh stack. Nevertheless, utilizing BLE Mesh for WSNs with a very low polling rate (i.e. WSN for Train Integrity) is superfluous.

Taking a closer look at the literature, research performed in [36] illustrates that the energy consumption used for data transmission of BLE is 30 % lower than that of Wi-Fi. Furthermore, research proposed in [37] illustrates that BLE 4.2 has a maximal data throughput of 221.7 kbps. In [38], it becomes clear that the power consumption is lower with each new version, even though the data throughput increases significantly. This is done by decreasing the transmission rate, but sending the same amount of data. The results in an overall lower power consumption per given data volume. Taking the complete history of the different Bluetooth versions into account and literature proposed in [39, 40], provides the required proof that Bluetooth was developed to be energy efficient and has always had a decent data throughput compared to its energy consumption. Therefore, this technology is best suited for all sorts of WSNs.

1.3.1 Blind spot detection

In literature, this topic is described and studied in different ways. In [41] a system is proposed where radar, camera and ultrasonic data is fused to detect a pedestrian in the blind spot. Three cameras are mounted on the car (side mirrors and central mirror), two ultrasonic sensors are deployed on the stop lights and six radar units are installed around the car (one in front, above the headlights, on the trunk and one on each side door). When a pedestrian is detected, the driver will receive an alert. In total, this system utilizes eleven sensors around a normal car and no real-life measurements were proposed. Furthermore, when integrating a truck with trailer, the amount of sensors increases significantly and makes the total system more expensive. [42] proposes a blind spot detection system based on ultrasonic

sensors. Here, four cameras were mounted on the cabin of the truck and four ultrasonic sensors were mounted alongside the truck. Based on some real-life accidents, the system test showed that 68 % of the desired alerts were missed when they occurred in front of the front axle. The ultrasonic system achieved a detection rate of 48 % alongside the nearside zone. This means that 32 % and 52 % were missed, respectively. Since both systems alarm the truck driver, all the responsibility lays with the truck driver. Therefore, the pedestrian will never know of this potential blind spot accident and learn from it. In [43] a 360° camera system is proposed to detect and track moving objects. When mounting the camera on a truck, the proposed system gives a false positive ratio of 5.8 % resulting in a large detection rate. Nevertheless, it only warns the truck driver, camera systems are more expensive than radar systems and there could be some privacy issues. Furthermore, there are limitations due to soiled camera lenses.

In conclusion, literature proposes sufficient solutions to detect vulnerable road user (VRU) in the blind spot of trucks. For some of these systems, the detection rate is low due to some limitations, but the rate is still larger than without. Nevertheless, most of these systems alert only the truck driver. This means that, all responsibility lays with the truck driver and a false safety feeling could exist with all the VRUs. Combined with a very complex set-up and/or expensive system, this slows down the roll-out on current and new trucks.

1.3.2 Fall detection

Much work is performed in individual fall prevention by extensive physical training of the elderly, or "Active Ageing" [44] as they are denoted by the World Health Organization (WHO). By training during the adult life and continuing this at older ages, a strong muscular strength and cardiovascular output is achieved. By keeping this up, the likelihood of a fatal fall accident is drastically reduced. Nevertheless, falls still occur and have to be detected.

Literature provides multiple solutions [45] to this problem. First, there exist camera based solutions [46]. In [47] a central camera is positioned in a room that tracks the movement of a body. By utilizing a machine learning (ML) algorithm, the system is trained to detect a fallen person. Similar research is performed in [48] and [49]. Here, a deep learning algorithm is used to train the system to detect falls. Both systems use a basic camera positioned in the room of an elderly. These systems [48] and [49] have an F_1-score of close to 99.94 % and 99.98 % on detecting falls and non-fall events, respectively. The F_1-score is a measure to illustrate the algorithm accuracy on a dataset. It is used to evaluate binary classification systems, where the classes are 'positive' or 'negative'. However, these camera systems are

expensive in purchase and installation. Furthermore, some questions arise about the privacy since these cameras are continuously recording.

Second, there are several radar based solutions. In [50] a radar and Recurrent Neural Network (RNN) is used to detect falling persons. This results in a 98 % detection out of 50 falls, but no activities of daily livings (ADLs) were used to train and test the algorithm. Similar research is performed in [51], where an ultra-wideband (UWB) radar is utilized. With the proposed CNN algorithm, an F_1-score of 91.9 % is reached. Just as in [50], no ADLs were used during the training of the algorithm, so these F_1-scores are not representative. Another type of radar is based on infrared frequencies [52]. This system reaches an F_1-score of 92 % with the proposed support vector machine (SVM) classifier. These systems were developed in square, almost empty offices, while most nursing homes room have furniture, a built-in bathroom and often visitors. Furthermore, these systems are tested on personal computers (PCs) without memory or power limitations.

Third and final, there are the wearable fall detection systems. These consist of a wearable or a smart device that is worn on the body and contains an accelerometer. In [53] the accelerometer continuously sends its data to a PC via a BLE link. An algorithm on the PC determines if a fall occurred. Next, there are the smart devices that utilize a ML algorithm [54, 55] to determine if a fall occurred. In an updated step, an accelerometer is integrated on a smart board with integrated MCU that runs a CNN algorithm [56] to detect a fall. By utilizing an ML of a CNN algorithm or the computing force of a PC or MCU, very high F_1-scores are obtained. Nevertheless, these are not the most energy efficient solutions, since these algorithms have to run continuously and cannot be put into a deep sleep. Furthermore, to train these algorithms, training data is required. Retrieving fall data of elderly is difficult. There are free online databases containing all sorts of data of people falling in controlled circumstances. This will help to train the algorithm, but differences remain between simulated and real fall events.

1.3.3 Train integrity

A limited amount of research is proposed in current literature about WSN used for TI monitoring. Most of the proposed networks contain several sensors around the train wagon and transfer their data to a Central Node (CN) via various wireless communication protocols like XBee [57]. In some occasions, a General Packet Radio Service (GPRS) or Global System for Mobile Communications (GSM) module is added to the CN that transfers data over a cellular network to the main station at the maintenance hall or the locomotive [58]. Since this is not energy efficient, a lot of research is

performed in developing energy harvesters (EHs) for these systems. In [59], an EH is developed based on the piezoelectric effect, which is placed inside a passenger train wagon. The harvested energy reaches a peak of 0.72 µJ/h. When the vibration increases to 19.5 m/s^2 the harvested energy reaches a level of about 0.2 mJ/h which is enough to transfer data packages. This resulted in the research proposed in [60] and in [61] where the energy is generated via an EH inside a wheel bearing or an accelerometer, respectively. This last one is an ideal solution, since the accelerometer can be used to detect movement.

1.4 Own Contribution

This dissertation presents the research performed to develop sensor nodes for WSN utilizing BLE as a main communication protocol for on-body and industrial IoTs. First, a blind spot detection and warning system was developed that will continuously scan for vulnerable road user. When coming too close, this is detected by a self-developed rule-based algorithm based on RSSI measurements, warning the truck driver and VRUs. Hence, there is a shared responsibility. Since leveraging BLE results in, a low-cost, low-power and low latency system. To validate this system, custom-made hardware and software was developed. Afterwards, one of the nodes used in this system was miniaturized to fit inside the sidelights of a truck or his trailer.

Next, a fall detection and warning system for nursing homes is developed. This consists of a small, unobtrusive wearable that uses an accelerometer and a low-power rule-based algorithm that detects a fall of an elderly. Afterwards, an alert is send to the rest of the system warning the closest caretaker. For both the wearable and the other nodes, custom-made hardware and software are developed. In this way, a low-power, low-cost and easy implementable system is developed.

Finally, measurements are performed on train wagons to find a suitable antenna topology for WSN on trains. Some acceleration measurements are performed to make the WSN energy efficient. Based on an extensive measurement campaign, several simulations are performed.

1.5 Outline

This book contains five chapters and two appendices. In this chapter, the context, motivation and state-of-the-art were presented, followed by the own contribution to the three proposed topics.

In Chapter 2, the blind spot detection and warning system to detect vulnerable road users (VRUs) is proposed. The system set-up with the

different nodes and the communication steps between them is elaborated. Next, the development of the hardware for each node is illustrated. This is followed by extensive simulations of the different parameters used in the self-written low-power rule based algorithm. Finally, the real-life measurement campaign and results are discussed.

In Chapter 3, the fall detection and warning system for nursing homes is proposed. The complete system set-up with different nodes is elaborated. Next, the developed hardware and self-developed rule based algorithm with integrated filtering is proposed. Next, the performed simulations and measurements on open-source datasets are discussed and compared to the performance of a CNN algorithm. Finally, a power analysis is performed to estimate the battery lifetime.

In Chapter 4, the measurements performed to make a WSN for TI power efficient and find an optimal antenna for the wireless communication. First, the measurement set-ups are elaborated followed by an extensive discussion on the received results for the acceleration and RF-measurements.

Chapter 5, presents the conclusion of this dissertation. The important improvements of these topics in comparison of the state-of-the-art are listed. In addition, Appendix A describes the miniaturization of the Detection Node (DN) presented in Chapter 2. In appendix B, the further development of the hardware for the other nodes of the fall detection and warning system proposed in Chapter 3 is elaborated, followed by a presentation of the measurement results.

References

[1] ABI Research. *Bluetooth Smart Will Drive Cumulative Bluetooth Enabled Device Shipments to 20 billion by 2017.* ABI Research, Aug 2012. Accessed on October 18, 2022, [Online] https://www.abiresearch.com/press/bluetooth-smart-will-drive-cumulative-bluetooth-en/.

[2] Bluetooth Special Interest Group. *2022 Market Update.* Accessed on October 18, 2022, [Online] https://www.bluetooth.com/2022-market-update/.

[3] Grand View Research inc. *Wearable Technology Market Size Worth $118.16 Billion By 2028.* Grand View Research inc., Oct 2018. Accessed on October 18, 2022, [Online] https://www.grandviewresearch.com/press-release/global-wearable-technology-market.

[4] Z. Lou, L. Wang, K. Jiang, Z. Wei, and G. Shen. *Reviews of Wearable Healthcare Systems: Materials, Devices and System Integration.* Materials Science and Engineering: R: Reports, 140:100523, 2020. Available from: https://www.sciencedirect.com/science/article/pii/S0927796X19301251, doi:https://doi.org/10.1016/j.mser.2019.100523.

[5] VIAS Institute. *Stijging aantal verkeersdoden in Vlaanderen vorig jaar, daling in Brussel en Wallonië.* Accessed on October 18, 2022, [Online] https://www.vias.be/.

[6] VIAS Institute. *Road Safety Barometer.* https://www.vias.be/en/research/road-safety-monitoring-survey/. Accessed on October 18, 2022.

[7] VIAS institute. *Briefing 'Dodehoekongevallen'*, 2022. Accessed on October 18, 2022, [Online] www.vias.be/briefing.

[8] K. Bucsuházy, E. Matuchová, R. Zůvala, P. Moravcová, M. Kostíková, and R. Mikulec. *Human Factors Contributing to the Road Traffic Accident Occurrence.* Transportation Research Procedia, 45:555–561, 2020. Transport Infrastructure and systems in a changing world. Towards a more sustainable, reliable and smarter mobility. TIS Roma 2019 Conference Proceedings. Available from: https://www.sciencedirect.com/science/article/pii/S2352146520302192, doi:https://doi.org/10.1016/j.trpro.2020.03.057.

[9] World Health Organization. *Falls.* Accessed on October 18, 2022, [Online] https://www.who.int/news-room/fact-sheets/detail/falls.

[10] World Health Organization. *Number of people over 60 years set to double by 2050; major societal changes required.* Accessed on October 18, 2022, [Online] https://www.who.int/news/item/30-09-2015-who-number-of-people-over-60-years-set-to-double-by-\2050-major-societal-changes-required.

[11] M. T. Lazarescu and P. Poolad. *Asynchronous Resilient Wireless Sensor Network for Train Integrity Monitoring.* IEEE Internet of Things Journal, 8(5):3939–3954, 2021. doi:10.1109/JIOT.2020.3026243.

[12] L. Francés-Morcillo, P. Morer-Camo, M. I. Rodríguez-Ferradas, and A. Cazón-Martín. *Wearable Design Requirements Identification and Evaluation.* Sensors, 20(9), 2020. Available from: https://www.mdpi.com/1424-8220/20/9/2599, doi:10.3390/s20092599.

[13] K. Maharatna, E. B. Mazomenos, J. Morgan, and S. Bonfiglio. *Towards the Development of Next-Generation Remote Healthcare System: Some Practical Considerations.* In 2012 IEEE International Symposium on Circuits and Systems (ISCAS), pages 1–4, 2012. doi:10.1109/ISCAS.2012.6270390.

[14] WiFi Alliance. Accessed on October 18, 2022, [Online] https://www.wi-fi.org/.

[15] IEEE Standard Association. *IEEE Standard for Information Technology - Telecommunications and Information Exchange Between Systems - Local and Metropolitan Area Networks - Specific Requirements - Part 11: Wireless LAN Medium Access Control (MAC) and Physical Layer (PHY) Specifications.* Accessed on October 18, 2022, [Online] https://standards.ieee.org/ieee/802.11/3605/.

[16] Z-Wave Alliance. Accessed on October 18, 2022, [Online] https://z-wavealliance.org/.

[17] ZigBee Alliance. Accessed on October 18, 2022, [Online] https://csa-iot.org/all-solutions/zigbee/.

[18] I. Rašović and Z. Mijanovic. *Proposal of an Industrial Communication System Based on ZigBee Technology.* In 2020 24th International Conference on Information Technology (IT), pages 1–4, 2020. doi:10.1109/IT48810.2020.9070659.

[19] IEEE Standard Association. *IEEE Standard for Information technology– Local and Metropolitan Area Networks– Specific Requirements– Part 15.4: Wireless Medium Access Control (MAC)*

and Physical Layer (PHY) Specifications for Low Rate Wireless Personal Area Networks (WPANs). Accessed on October 18, 2022, [Online] https://standards.ieee.org/ieee/802.15.4/3582/.

[20] S. Zeadally, F. Siddiqui, and Z. Baig. *25 Years of Bluetooth Technology.* Future Internet, 11(9), 2019. Available from: https://www.mdpi.com/1999-5903/11/9/194, doi:10.3390/fi11090194.

[21] Bluetooth Special Interest Group. *Bluetooth Wireless Technology.* Accessed on October 18, 2022, [Online] https://www.bluetooth.com/learn-about-bluetooth/tech-overview/.

[22] C. Gomez, J. Oller, and J. Paradells. *Overview and Evaluation of Bluetooth Low Energy: An Emerging Low-Power Wireless Technology.* Sensors, 12(9):11734–11753, 2012. Available from: https://www.mdpi.com/1424-8220/12/9/11734, doi:10.3390/s120911734.

[23] J. Tosi, F. Taffoni, M. Santacatterina, R. Sannino, and D. Formica. *Performance Evaluation of Bluetooth Low Energy: A Systematic Review.* Sensors, 17(12), 2017. Available from: https://www.mdpi.com/1424-8220/17/12/2898, doi:10.3390/s17122898.

[24] K. Townsend, C. C. Akiba, and R. Davidson. *Getting Started with Bluetooth Low Energy: Tools and Techniques for Low-Power Networking.* O'Reilly Media, Inc, USA, 2014.

[25] G. Naresh. *Inside Bluetooth Low Energy, second Edition.* Artech House, 2016.

[26] *Bluetooth Core Specification 4.2.* Accessed on October 18, 2022, [Online] https://www.bluetooth.com/specifications/specs/core-specification-4-2/.

[27] Bluetooth Special Interest Group. *Bluetooth Core Specification Version 5.0.* Accessed on October 18, 2022, [Online] https://www.bluetooth.com/bluetooth-resources/bluetooth-5-go-faster-go-further/.

[28] M. Woolley. *Bluetooth Core Specification v5.1.* Bluetooth Special Interest Group, 2019. Accessed on October 18, 2022, [Online] https://www.bluetooth.com/bluetooth-resources/bluetooth-core-specification-v5-1-feature-overview/.

[29] Bluetooth Special Interest Group. *How AoA & AoD Changed the Direction of Bluetooth Location Services.* Accessed on October 18, 2022, [Online] https://www.bluetooth.com/blog/new-aoa-aod-bluetooth-capabilities/.

[30] G. Pau, F. Arena, Y. E. Gebremariam, and I. You. *Bluetooth 5.1: An Analysis of Direction Finding Capability for High-Precision Location Services.* Sensors, 21(11), 2021. Available from: https://www.mdpi.com/1424-8220/21/11/3589, doi:10.3390/s21113589.

[31] Bluetooth Special Interest Group. *Bluetooth Mesh Networking - An Introduction for Developers.* Accessed on October 18, 2022, [Online] https://www.bluetooth.com/bluetooth-resources/bluetooth-mesh-networking-an-introduction-for-developers/.

[32] Bluetooth Special Interest Group. *Mesh networking is Blue.* Accessed on October 18, 2022, [Online] https://www.bluetooth.com/learn-about-bluetooth/recent-enhancements/mesh/.

[33] S. M. Darroudi and C. Gomez. *Bluetooth Low Energy Mesh Networks: A Survey.* Sensors, 17(7), 2017. Available from: https://www.mdpi.com/1424-8220/17/7/1467, doi:10.3390/s17071467.

[34] M. Baert, J. Rossey, A. Shahid, and J. Hoebeke. *The Bluetooth Mesh Standard: An Overview and Experimental Evaluation.* Sensors, 18(8), 2018. Available from: https://www.mdpi.com/1424-8220/18/8/2409, doi:10.3390/s18082409.

[35] S. M. Darroudi, R. Caldera-Sànchez, and C. Gomez. *Bluetooth Mesh Energy Consumption: A Model.* Sensors, 19(5), 2019. Available from: https://www.mdpi.com/1424-8220/19/5/1238, doi:10.3390/s19051238.

[36] G. D. Putra, A. R. Pratama, A. Lazovik, and M. Aiello. *Comparison of Energy Consumption in Wi-Fi and Bluetooth Communication in a Smart Building.* In 2017 IEEE 7th Annual Computing and Communication Workshop and Conference (CCWC), pages 1–6, 2017. doi:10.1109/CCWC.2017.7868425.

[37] F. J. Dian, A. Yousefi, and S. Lim. *A practical Study on Bluetooth Low Energy (BLE) Throughput.* In 2018 IEEE 9th Annual Information Technology, Electronics and Mobile Communication Conference (IEMCON), pages 768–771, 2018. doi:10.1109/IEMCON.2018.8614763.

[38] P. Bulić, G. Kojek, and A. Biasizzo. *Data Transmission Efficiency in Bluetooth Low Energy Versions.* Sensors, 19(17), 2019. Available from: https://www.mdpi.com/1424-8220/19/17/3746, doi:10.3390/s19173746.

[39] K.-H. Chang. *Bluetooth: a Viable Solution for IoT? [Industry Perspectives].* IEEE Wireless Communications, 21(6):6–7, 2014. doi:10.1109/MWC.2014.7000963.

[40] A. Nikoukar, S. Raza, A. Poole, M. Güneş, and B. Dezfouli. *Low-Power Wireless for the Internet of Things: Standards and Applications.* IEEE Access, 6:67893–67926, 2018. doi:10.1109/ACCESS.2018.2879189.

[41] S. Shirahmad Gale Bagi, B. Moshiri1, H. Gharaee Garakani, and M. Khoshnevisan. *Blind Spot Detection System in Vehicles Using Fusion of Radar Detections and Camera Verification.* International Journal of Intelligent Transportation Systems Research, 19:389–404, 2021. doi:https://doi.org/10.1007/s13177-021-00254-5.

[42] R. J. Frampton and J. E. Millington. *Vulnerable Road User Protection from Heavy Goods Vehicles Using Direct and Indirect Vision Aids.* Sustainability, 14(6), 2022. Available from: https://www.mdpi.com/2071-1050/14/6/3317, doi:10.3390/su14063317.

[43] C. Premachandra, S. Ueda, and Y. Suzuki. *Detection and Tracking of Moving Objects at Road Intersections Using a 360-Degree Camera for Driver Assistance and Automated Driving.* IEEE Access, 8:135652–135660, 2020. doi:10.1109/ACCESS.2020.3011430.

[44] World Health Organization. *WHO Global Report on Falls Prevention in Older Age.* Technical report, World Health Organization, 2007. Accessed on October 18, 2022, [Online] https://www.who.int/ageing/projects/falls_prevention_older_age/en/.

[45] M. E. Karar, H. I. Shehata, and O. Reyad. *A Survey of IoT-Based Fall Detection for Aiding Elderly Care: Sensors, Methods, Challenges and Future Trends.* Applied Sciences, 12(7), 2022. Available from: https://www.mdpi.com/2076-3417/12/7/3276, doi:10.3390/app12073276.

[46] S. Rastogi and J. Singh. *Human Fall Detection and Activity Monitoring: a Comparative Analysis of Vision-Based Methods for Classification and Detection Techniques.* Soft Comput, 26:3679–3701, 2022. Available from: https://doi.org/10.1007/s00500-021-06717-x.

[47] D. R. Beddiar, M. Oussalah, and B. Nini. *Fall Detection Using Body Geometry and Human Pose Estimation in Video Sequences.* Journal of Visual Communication and Image Representation, 82:103407, 2022. Available from: https://www.sciencedirect.com/science/article/pii/S1047320321002728, doi:https://doi.org/10.1016/j.jvcir.2021.103407.

[48] S. Saurav, R. Saini, and S. Singh. *Vision-based Tchniques for Fal Detction in* 360 *Videos Using Deep learnin: Dataset and Baseliner Results* Multimedia Tools and Applications, 81:14173–14216, 2022. Available from: https://doi.org/10.1007/s11042-022-12366-5, doi:10.1007/s11042-022-12366-5.

[49] S. B. P. G. Anitha. *Vision Based Real Time Monitoring System for Elderly Fall Event Detection Using Deep Learning.* Computer Systems Science and Engineering, 42(1):87–103, 2022. Available from: http://www.techscience.com/csse/v42n1/45733, doi:10.32604/csse.2022.020361.

[50] F. Jin, A. Sengupta, and S. Cao. *mmFall: Fall Detection Using 4-D mmWave Radar and a Hybrid Variational RNN AutoEncoder.* IEEE Transactions on Automation Science and Engineering, 19(2):1245–1257, 2022. doi:10.1109/TASE.2020.3042158.

[51] P. Wang, Q. Li, P. Yin, Z. Wang, Y. Ling, R. Gravina, and Y. Li. *A Convolution Neural Network Approach for Fall Detection Based on Adaptive Channel Selection of UWB Radar Signals.* Neural Computing and Applications, pages 1433–3058, 2022. Available from: https://doi.org/10.1007/s00521-021-06795-w, doi:10.1007/s00521-021-06795-w.

[52] Y. Yang, H. Yang, Z. Liu, Y. Yuan, and X. Guan. *Fall detection system Based on Infrared Array Sensor and Multidimensional Feature Fusion* Measurement, 192:110870, 2022. Available from: https://www.sciencedirect.com/science/article/pii/S0263224122001555, doi:https://doi.org/10.1016/j.measurement.2022.110870.

[53] W.-Y. Lin, C.-H. Chen, and M.-Y. Lee. *Design and Implementation of a Wearable Accelerometer-Based Motion/Tilt Sensing Internet of Things Module and Its Application to Bed Fall Prevention.* Biosensors, 11(11), 2021. Available from: https://www.mdpi.com/2079-6374/11/11/428, doi:10.3390/bios11110428.

[54] O. Ribeiro, L. Gomes, and Z. Vale. *IoT-Based Human Fall Detection System.* Electronics, 11(4), 2022. Available from: https://www.mdpi.com/2079-9292/11/4/592, doi:10.3390/electronics11040592.

[55] M. Fáñez, J. R. Villar, E. de la Cal, V. M. González, and J. Sedano. *Improving wearable-based Fall Detection with Unsupervised Learning.* Logic Journal of the IGPL, 30(2):314–325, 12 2020. Available from: https://doi.org/10.1093/jigpal/jzaa064, doi:10.1093/jigpal/jzaa064.

[56] F. Amato, W. Balzano, and G. Cozzolino. *Design of a Wearable Healthcare Emergency Detection Device for Elder Persons.* Applied Sciences, 12(5), 2022. Available from: https://www.mdpi.com/2076-3417/12/5/2345, doi:10.3390/app12052345.

[57] N. Barkovskis, A. Salmins, K. Ozols, M. A. Moreno García, and F. P. Ayuso. *WSN Based on Accelerometer, GPS and RSSI Measurements for Train Integrity Monitoring.* In 2017 4th International Conference on Control, Decision and Information Technologies (CoDIT), pages 0662–0667, 2017. doi:10.1109/CoDIT.2017.8102670.

[58] A. Lo Schiavo. *Fully Autonomous Wireless Sensor Network for Freight Wagon Monitoring.* IEEE Sensors Journal, 16(24):9053–9063, 2016. doi:10.1109/JSEN.2016.2620149.

[59] M. Saliya, N. Kouvelas, R. V. Prasad, and N. Hokke. *Characterizing and Optimizing Piezo Harvesters for Train Interiors.* In 2020 IEEE SENSORS, pages 1–4, 2020. doi:10.1109/SENSORS47125.2020.9278637.

[60] Y. Gong, S. Wang, Z. Xie, T. Zhang, W. Chen, X. Lu, Q. Zeng, Y. Gao, and W. Huang. *Self-Powered Wireless Sensor Node for Smart Railway Axle Box Bearing via a Variable Reluctance Energy Harvesting System.* IEEE Transactions on Instrumentation and Measurement, 70:1–11, 2021. doi:10.1109/TIM.2021.3076857.

[61] L. Wang, T. He, Z. Zhang, L. Zhao, C. Lee, G. Luo, Q. Mao, P. Yang, Q. Lin, X. Li, R. Maeda, and Z. Jiang. *Self-sustained autonomous wireless sensing based on a hybridized TENG and PEG vibration mechanism.* Nano Energy, 80:105555, 2021. Available from: https://www.sciencedirect.com/science/article/pii/S2211285520311290, doi:https://doi.org/10.1016/j.nanoen.2020.105555.

2

Bluetooth-Low-Energy-Based Detection and Warning System for Vulnerable Road Users in the Blind Spot of Vehicles

Nick De Raeve, Matthias de Schepper, Jo Verhaevert, Patrick Van Torre and Hendrik Rogier

Published in MDPI Journal of sensors, vol. 20, no. 9, p. 2727, May 2020.

⋆⋆⋆

Blind spot road accidents are a frequently occurring problem. Every year too many deaths are caused by this phenomenon, even though a lot of money is invested in raising awareness and in the development of prevention systems. In this chapter, a blind spot detection and warning system is proposed, relying on Received Signal Strength Indicator (RSSI) measurements and Bluetooth Low Energy (BLE) wireless communication. The received RSSI samples are threshold-filtered, after which a weighted average is computed with a sliding window filter. The technique is validated by simulations and measurements. Finally, the strength of the proposed system is demonstrated with real-life measurements.

2.1 Introduction & related work

On Belgian roads, every year approximately 50 people are involved in blind spot accidents [1], of which approximately 10 % end lethally. Annually, the government invests a lot to raise the awareness of this problem. However, the danger still exists, mainly due to the lack of reliable communication between the truck driver and the vulnerable road user. Therefore, in this chapter we propose a blind spot detection and warning system that makes both parties aware of a potential blind spot danger.

Most systems which are developed and sold on the market are camera-based or radar-based. In most cases, camera systems use visual parameters to detect vehicles in the blind spot through post-processing machine learning algorithms [2–4]. Their big advantage is the visualization of a potential accident. At night, when compared to daytime, special camera systems are needed and the detection rate is inevitably reduced. In [5, 6] an improved solution for detection at nighttime was introduced. However, since the detection is based on images, all cameras have to stay clean, which is often problematic in the truck's operating conditions. Furthermore, when a truck makes a turn, the cameras lose the observation position as well as the detection region. In contrast, radar-based systems can be applied in real-life situations [7]. Their biggest advantage is their versatility, since these systems can operate during day- and nighttime. Most studies, however, show that only motorized vehicles are detected, and not vulnerable road users. It is easy to understand that radar detection for vulnerable road users is problematic, due to their fairly small radar cross section in combination with significant clutter on a realistic radar image. In most situations, rain, snow, trash bins, etc. are also detected, leading to many unwanted false positives. In this chapter, a Bluetooth Low Energy (BLE)-based detection and warning system where both the truck driver and the vulnerable road user are warned for a potential danger, is proposed. Moreover, as the system is based on Radio Frequency (RF) communication, the major problems of camera- and radar-based detection systems are solved.

Publications based on reconstruction reports of heavy good vehicle accidents confirm that most of the vulnerable road users are on the right side of the truck at the moment of the accident [8, 9]. In Figure 2.1 different zones around the truck are visualized. The areas with the double blue lines are visible from the truck driver's seat, directly through the windows. The areas with orange solid and dashed lines are visible via the truck's mirrors, when deployed as regulated by law. The areas with the red squares are not visible from inside the cabin through the windows and/or the mirrors. These areas are called the blind spots. Important to mention here is that all

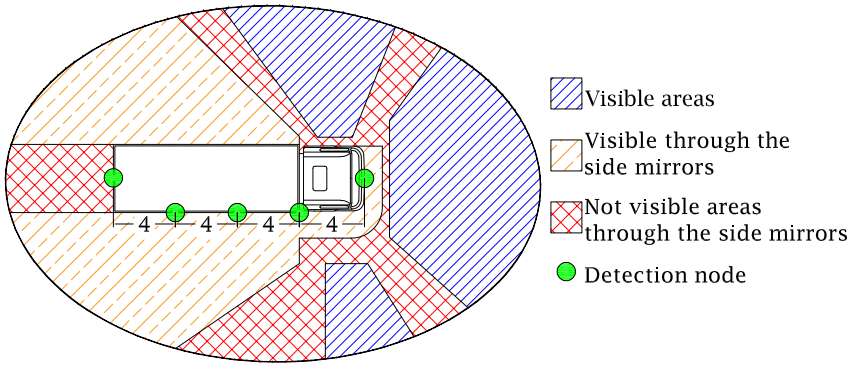

Figure 2.1: Truck with all detection nodes (green dots) mounted and all blind spots around a truck. Double blue lines are areas visible through the windshield, the orange solid and dashed lines are the areas visible through the side mirrors and the red crossed lines are not visible through the side mirrors, also known as the blind spot area.

areas are drawn based on the position of the truck in Figure 2.1. When the truck turns to the right, the area visible through the mirrors decreases and the blind spot area increases. Furthermore, mirrors are a passive system and will not alert the truck driver of potential danger. In this chapter, we propose a blind spot detection and warning system based on BLE, warning both the truck driver and the vulnerable road user for a possible blind spot accident. Although the system can be used by all kinds of cyclists, the rest of the sections focuses on pedestrians as vulnerable road users.

This chapter presents the hardware implementation of the different nodes and the design of a small sensor or wearable. Moreover in Section 2.2, the communication protocol between the different nodes and the applied filtering are discussed. Next, the performed simulations and real-life measurements that validate the system's operation are detailed in Section 2.3 and Section 2.4. This chapter ends with a conclusion formulated in Section 2.5.

2.2 Design

The system proposed in this chapter creates a complete detection area around the right side of the truck. Therefore, Figure 2.1 also shows detection nodes attached to the truck in order to detect objects and persons in the blind spots. Therefore, at the front of the truck a detection node is deployed and also one at the rear of the truck, as well as uniformly distributing three nodes along the right side. The vulnerable road user is equipped

with a small sensor or wearable, that can wirelessly connect to a detection node. Hence, the vulnerable road user can detected these detection nodes when entering the blind spot. In what follows, the detailed hardware implementation of the designed nodes is described and the software routines and filtering algorithms are explained.

2.2.1 Hardware implementation

The communication between the nodes in the proposed system is based on BLE. This communication standard was selected for the low power capabilities, minimal complexity, low price, easy connectivity with smartphone applications and compatibility of future versions. Furthermore, Silicon Labs provides multiprotocol chips, including BLE, making their hardware suitable for the design of a proof-of-concept.

For this system, BLE4.2 is the minimal required version. All previous versions used a one-to-one communication protocol, while starting from BLE4.2 one-to-many is possible. The entire required data throughput is limited and higher versions of the BLE-standard are not necessary, limiting also the power usage [10].

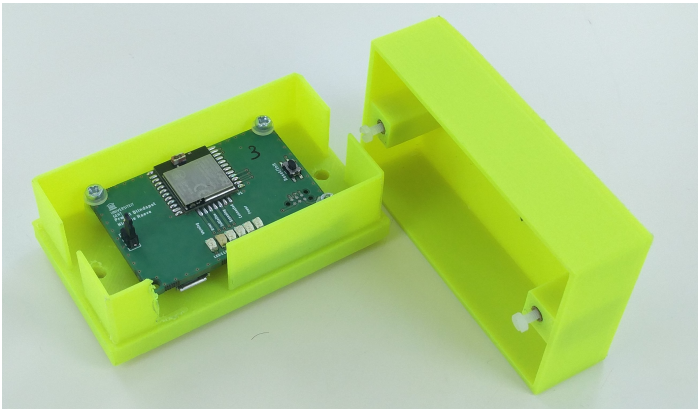

Figure 2.2: Designed detection node in its fluorescent housing.

The design of the hardware relies on BGM111 modules from Silicon Laboratories [11]. These modules use the BLE4.2 stack [12] and contain an on-board 32-bit, 38.4 MHz Advanced RISC Machines (ARM) Cortex M4 [13] microcontroller with Digital Signal Processing (DSP) instruction set, combined with an integrated antenna. In order to have an optimal maximal range, the data sheet of the BGM111 prescribes an empty space of at least 16 mm around both sides of the System-on-Chip (SoC). Furthermore, a TAG-connect [14] connector was used to program all different nodes via the

Serial Wire Debug (SWD) protocol [15]. As power supply LiPo batteries of 3.3 V [16] are used.

Figure 2.2 shows the designed Printed Circuit Board (PCB) for the detection node. Some leds were added for initialization and debugging purposes. As protection PCB plastic boxes were 3D-printed. A neodymium magnet is glued at the bottom side of the box to attach the node alongside the truck.

The wireless starter kit accompanying the BGM111 module from Silicon Laboratories [17] is used as central node. This development board contains a small Liquid Crystal Display (LCD) screen, LED, push buttons, etc. but also the necessary circuitry to debug and log all necessary data.

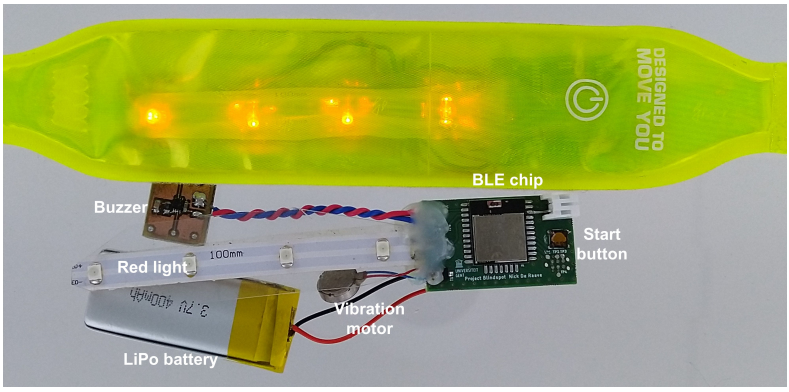

Figure 2.3: Designed wearable next to its housing.

Figure 2.3 shows the designed wearable and buzzer PCB next to its flexible housing. A light band worn by runners, cyclists and pedestrians, was chosen. The main PCB contains the BLE module and the peripheral components to activate the module and to set the outputs. Also here, the size of the PCB is very important. To fit the PCB inside the package, the width at both lateral sides of the SoC was reduced to 11 mm, yielding a decrease by approximately 10 % in maximum range, according to the data sheet.

The second PCB of Figure 2.3 contains the buzzer. On this PCB, an oscillator was implemented based on NAND gates with a built-in Schmitt trigger. According to the data sheet of the buzzer [18], a signal between 4 to 8 kHz is necessary to receive the highest pitch. Realized with in-house components, a frequency of 5.4 kHz was measured with a Rigol DS1054Z oscilloscope. Furthermore, leds and a vibration motor were added for flashing and vibrating in case of an alert.

2.2.2 Software

In this section, a global overview of the communication steps is given. The sequence diagram in Figure 2.4 pictures these steps. After initialization, the detection nodes send advertisement packets. The wearable records the Received Signal Strength Indicator (RSSI) levels of the received packets of the different detection nodes in a database. When the buffer is full, the wearable algorithm calculates the alert level for each detection node. If there is an alert, the wearable makes a connection with the corresponding detection node and alerts it. Afterwards, this detection node immediately disconnects from the wearable and sends a message to the central node to alert it.

At this point, the truck driver and the vulnerable road user are both alerted of each other's presence. This subsequently enables both parties to take the required measures to avoid a blind spot accident. In the following subsections, the communication steps of the different nodes and the filtering technique implemented in the algorithm are discussed in more detail. Also, a more detailed interpretation of the buffer size and the weights for the alert calculation is given.

2.2.2.1 Wearable

The designed wearable contains a push button to switch on the system. After the initialization of the complete database, the device starts scanning for advertising messages from the detection nodes [19]. The wearable runs three main software routines. The first one is the initialization routine, the second adds the RSSI levels to the database and a last one checks the database. Figure 2.5 illustrates in the top part the initialization of the wearable, while the bottom part shows the function to add the RSSI levels to the database. In the first software routine, the leds of the wearable light up, while it starts scanning for advertisement messages with predefined data. The second software routine adds the received RSSI levels to the corresponding buffers inside the database. At the same time, a timer-controlled routine runs in the background and checks this database. If no more packages from a specific detection node are received, this timer-controlled routine clears the database entity so it can be reused.

The third and final software routine checks the database, as can be seen in Figure 2.6. The wearable continuously scans for advertisement packets. In order to have a fast response, the system pauses scanning after every five received packages and then checks the database. In this way, with an advertisement interval of 20 ms, every 100 ms the database with all received RSSI samples in multiple buffers is checked. When one of these buffers is

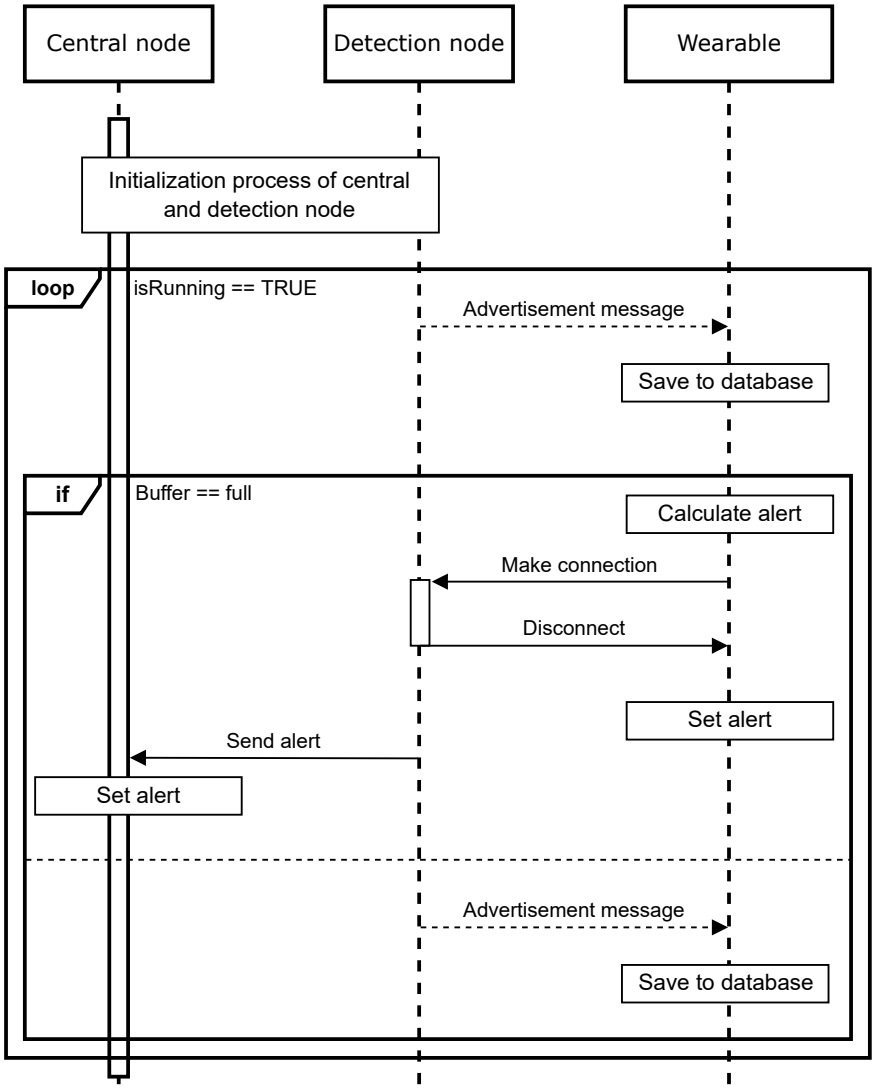

Figure 2.4: Sequence diagram of the designed system starting from the point when the wearable is activated.

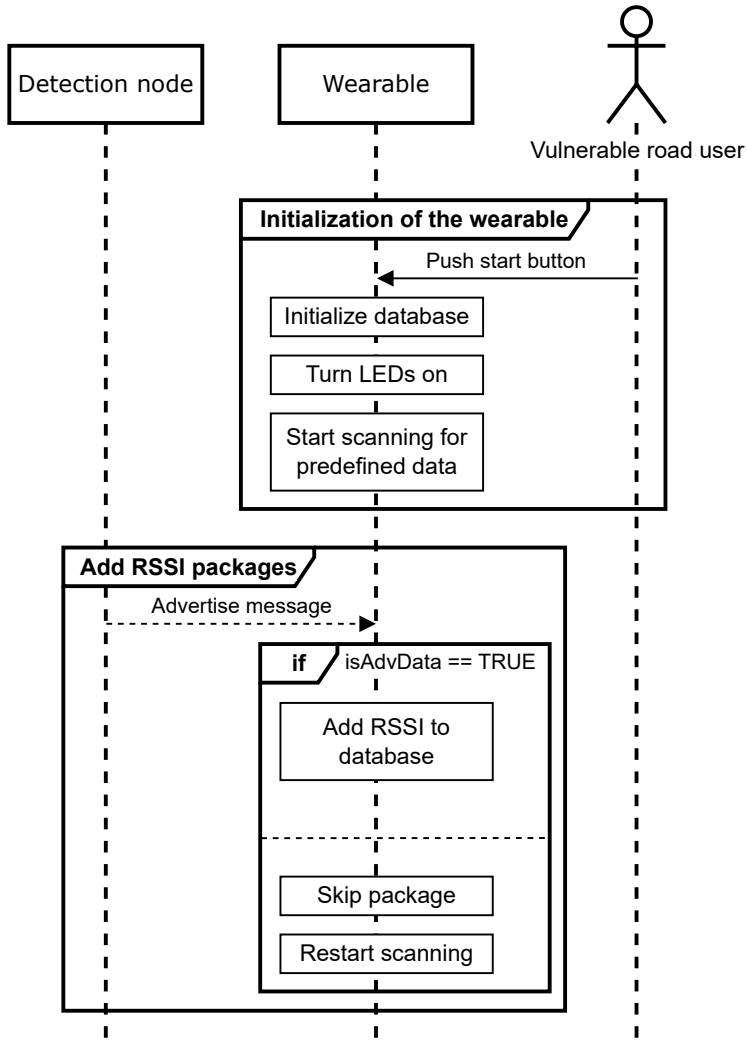

Figure 2.5: Sequence diagrams of the wearable with the initialization and add RSSI levels to database software routine.

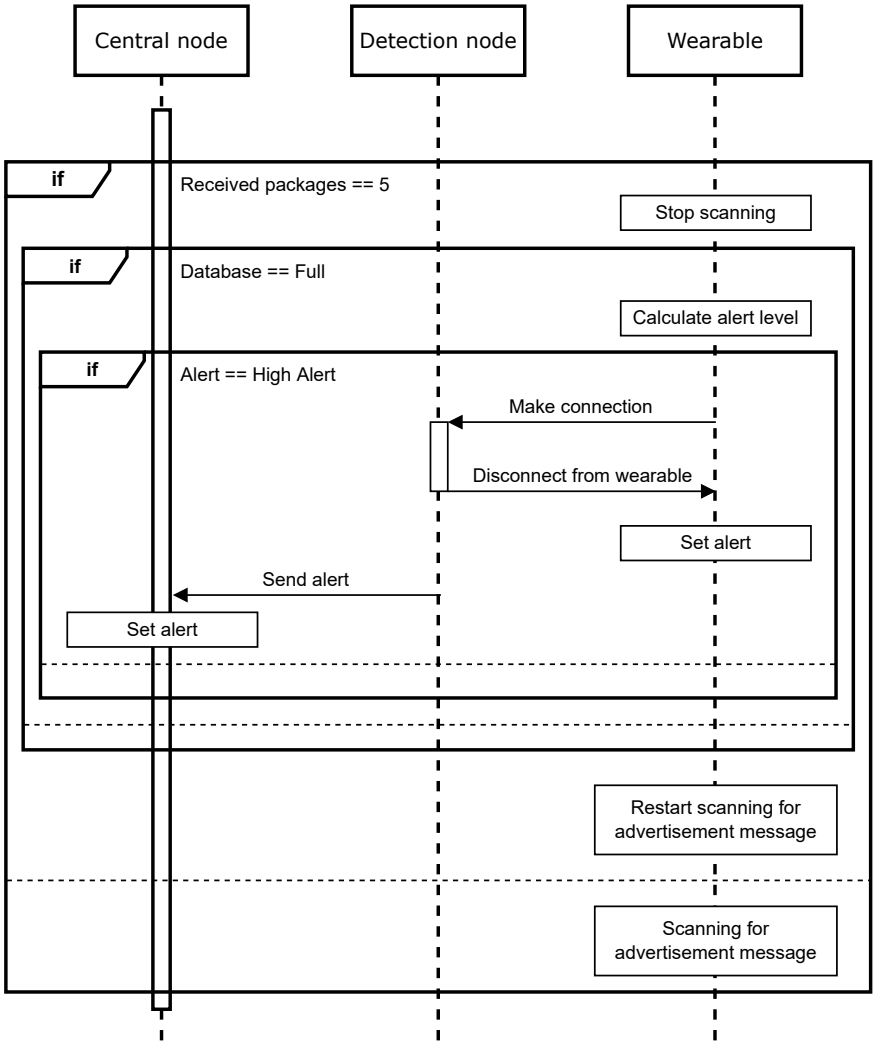

Figure 2.6: Sequence diagram of the wearable with the check database software routine.

full, the algorithm filters all RSSI samples, calculates the average value and determines the alert level. If the level is 'high', the routine connects to the detection node. Once the connection is made, the detection node immediately disconnects from the wearable and sends the corresponding alert to the alert level characteristic of the central node [12]. Because the connection is immediately disconnected, the wearable sets the alert and restarts scanning for new advertisement messages. When an alert-level-characteristic message is received, the central node also sets the corresponding alert.

2.2.2.2 Detection and central node

The next sequence diagram (Figure 2.7) shows the initialization procedure of the central and detection nodes. When the button on the central node is pushed, the initialization is started and the central node advertises. In a second step, the button on the first detection node is pushed. This detection node starts scanning for the advertising messages from the central node. When this message is received, the detection node makes a connection and requests a handle for the immediate alert service and for the alert level characteristic [12]. These handles contain the addresses of the memory allocations inside the BLE stack. Afterwards, the detection node sends an acknowledgment and starts scanning for 'start' packages. The first detection node is now completely initialized and is waiting to start advertising. The same steps are repeated consecutively for every detection node.

When all detection nodes are connected, the central node then advertises 'start' and goes in a waiting state. In total ten 'start' messages are used, in order to have redundancy. When receiving these 'start' messages, the detection node scans for packages sent by the wearable. During initialization, the central node and detection node save the addresses from the other nodes. The next time the system is activated, the nodes can just connect and start advertising without the need of the complete initialization process. If a node fails, the addresses can be adapted by reinitializing the complete system.

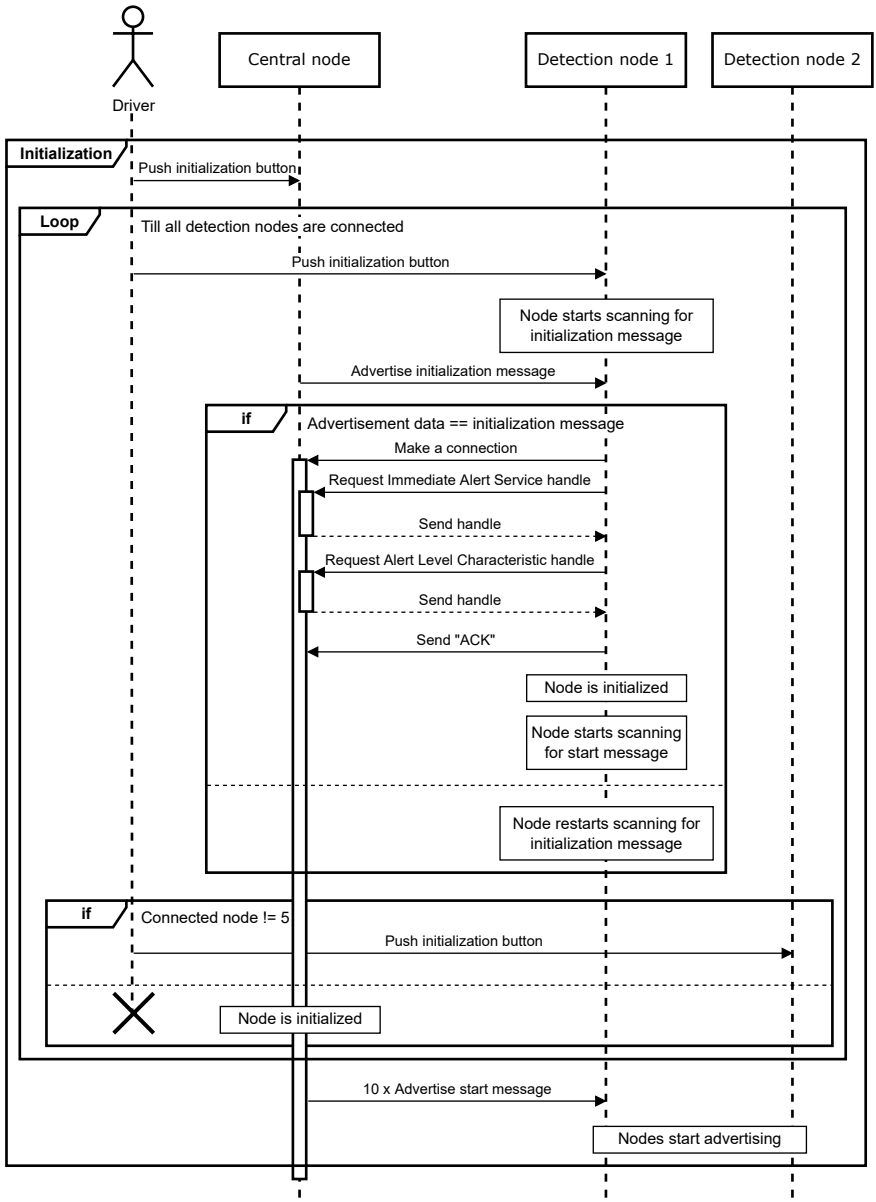

Figure 2.7: Sequence diagram of the initialization between detection node and central node.

2.2.3 Filtering

The detection system has to rely on very volatile RSSI levels, hence requiring extensive filtering. The recorded signal levels are influenced by several radio-wave-propagation effects. Path loss causes a gradual attenuation of the signals when the distance between the transmit and receive antennas increases. Shadowing and multipath fading cause these signals to fluctuate significantly during the recorded trajectory. Shadowing is inevitably caused by the human body on which the wearable is worn. As the body is situated into the radio-wave-propagation path, signals are variably attenuated depending on body orientation and posture. While walking, the arm on which the wearable is worn also moves, causing signal fluctuations. Additionally, multipath fading results in quick signal variations. The physical reason for this phenomenon is the interference between signals that travel along different paths. Metal obstacles cause the strongest reflections, but also trees and buildings play an important role. The operating frequency of the detection system is 2.45 GHz, corresponding to a wavelength of 12 cm. Due to alternating destructive and constructive interference the signal fluctuates rapidly, even with small displacements of the transmitter and/or receiver.

A lot of research was performed in order to improve the detection based on RSSI levels and to mitigate radio propagation related effects [20, 21]. Most of these algorithms require a lot of resources in terms of calculations and memory, hence they are mostly performed in post-processing. To retain real-time behaviour, two basic filtering systems are proposed. The first filter was implemented in order to suppress outlier RSSI samples due to path loss, shadowing and fading. In this filter received RSSI samples smaller than a certain threshold level are replaced by that threshold value.

$$RSSI_{avg} = w_1.\frac{\sum_{i=Q_{2,3}} RSSI_{sort,i}}{\left\lfloor \frac{k}{2} \right\rfloor} + w_2.RSSI_{k+1} \tag{2.1}$$

The second filter is a weighted average filter with sliding window [22]. This filter is implemented in order to smoothen the received RSSI samples and to calculate the average value, as is shown in Formula 2.1. All values in these buffers are expressed in dBm.

The proposed filter consists of a buffer that is filled with RSSI samples. When the buffer is completely full, the buffer is sorted ($RSSI_{sort}$) and the average is calculated with the RSSI samples in the interquartile range between the 0.25 and 0.75 quartile, visualized by Q_2 and Q_3 in Figure 2.8. The size of the buffer is represented by k and the summation of the selected RSSI samples is divided by the floored value of $k/2$. Afterwards, the av-

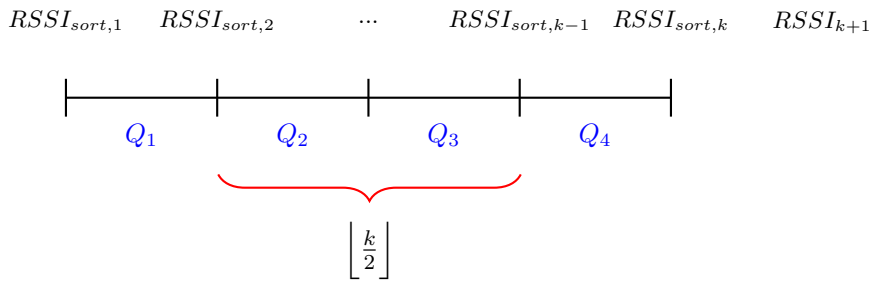

Figure 2.8: Graphical representation of the average filter with sliding window. k represents the buffer size, Q_{1-4} represents the quartiles of the buffer.

erage is multiplied by the weight w_1. In a next step, a new RSSI sample ($RSSI_{k+1}$) is multiplied by the weight w_2 and added to the average of the sorted buffer. These weights are calculated based on Formulas 2.2 and 2.3. Figure 2.9 illustrates how the weights are generated. x_1 and x_2 represents the number of RSSI samples that are being used to calculate the weight. The denominator is half the size of the buffer plus one, because of the last added RSSI sample ($RSSI_{k+1}$).

$$w_1 = \frac{x_1}{\lfloor \frac{k}{2} \rfloor + 1} \tag{2.2}$$

$$w_2 = \frac{x_2}{\lfloor \frac{k}{2} \rfloor + 1} \tag{2.3}$$

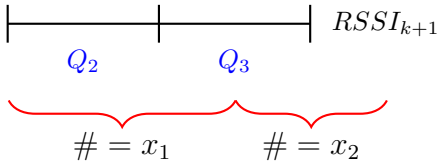

Figure 2.9: Graphical representation of the weight calculation.

2.3 Measurements

In this section, two measurement setups are analysed and different simulations are explained in detail. From these simulations, the parameters for the final algorithm were extracted. To conclude this section, results with the optimized algorithm are shown.

2.3.1 Measurement setup

2.3.1.1 Static RSSI measurement

A first measurement campaign was set up to find the most appropriate threshold level. It is important to note that the accurate conversion from RSSI levels to distances is not possible, but ranges of RSSI levels corresponding to different distances can be determined. To obtain this feeling, some static measurements were performed and are schematically illustrated in Figure 2.10. A detection node was fixed against a metal container building at a height of 1.2 m (as is shown in Figure 2.11). This metal structure replicated a metal trailer of a truck. At a distance of 1 m, 250 RSSI samples were logged while the test person was standing still. The same measurement was repeated at distances varying from 1 to 8 m in steps of 1 m.

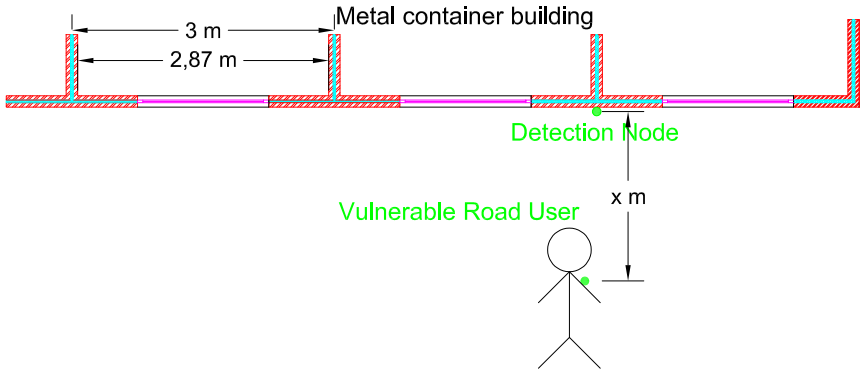

Figure 2.10: Top view of the static measurement setup against a metal container building. X represents the distance between the vulnerable road user with the wearable and the detection node mounted at a height of 1.2 m. *X varies from* 1 *to* 8 m *in steps of* 1 m

Next, the measured data is filtered with a moving average filter. A window size of 7 measurements was chosen because, given the measurement rate, the average speed of the user and the small-scale fading pattern occurring at 2.45 GHz, this window size offered the best compromise between sufficient smoothing and limited delay. Figure 2.12 shows the filtered data at each distance, together with the unfiltered data as dots. There is a clear difference in RSSI levels between 1 m and 2 m. Starting from 3 m, overlapping ranges occur. Since the system has to start detecting vulnerable road users at a minimum distance of 8 m or more, a threshold level of −65 dBm was selected. At a distance of 3 to 4 m, the system has to give an alert. So an RSSI alert level of 10 dBm higher was selected.

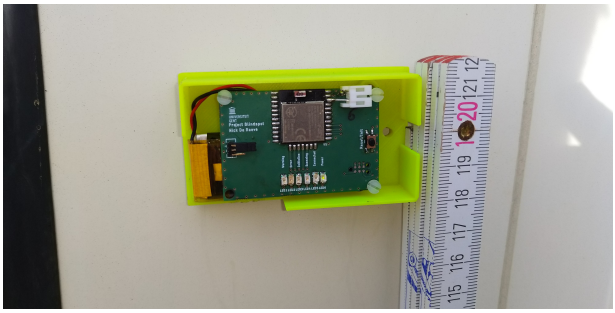

Figure 2.11: Detection node mounted against the metal container building at a height of 1.2 m

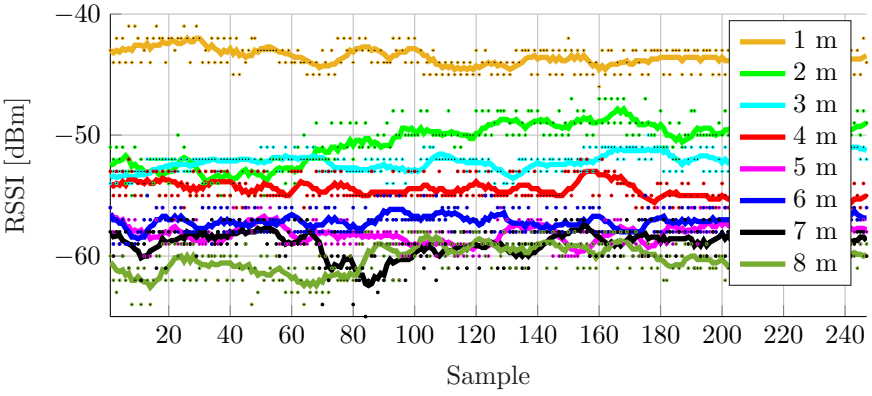

Figure 2.12: Averaged RSSI levels at distances of 1 m *to* 8 m *in steps of* 1 m.

Having this knowledge and knowing that the maximum length of a truck with trailer in Europe is 16.5 m. It can be concluded that that 5 detection nodes provided sufficient coverage since the maximum distance between these nodes is approximately 3.3 m. Furthermore, the 5 nodes provide us with the possibility that the truck driver have a better view at which point the pedestrian is detected.

2.3.1.2 Dynamic RSSI measurement

To obtain the optimal parameters for Formulas 2.1, 2.2 and 2.3, a number of dynamic RSSI measurements are performed. Figure 2.13 shows the measurement setup. Also here, the detection node was deployed on a metal container building at a height of 1.2 m. To simulate a vulnerable road user walking beside a truck, a test person walks at a distance of 4 m in front of the metal container building, starts at 6 m before and ends 6 m beyond the

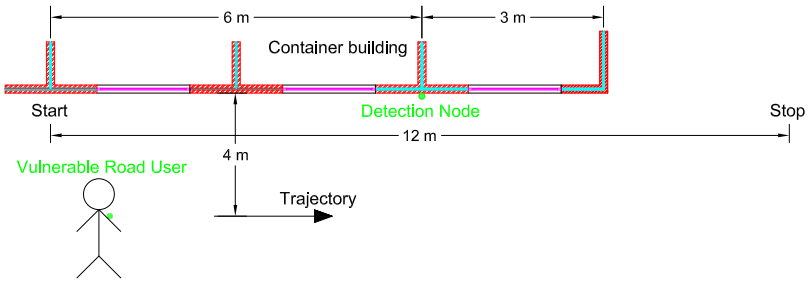

Figure 2.13: Top view of the dynamic measurement setup. The detection node is mounted at a height of 1.2 m. *A test person wearing the wearable walks in front of the metal container building at a distance of* 4 m. *The test person follows a trajectory that starts at a distance of* 6 m *before and ends* 6 m *beyond the detection node.*

node, covering a trajectory of 12 m. In three different runs, RSSI samples, received by the test person, are logged and used in the following simulations to determine the parameters of both filters.

2.3.2 Threshold filtering

The first filter compares each RSSI level to a fixed threshold value, as is defined in Subsection 2.3.1.1. The comparison itself can be done via different filtering techniques. The first technique is the minimum threshold filtering: every RSSI value lower than the threshold value is replaced by the threshold value. The second proposed technique is the step 1 dB filter: every RSSI value lower than the threshold is replaced by the previous value minus 1 dB. The same idea is used for the third technique with a step of 2 dB, although the RSSI measurement resolution of the used hardware is 1 dB.

Figure 2.14 presents the RSSI samples filtered by the three techniques, the original data and the discarded data points. The optimal threshold has already been derived earlier, and is represented as a solid black line. Starting from sample 55, the effect of the different techniques becomes visual. The step 1 dB (dashed green line with right triangles) and 2 dB (dashed blue line with left triangles) techniques result in RSSI levels with a much lower value than the original ones. Especially in areas with many discarded points, the negative influence becomes even larger. In contrast, the minimum filtering technique yields the most acceptable result. All discarded points are replaced by the threshold value which results in a more acceptable effect. Therefore, the minimum technique was selected as the preferred filtering technique for the first filter. A threshold level of −65 dBm was

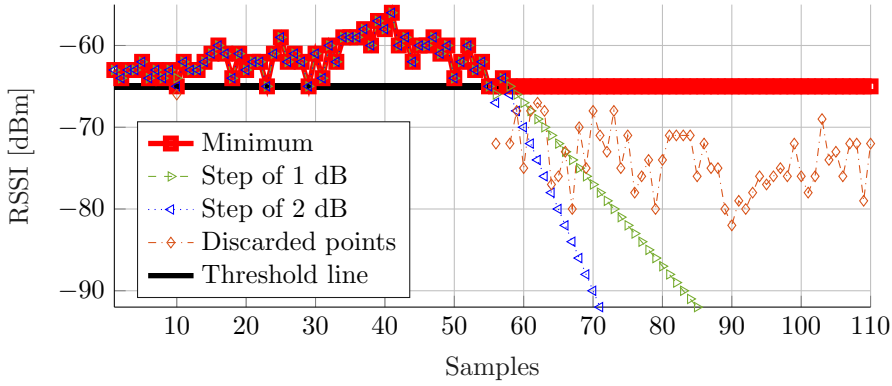

Figure 2.14: RSSI samples filtered by three different threshold filtering techniques.

selected based on the measurements performed in Section 2.3.1.1. These RSSI levels where received at a distance of approximately 8 m. In this way, there is a kind of prefiltering on the received values resulting in a faster and more accurate alert calculation.

2.3.3 Weighted average filter with sliding window

For the weighted average filtering given by Formula 2.1, a number of simulations were performed to find the best suited buffer size and weights. In order to find these parameters, the best result of the buffer size is used in the simulations for the weights and vice versa. Figure 2.15 shows the minimum threshold filtered data that is used in every next simulation.

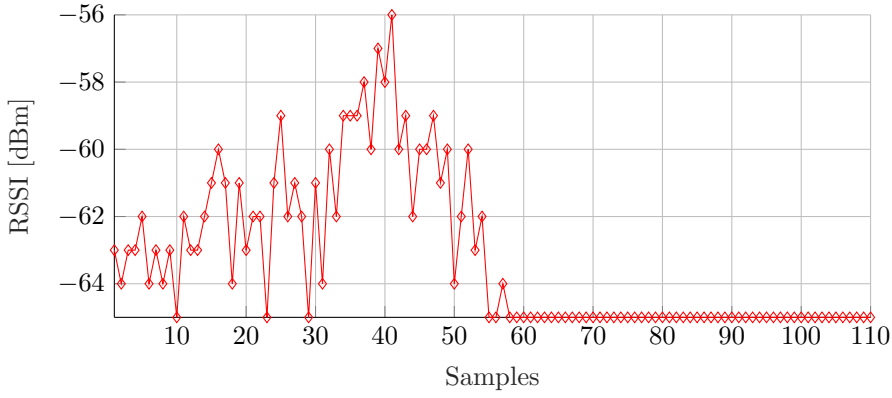

Figure 2.15: Minimum threshold filtered RSSI samples.

In Figure 2.16, it can be seen that the size of the buffer has a large influence indeed. This size needs to be chosen carefully: the larger the buffer, the more smoothing effect. However, the buffer has to be filled in a reasonable time. Advertisement packets are sent at 20 ms intervals. For a buffer size equal to 51, it takes 1.02 s to calculate the first alert. For small buffer sizes, the obtained average value is by far too small compared to the original data points of Figure 2.14. Therefore, a buffer size of 31 was selected as the best compromise, offering an acceptable delay in combination with sufficient sensitivity. In case of an alert, a connection is made to the corresponding detection node, alerting it. This alert is forwarded by the detection node to the central node, resulting in a connection time or latency limited to 620 ms.

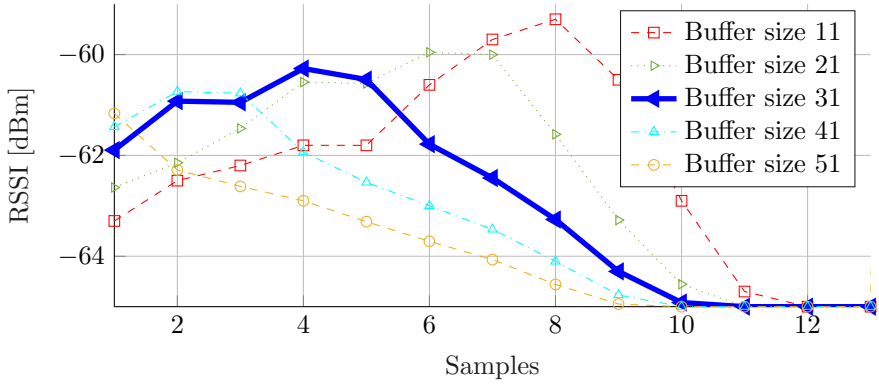

Figure 2.16: Weighted average filtering with different buffer sizes.

For the weight, a similar conclusion can be drawn. Figure 2.17 demonstrates the effects of different weights. Since the buffer contains the most information, 50 % as a lower bound for w_2 was set. Earlier a buffer size of 31 had been selected, resulting in an average calculation based on the middle 15 values (between the 0.25 and 0.75 quartile). The denominator of Formulas 2.2 and 2.3 was set to 16. As can been seen in the figure, 68.75 % or 11/16 for w_1 gives the smoothest result. Furthermore, this value still attributes sufficient weight (w_2) to the most recently added sample (31.25 % or 5/16).

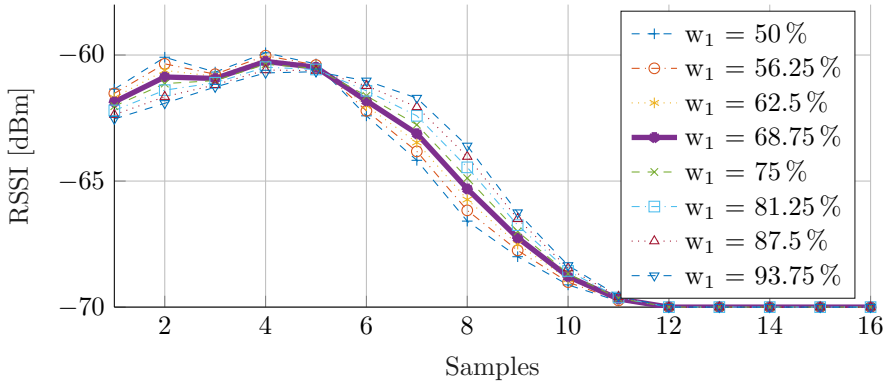

Figure 2.17: Weighted average filtering with different weights.

2.3.4 Optimized algorithm

In order to verify the selected threshold filtering, buffer size and weights, the simulations were repeated for three other data sets. All runs were filtered separately and the average value is presented in the graphs, where the measurement spread with minimum and maximum for the selected parameters is also represented.

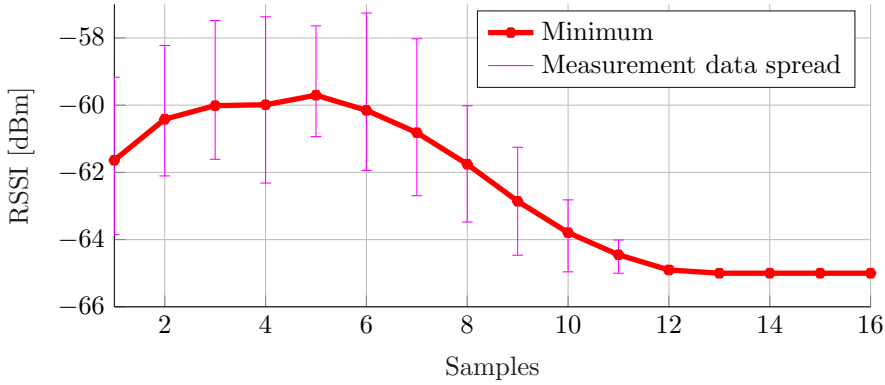

Figure 2.18: Threshold filtering with mean, minimum and maximum for three data sets.

The result of the selected threshold filter is displayed in Figure 2.18. For every RSSI sample the minimum and maximum value of all runs are displayed, showing the performance of this threshold filter.

Figure 2.19 shows the variation in RSSI levels for a buffer size of 31. Taking the measurement spread into account, similar results are obtained.

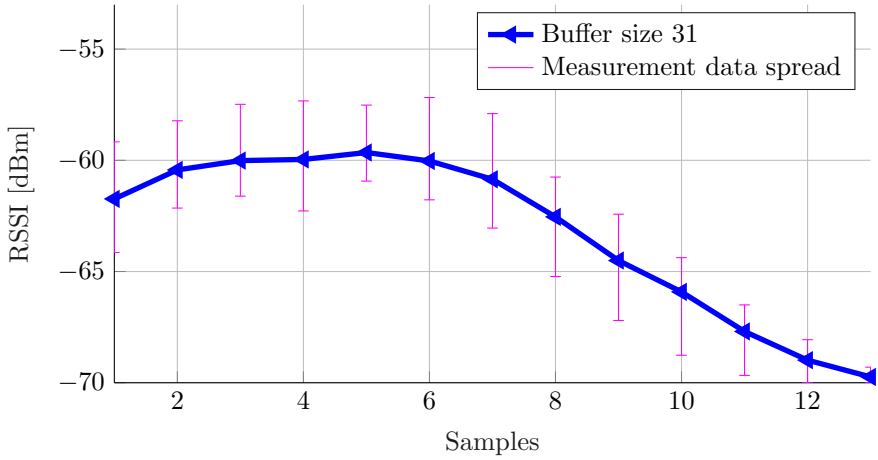

Figure 2.19: Weighted average filtering with different buffer sizes for three data sets.

Figure 2.20 demonstrates the result of the weight simulation for the three runs. The measurement spread for 68.75 % has an acceptable effect for the different data sets.

2.4 Real-life Measurements

Based on real-life measurements, the performance of designed hardware and the realization of the optimized algorithm are validated. After the description of a general test, also the system behaviour for a big group of people is handled.

2.4.1 General test

As a general test, the system was mounted on a truck and multiple secondary school teenagers were equipped with a wearable, worn on the left upper arm. One at a time, a pupil approached the truck from the back or the front. The start position of everyone was 20 m away from the truck. From the moment the pupil started to walk towards the truck, the wearable was activated. Figure 2.21a shows a pupil receiving his second alert, with the wearable blinking.

During this test, the general operation of the system was validated. At the start of the test, it was experienced that −65 dBm is a little bit too low. Therefore, the threshold level was changed to −70 dBm. This increased the detection distance by approximately 3 m and when starting from the rear

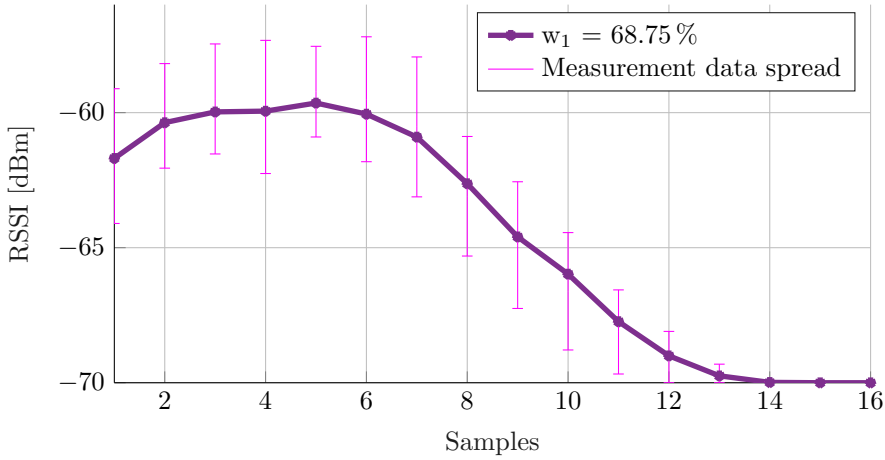

Figure 2.20: Weighted average filtering with different weights for three data sets.

(a) Pupil receiving second alert.

(b) Group of ten receiving an alert.

Figure 2.21: Pupils receiving alert during real-life measurements.

end of the truck, the first alert was received at a distance of around 8 m. Coming from the other side, the alert was received much later, resulting in a distance of roughly 3.5 m from the truck. This can be explained by the fact that the wearable was worn at the left upper arm and was hence oriented away from the detection nodes.

2.4.2 Large group of people

Other tests were carried out with more than one person at a time: with five, ten and twenty pupils respectively.

Five persons walk in a small group towards the truck starting from approximately 20 m from behind the truck (Figure 2.22). The first alert was received by persons in position one and two, followed by an alert for the pupil in the third position. The pupils in position four and five received the alert from the moment they passed the others. This test shows that

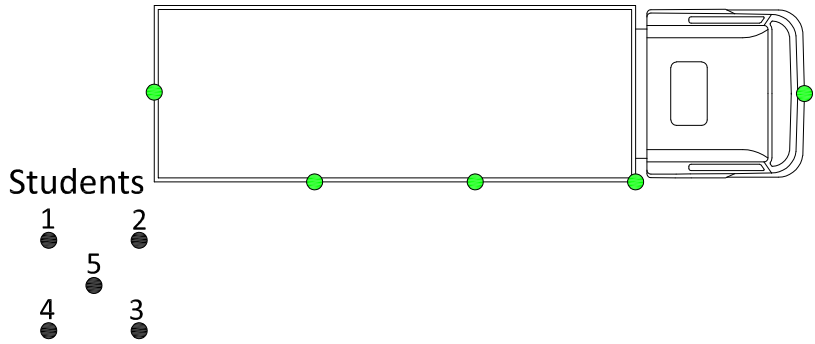

Figure 2.22: Top view of the real-life measurement test with big group of people. Five persons in a small group walked towards the truck starting at a distance of approximately 20 m *behind the truck.*

the RSSI levels for pupil four and five are influenced by the others around them. When there is a Line-of-Sight (LoS) connection, the system performs perfectly.

(a) Start from behind truck.

(b) Start from before truck.

Figure 2.23: Group of twenty pupils receiving alert during measurement.

The test with a group of ten was in a random position. As can been seen in Figure 2.21b, the first time the teenagers walked towards the truck starting from 20 m behind the truck and the second time from the front of the truck. Pupils with an LoS connection received the earliest alert just-in-time. Repeated with twenty persons (see Figure 2.23a), alerts were received at various times. Once the teenagers started before the truck (see Figure 2.23b) and the wearable on the left upper arm was obstructed by the different bodies, alerts were received much later. However, all people on the side of the truck received a fast alert.

2.4.3 Verification measurement

In order to test the system progressively, the same tests were repeated with a larger truck (16.5 m) and 30 other persons (see Figure 2.24a and Figure 2.24b). This way, the entire system was tested with a larger group and employing the longest truck allowed on Belgian roads.

(a) Group of two received alerts.

(b) Group of four received alerts.

Figure 2.24: Pupils receiving alert during the verification measurement campaign.

Just like in previously described real-life measurements, the test persons walked by in different group sizes and positions. Also here, the proposed system performed as intended. For students starting from the back, the first alert was received at a distance of approximately 8 m, measured from the back of the trailer and confirming the results described above.

2.5 Conclusion

In this chapter, a blind spot detecting and warning system based on Bluetooth Low Energy (BLE) wireless communication is proposed, relying on Received Signal Strength Indicator (RSSI) measurements. The system consists of five detection nodes around the truck who advertise their presence. The vulnerable road user utilizes a wearable that scans these advertisement packets. The algorithm inside the wearable interprets these messages and applies filtering on the RSSI levels of them.

The algorithm itself consists of two filters: the threshold filter and the weighted average filter with sliding window. Based on static RSSI measurements, the threshold level was fixed at -65 dBm. Later, during the real-life measurements, this value is lowered to -70 dBm. From the threshold simulations, the minimum technique is selected as the preferred threshold filter. Dynamic RSSI measurements are performed to find the best suited buffer size and weights to be used. A buffer size of 31 is proposed and for the weights w_1 and w_2 the values 68.75 % or 11/16 and 31.25 % or 5/16 are suggested, respectively. The first alert is received in 620 ms.

During the real-life measurement, the system performed reliably well. The first alert for a vulnerable road user starting from the back of the truck is received at approximately 8 m. The test with multiple vulnerable road users at the same time lead to the same results. When the wearable is surrounded by many people, the alert is received slightly later. In a group of people, only a few need to wear the wearable in order to receive an alert, the complete group will be alerted due to the light and sound effect of the others.

A blind spot detection and warning system is proposed, relying on RSSI measurements and BLE wireless communication. Compared to camera- and radar-based systems, the proposed system is based on RF communication and uniquely identifies only all vulnerable road users. The system warns both the truck driver and the vulnerable road user for a potential danger.

Acknowledgment

The author wants to express his gratitude to the Flemish government, Departement Mobiliteit en Openbare Werken for the funding of this research and to the Provincial Technical Institute in Zottegem and Snel Logistics Solutions for their cooperation during the real-life measurements.

Funding

This work was supported by the Flemish government, Departement Mobiliteit en Openbare Werken.

References

[1] Veiligverkeer.be. *Cijfers en Ongevallen Dode Hoek.* https://www.veiligverkeer.be/inhoud/cijfers-en-ongevallen-dode-hoek/.

[2] S. Chang, C. Tsai, and J. Guo. *A Blind Spot Detection Warning System Based on Gabor Filtering and Optical Flow for E-Mirror Applications.* In 2018 IEEE International Symposium on Circuits and Systems (ISCAS), pages 1–5, May 2018.

[3] J. W. Baek, E. Lee, M. Park, and D. Seo. *Mono-Camera Based Side Vehicle Detection for Blind Spot Detection Systems.* In 2015 Seventh International Conference on Ubiquitous and Future Networks, pages 147–149, July 2015. doi:10.1109/ICUFN.2015.7182522.

[4] S. Baek, H. Kim, and K. Boo. *Robust Vehicle Detection and Tracking Method for Blind Spot Detection System by Using Vision Sensors.* In 2014 Second World Conference on Complex Systems (WCCS), pages 729–735, Nov 2014. doi:10.1109/ICoCS.2014.7060984.

[5] Y. Chen, B. Wu, H. Huang, and C. Fan. *A Real-Time Vision System For Nighttime Vehicle Detection and Traffic Surveillance.* IEEE Transactions on Industrial Electronics, 58(5):2030–2044, May 2011. doi:10.1109/TIE.2010.2055771.

[6] C. T. Chen and Y. S. Chen. *Real-Time Approaching Vehicle Detection in Blind Spot Area.* In 2009 12th International IEEE Conference on Intelligent Transportation Systems, pages 1–6, Oct 2009. doi:10.1109/ITSC.2009.5309876.

[7] G. Liu, L. Wang, and S. Zou. *A Radar-Based Blind Spot Detection and Warning System for Driver Assistance.* In 2017 IEEE Second Advanced Information Technology, Electronic and Automation Control Conference (IAEAC), pages 2204–2208, March 2017. doi:10.1109/IAEAC.2017.8054409.

[8] VIAS. *Ongevallen met Vrachtwagens - Fase 1.* https://www.vias.be/publications/Ongevallen%20met%20vrachtwagens%20%E2%80%93%20Fase%201/Ongevallen_met_vrachtwagens_%E2%80%93_Fase_1.pdf.

[9] VIAS. *In-Depth Investigation of Crashes Involving Heavy Goods Vehicles.* https://www.vias.be/publications/Ongevallen%20met%20vrachtwagens%20%E2%80%93%20Fase%202/Accidents_involving_trucks_%E2%80%93_Phase_2.pdf.

[10] P. Bulić, G. Kojek, and A. Biasizzo. *Data Transmission Efficiency in Bluetooth Low Energy Versions.* Sensors, 19(17):3746, Aug. 2019. doi:10.3390/s19173746.

[11] Silicon Laboratories. *BGM111 Blue Gecko Bluetooth module data sheet.* https://www.silabs.com/documents/public/data-sheets/BGM111_datasheet.pdf.

[12] Bluetooth Special Interest Group. *Specification of the Bluetooth System, Covered Core Package Version 4.2.* https://www.bluetooth.com/specifications/archived-specifications/.

[13] ARM. https://www.arm.com/products/silicon-ip-cpu. Accessed on October 18, 2022.

[14] T. Connect. *TAG Connect.* http://www.tag-connect.com/.

[15] Silicon Laboratories. *Programming Internal Flash Over the Serial Wire Debug Interface.* https://www.silabs.com/documents/public/application-notes/an0062.pdf. Accessed on October 18, 2022.

[16] J & A. *Lithium-ion Polymer Battery, Specification Model: JA-803450P.* https://www.olimex.com/Products/Power/BATTERY-LIPO1400mAh/resources/JA803450-Spec-Data-Sheet--J-A.pdf.

[17] Silicon Laboratories. https://www.silabs.com/products/development-tools/wireless/bluetooth/bluegecko-bluetooth-low-energy-module-wireless-starter-kit.

[18] Murata. *Buzzer murata PKLCS1212E4001-R1.* https://www.murata.com/en-eu/api/pdfdownloadapi?cate=cgsubSounders&partno=PKLCS1212E4001-R1.

[19] M. Nikodem and M. Bawiec. *Experimental Evaluation of Advertisement-Based Bluetooth Low Energy Communication.* Sensors, 20(1):107, Dec. 2019. doi:10.3390/s20010107.

[20] G. Li, E. Geng, Z. Ye, Y. Xu, J. Lin, and Y. Pang. *Indoor Positioning Algorithm Based on the Improved RSSI Distance Model.* Sensors, 18(9):2820, Aug. 2018. doi:10.3390/s18092820.

[21] D. Cannizzaro, M. Zari, D. J. Pagliari, E. Patti, E. Macii, M. Poncino, and A. Acquaviva. *A Comparison Analysis of BLE-based Algorithms for Localization in Industrial Environments.* Electronics, 9(1):44, Dec. 2019. doi:10.3390/electronics9010044.

[22] S. Onofre, P. M. Silvestre, J. P. Pimentão, and P. Sousa. *Surpassing Bluetooth Low Energy limitations on distance determination.* In 2016 IEEE International Power Electronics and Motion Control Conference (PEMC), pages 843–847, Sept 2016. doi:10.1109/EPEPEMC.2016.7752104.

3

Bluetooth-Low-Energy Based Fall Detection and Warning System for Elderly People in Nursing Homes

Nick De Raeve, Adnan Shahid, Matthias de Schepper, Eli De Poorter, Ingrid Moerman, Jo Verhaevert, Patrick Van Torre and Hendrik Rogier

Published in Hindawi Journal of sensors, vol. 2022, Article ID 9930681, 14 pages, Jan 2022.

⋆⋆⋆

Due to the ever growing population of elderly people, there is a dramatic increase in fall accidents. Currently, multiple ideas exist to prevent the elderly from falling, by means of technology or individualised fall prevention training programs. Most of them are costly, difficult to implement or less used by the elderly and they do not deliver the required results. Furthermore, the increasingly older population will also impact the workload of the medical and nursing personnel. Therefore, we propose a novel fall detection and warning system for nursing homes, relying on Bluetooth Low Energy (BLE) wireless communication. This chapter describes the hardware design of a fall-acceleration sensing wearable for the elderly. Moreover, this chapter also

focuses on a novel algorithm for real-time filtering of the measurement data as well as on a strategy to confirm the detected fall events, based on changes in the person's orientation. In addition, we compare the performance of the algorithm to a machine learning procedure using a convolutional neural network (CNN). Finally, the proposed filtering technique is validated via measurements and simulation. The results show that the proposed algorithm as well as the CNN both result in an excellent accuracy when validating on a common database.

3.1 Introduction

Fall accidents are a large risk in the life of elderly people and form one of the most important public health problems in the ageing population [1]. Research shows that, from the age of 65 on, the number of fall accidents rises dramatically [2, 3], often with a lethal ending. Furthermore, it is found that individualised fall prevention training programs [4, 5] do not have the intended results. All these fall injuries have a large influence on the health system [6]. Moreover, they definitely impact the workload of the medical and nursing personnel, since they have to constantly check if an elderly person has fallen. This causes stress for the personnel and can lead to mental or physical problems. Current literature proposes multiple solutions to lower the number of fall accidents with lethal endings, by alerting the personnel faster. Accordingly, the workload of the medical and nursing personnel is lowered as well. However, many of these solutions are very expensive, difficult to implement or hindered by privacy regulations. Therefore, we propose a low-cost fall detection and warning system for nursing homes based on Bluetooth Low Energy (BLE)5.1 [7]. The proposed system consists of four different nodes, all using BLE5.1 or Bluetooth Mesh as a wireless communication platform.

The novel contributions of this system is as follows. A truly wearable node for fall detection is developed, complemented with victim localization and staff alerting functionality and based on a single-chip solution, exploiting BLE5.1. Thereby a novel reliable physics-based fall detection algorithm that does not require any training is conceived and the proposed algorithm is compared with machine learning (ML) using convolutional neural networks (CNNs).

This chapter describes the design and implementation of a fall detection wearable for the elderly. First, an overview is presented of the current literature, followed by a detailed explanation of the hardware implementation and algorithm used to reliably detect and confirm a fall. The detection is triggered by acceleration and the conformation is based on orientation

change. Next, there is an overview of all measurements and simulations that are used to construct and validate the algorithm, followed by measurement analysis and conclusions.

3.2 Related Work

In current literature, multiple fall detection systems are proposed [8–14]. These detection systems can be split up in three different groups, as can be seen in Figure 3.1.

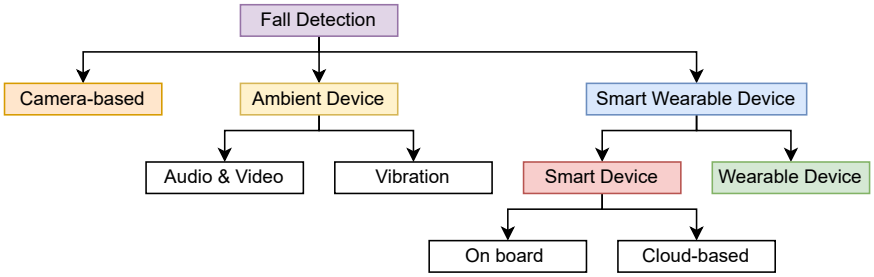

Figure 3.1: Classification of fall detection systems

A first group is formed by camera-based systems [15–19]. By means of a camera implemented in a room or on a person, a fall is detected based on an extensive algorithm that runs on a personal computer (PC). Even though these systems work well, they have some disadvantages. Most of them have a limited coverage area, have a very high cost and can be hindered by privacy regulations. Furthermore, it is important to notice that none of these systems communicate to provide the necessary help when a fall occurs. Since these systems rely on a different principle, we do not go into further detail.

A second group consists of ambient device systems [8–10, 20–23]. This group can be split up into two subgroups. The first subgroup utilises vibration to determine whether a fall occurred. Sensors are mounted in a room, on a floor [21] etc., to monitor the environment and to detect a fall. Accelerometers are integrated into the walls [20] and continuously scan for vibration, while an algorithm detects a fall based on these wall sensors. The second subgroup attempts to fuse audio and visual data. The system proposed in [23] combines accelerometer and camera data to determine whether a fall has occurred. Just like camera-based systems, these have an even higher implementation cost. Moreover, they can only detect a fall, but they cannot determine which elderly person has fallen, nor can they send vital parameters to the nursing personnel. Most of these systems are prone

to generating false alerts, which is stressful for the personnel and can lead to carers paying less attention to the alerts.

A final group of solutions consists of wearable systems. We have opted to divide these systems in two subgroups. The first and biggest subgroup consists of systems that are based on a smart device with integrated accelerometer or gyroscope sensors [24–29]. In a next step, these systems can be divided in categories, based on where most of the processing is performed. In the systems proposed in [24, 26], the accelerometer data are transferred to the cloud or to a PC, where a post-processing algorithm detects a fall. In the cloud, multiple algorithm types can be used to determine whether a person has fallen. In current literature, a lot of research is performed on machine learning algorithms [30–39] that detect falls. However, these systems require a lot of training data, which is difficult to obtain. Furthermore, such systems consume a lot of power. Secondly, there are the smart device systems that perform all necessary calculations on the device itself [27, 28]. In this way, there is no unnecessary transfer of data to the cloud.

The second type of smart wearable devices are the ones where a dedicated wearable will detect a fall. Note that research confirms that elderly people prefer not to wear (obtrusive) smart devices [40, 41]. A truly unobtrusive wearable [42–46] generally only contains a microcontroller (MCU) and an accelerometer or gyroscope sensor. The MCU will determine whether a fall has occurred, based on movement or posture changes of the person wearing the device. The device is energy efficient consumes little energy and the wearable does not hinder the elderly people. Since these wearables do not look like smart devices or do not require any input actions from elderly people, the likelihood of acceptance increases. However, such wearables often do not communicate with the carers. A selected group of fall detection systems uses a gyroscope [47–52] to detect a fall or even the typical movements just before a fall occurs.

There are also several commercially available products. Most of these products [53–55] will make a call to the emergency services when a fall event is observed. In most situations, the detection is based on accelerometer or gyroscope data that are fused together. The detection occurs with a smartphone, smartwatch or dedicated wearable. Disadvantages of these systems are the smart technology. It is a known fact [40, 41] that elderly do not like to wear smart devices, especially when they are not unobtrusive. There are also some radar-based solutions [56, 57]. These are placed inside the room and detect falling persons. When a fall occurs, the system calls the emergency service. Radar solutions have promising effects, but can suffer image clutter caused by furniture in the room. Other products do not only detect when a person falls, but also try to prevent a serious fall.

The product proposed in [58] is a belt worn around the waist that uses a fusion of different sensors to detect if a person is going to fall. If so, an airbag is deployed and a predefined phone number is called. Compared to our solution, it is very difficult to wear this wearable in an unobtrusive way.

Since the system proposed in this chapter only has to detect whether a fall occurred, we opted to use only an accelerometer instead of a gyroscope for several reasons. First, current state-of-the-art micro-electro-mechanical systems (MEMS) accelerometers consume less energy in comparison to gyroscopes. Next, determining the orientation of a person based on 3-D accelerometer measurements of the gravitational vector is straightforward. Finally, MEMS accelerometers only measure angular speed in rad/s, which needs to be integrated to find the angle. However, bias and drift are known to produce deviations in the angles produced. The following sections will further explain how the accelerometer detects the fall acceleration as well as changes in orientation of the falling person.

3.3 Design

Based on the advantages and disadvantages of the previously mentioned systems, the following system requirements for the patient wearable were adopted:

1. More than 90 % of the falls detected
2. Less than 10 % false alerts
3. Compact and unobtrusive
4. Battery lifetime of up to 7 days

The proposed system consists of four different nodes, Figure 3.2 provides a ground plan of a typical room in a nursing home that is equipped with the system and Figure 3.3 illustrates the communication steps between the different nodes. The first node, the patient wearable (green dot), is worn around the waist. This node uses BLE5.1 as wireless communication platform and contains an accelerometer for measuring the movements of the elderly person. As soon as the node measures a fall, it starts advertising alert messages. For each alert, five subsequent advertisement packets are transmitted to ensure reliable reception. With this approach, system pairing and self-healing are not necessary.

The second node is the DN (red dot) and is placed in a central position of the room and scans for alert messages from the wearable. When detecting an alert, it pushes a message on the mesh network. This network

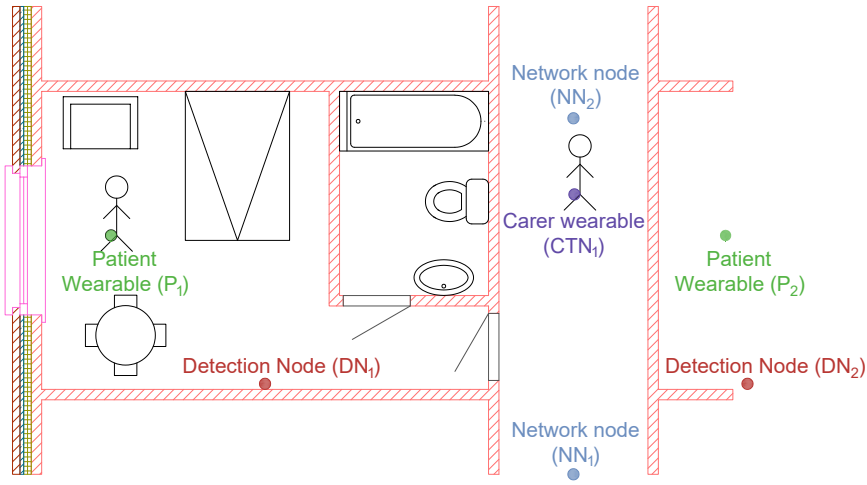

Figure 3.2: Ground plan of a room in a nursing home with the different nodes mounted. The patient wearable (green dot) (P) is worn by an elderly person who has fallen. The Detection Node (DN) (red dot) is mounted in a central position and communicates with the Network Nodes (NNs) (blue dot) mounted in the hallway. These nodes transfer messages to the Caretaker Node (CTN) equipped with a wearable/smartphone (purple dot).

is realised by the NNs (blue dots) that are placed in the corridors. These nodes transfer the alert messages to the closest carer wearable (purple dot), alerting the carer that patient X has fallen in room Y. Since each room is equipped with its DN, it is easy to map each node to a floor and room number. Additional information can be added to these alert messages or a continuous stream can be setup to visualise the vital parameters from the elderly person. Furthermore, by implementing the proxy feature [59, 60] in the mesh network, every BLE device can communicate on the network. In this way, the carer's wearable can be replaced by a smartphone application.

The proposed system is very energy efficient, allowing the patient wearable and CTN to be powered by batteries, it does not cause any issues with privacy, the installation costs are minimal, it is much cheaper than camera systems or extensive individualised training programs. Additionally, there is no need for advanced positioning systems or cellular communications, which would make such a system more expensive. Furthermore, since this network allows connection to smartphones, the nurses do not have to carry

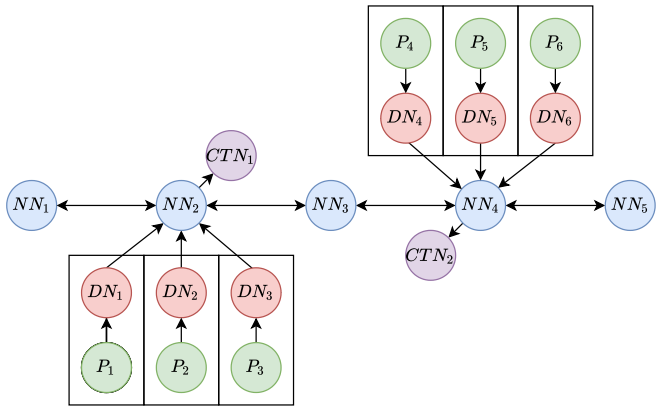

Figure 3.3: Graphical representation of the communication steps. The patient (P) wearable, represented in green, will detect a fall and send a message to the DN , represented in red. The number of the DN corresponds to the room number. This node transmits an alert message to the NNs, shown in blue. These nodes forward the message to the closest CTN, shown in purple. The carer can then perform the necessary actions.

extra devices. The following subsections describe the hardware design and the detection algorithm that is executed in the wearable, worn by the elderly person.

3.3.1 Hardware design

A number of specific requirements are imposed during the design process of the wearable. First, the wearable has to be unobtrusive to the end-user. Studies show that elderly do not easily adopt novel technology, especially when devices are too big or too complicated to use [40, 41]. Furthermore, based on research performed in [61, 62], the ideal position to mount this wearable is on the waist, which makes the unobtrusiveness even more important. Furthermore, the wearable needs to be energy efficient. The final requirement is the versatility. If the wearable is easy to configure with different sensors, it is more useful for doctors and carers to track or monitor patients in critical conditions. As mentioned before, BLE5.1 is an excellent choice as wireless communication platform, given its high energy efficiency [63]. Next, the use of the Generic Attribute (GATT) profiles [64], which are part of the BLE stack, makes it very easy to add more functionality. Furthermore, BLE5.1 has a high message capacity and can operate over a larger range compared to previous versions of BLE.

Figure 3.4 displays the layout of the PCB of the designed wearable. The

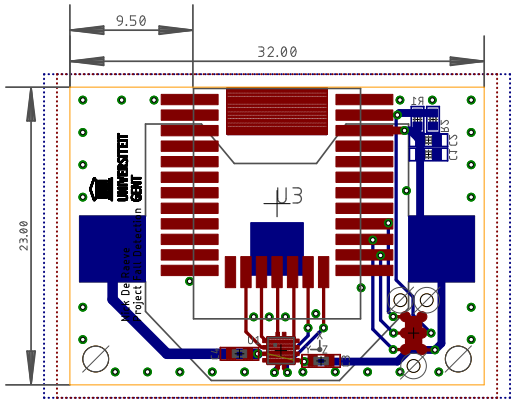

Figure 3.4: Designed Printed Circuit Board (PCB) (dimensions in mm)

design relies on the BGM13P wireless module from Silicon Laboratories [65]. This device uses the BLE5.1 stack and contains an on-board 32-bit 38.4 MHz Advanced RISC Machines (ARM) [66] Cortex-M4 MCU with Digital Signal Processing (DSP) instruction set. The ARM Cortex-M4 is a modern general-purpose MCU employed in many low-power systems. 32-bit processing enables efficient execution of the complex procedures necessary to deploy current-day wireless communication standards such as BLE. The ARM can handle this in a very power efficient way, compared to low-end 8-bit processors, which need much more instructions to achieve the same result. Moreover, modern ARM controllers also provide many power saving modes. Hence, in this application, the processor goes into sleep mode for a relatively long time between short bursts of activity, resulting in an energy efficient solution.

The BGM13P unit also includes an integrated antenna. The complete module has an overall size of 15×13 mm, which makes the wearable unobtrusive and much smaller than most smart devices, as is shown in Figure 3.5. To achieve an optimal communication range, the data sheet of the BGMP13P prescribes an empty space of at least 17 mm near the antenna. To ensure that the device remains unobtrusive to the wearer, the width of the PCB at both lateral sides of the System-on-Chip (SoC) was reduced to 9.5 mm, yielding a decrease by 10 % in maximum communication range, according to the data sheet. Furthermore, a TAG-connect [67] connector was used to program all different nodes via the Serial Wire Debug (SWD) protocol [68]. The power supply is a standard small battery of 3.3 V; a power analysis follows in Section 3.5. Based on previous experience, these modules have

been selected to implement this proof of concept.

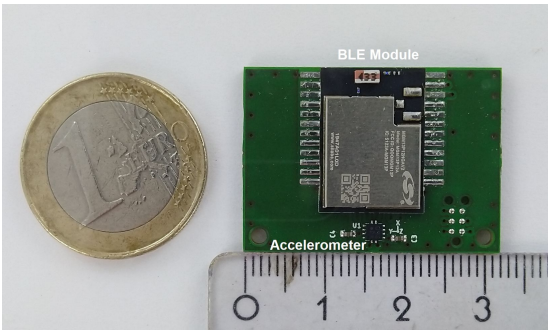

Figure 3.5: Fabricated PCB with a size of $32 \times 23 \times 10\,\text{mm}$

To measure the movements of the patient, the ultra-small, low-power, triaxial Bosch BMA280 [69] accelerometer was added. This sensor features an integrated low-pass filtering with a filtered-output data rate up to 500 Hz and an unfiltered data rate of 2 kHz. Furthermore, it possesses a resolution of 4096 LSB/g in the ± 2 g range, can be used in ± 2 g, ± 4 g, ± 8 g and ± 16 g range, communicates via an Serial Peripheral Interface (SPI) 3-wire communication link and contains an integrated temperature sensor. These properties make the accelerometer excellent to detect when a patient has fallen. The integrated temperature sensor is a valuable extra feature because if an elderly person falls and is lying on a cold floor, the body temperature can drop to a critical value and lead to hypothermia. By wearing this wearable under clothing, close to the body, the body temperature significantly influences the on-board temperature sensor and a decreasing body temperature can be detected. Taking all these measures into account, the patient's wearable is compact and unobtrusive and has an overall size of $32 \times 23 \times 10\,\text{mm}$. Hence, the third design requirement is met.

3.3.2 Algorithm design and filtering procedure

Since the node is constantly receiving the X, Y and Z acceleration values from the accelerometer at a high sample rate, filtering is necessary to reduce the amount of data. Figure 3.6 illustrates the flowchart of the applied filtering and decision tree. The algorithm can be split up in two branches. The first branch in red decides whether a fall occurred, based on the amplitude of the accelerometer data, and is called the acceleration branch. The second branch in green takes a decision based on the change of the spatial

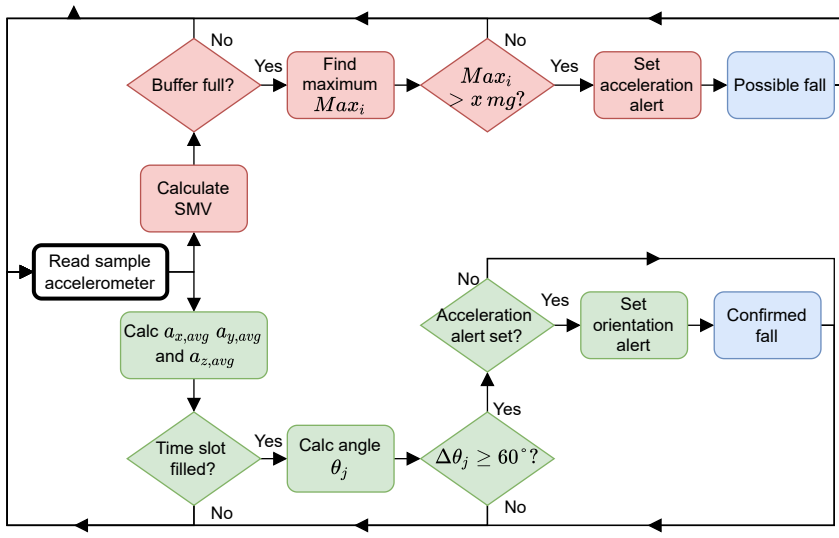

Figure 3.6: Flowchart of two branches used to filter accelerometer data and determine fall alerts. Acceleration branch coloured in red, orientation branch in green and decision tree in blue. Note that orientation change alone can never trigger an alert.

orientation and is called the orientation branch. At the end of each branch, in the decision tree, a measured fall is classified as a possible or confirmed fall, visualised in blue.

The analysis starts when the samples of the accelerometer are received. The acceleration branch calculates the Signal Magnitude Vector (SMV) as used in many related publications [8, 26–29, 32, 70] based on formula (3.1) and is expressed in $mg = 9.81 \times 10^{-3}\,\mathrm{m/s^2}$, where a_X, a_Y and a_Z are the measured accelerations expressed in mg along the X, Y and Z axis, respectively. The calculated SMV is stored in a buffer. When this buffer is full, the maximum SMV value is selected. This value has to be larger than a certain threshold value, which will be determined in Subsection 3.4.2. When this conditions is valid, the acceleration alert flag is set.

$$SMV = \sqrt{a_X^2 + a_Y^2 + a_Z^2} \tag{3.1}$$

The orientation branch calculates the average a_X, a_Y and a_Z based on a single exponential smoothing algorithm, as is expressed in formula 3.2 [71–73], with $a_{axis,avg,i}$ the average calculated for sample i along a certain axis expressed in mg, with $a_{axis,avg,i-1}$ the previously calculated average along that axis, with $a_{axis,i}$ a new sample along the same axis and with α a

damping factor, which is set to 0.1. Based on formula (3.3) and (3.4), for the given sample rate (subsection 3.4.2), this α value results in a time constant τ of 47.45 ms, which leads to a cut-off frequency of 3.35 Hz. Hence, (3.2) implements a low-pass filtering operation to reduce the noise of the accelerometer samples.

$$a_{axis,avg,i} = (1-\alpha).a_{axis,avg,i-1} + \alpha.a_{axis,i} \tag{3.2}$$

$$\alpha = 1 - e^{\frac{-\Delta T}{\tau}} \Rightarrow \tau = \frac{-\Delta T}{\ln(1-\alpha)} = 47.45\,\text{ms} \tag{3.3}$$

$$f_c = \frac{1}{2.\pi.\tau} = 3.35\,\text{Hz} \tag{3.4}$$

For every 250 ms of captured data, the calculated averages $\overline{a_{X,j}}$, $\overline{a_{Y,j}}$ and $\overline{a_{Z,j}}$ determine a vector $\vec{v_j}$ as in equation (3.5). Next, based on equation (3.6) the angle $\Delta\theta_j$ between of the new vector $\vec{v_j}$ and the previous vector $\vec{v}_{j-1}$ is calculated. When this $\Delta\theta_j$ is larger than or equal to 60°, the orientation alert flag is set, but only if the acceleration flag was set earlier. In a final step, the alert flags are checked. When both flags are set, the person definitely fell. Hence, a confirmed fall alert is sent to the carer's wearable. When only one of the flags is set, a normal fall alert is sent. Note that the latter case should still be interpreted as a very high probability of a fall event, although the fall is potentially less severe.

$$\vec{v_j} = \overline{a_{X,j}} \cdot \vec{X} + \overline{a_{Y,j}} \cdot \vec{Y} + \overline{a_{Z,j}} \cdot \vec{Z} \tag{3.5}$$

$$\Delta\theta_j = \arccos \frac{\vec{v}_{j-1}.\vec{v_j}}{\|\vec{v}_{j-1}\|.\|\vec{v_j}\|} \tag{3.6}$$

The main idea behind these branches and the associated conditions originates from looking at the amplitude flow of a fall (Figure 3.7) and the change in spatial orientation (Figure 3.8). Figure 3.7 illustrates the calculated SMV of a measured fall, with a theoretical fall profile fitted on the measurement data. The theoretical fall profile was described in [70]. Under normal conditions, the SMV is around 1 g or 9.81 m/s^2. When a fall occurs, the SMV first drops, followed by a steep positive peak, followed by a smaller peak and ending near 1 g again. Nearly always, the fall results in a different orientation, as can be seen in Figure 3.8.

The purpose of this wearable is to provide reliable fall detection without false positives. This is achieved by taking into account that the new maximum value should be larger than the previous maximum and that the difference between the two values should be larger than a predefined threshold expressed in *mg*. Employing this method, we are able to reliably find the peak and set the acceleration alert flag. Research performed in [70]

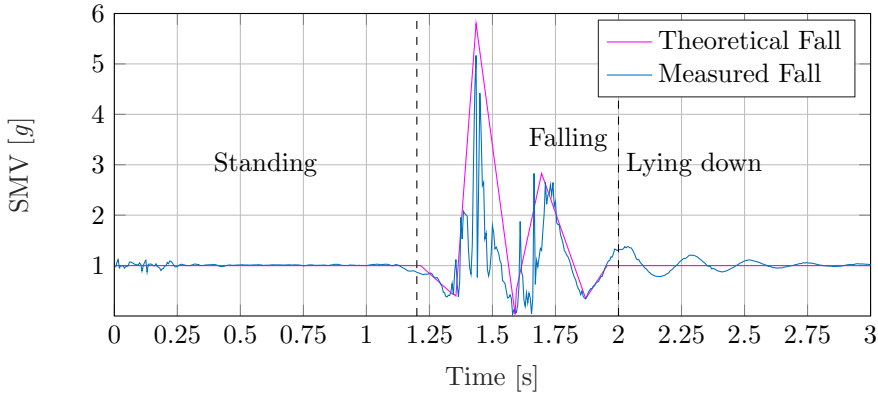

Figure 3.7: Graphical representation of the calculated SMV for a measured fall at a sample interval of 5 ms *compared to a fitted theoretical fall [70]. Both falls represent acceleration data of a test person standing before a fall, during the fall and lying down after a fall occurred.*

illustrates that while walking, ascending and descending stairs, there will never be a peak as large as when a fall occurs.

The main idea of the orientation branch is to confirm a fall by determining the different spatial orientations of the person before and after the fall event. The peak of the angle between two vectors measured before and after the fall with a time interval of 1 s in between is used to determine this condition. It is important that this time separation is large enough in order not to include accelerations measured during the fall, as this will disturb the orientation measurement. During the orientation measurement, the total acceleration should be predominantly caused by gravity, which can be confirmed by an SMV value approaching 1 g.

By calculating the moving averages of a_X, a_Y and a_Z with window size of 250 ms and transforming it to a vector, a more reliable orientation angle is obtained. This angle approaches the orientation of the gravity vector and is considered as a measurement of the gravity vector. The angle between two measured gravity vectors, taken 250 ms before the fall and 250 ms after the fall, provides valuable information to confirm the fall event.

An orientation difference around 90° is expected when a person's orientation changes from standing to lying down. However, a lower threshold value of 60° is proposed in order to account for situations where the elderly person falls on a nearby object and is not lying entirely flat. Note that the orientation alert flag is only set if an acceleration alert flag had already been set. Hence, an orientation change alone can never trigger a fall alert.

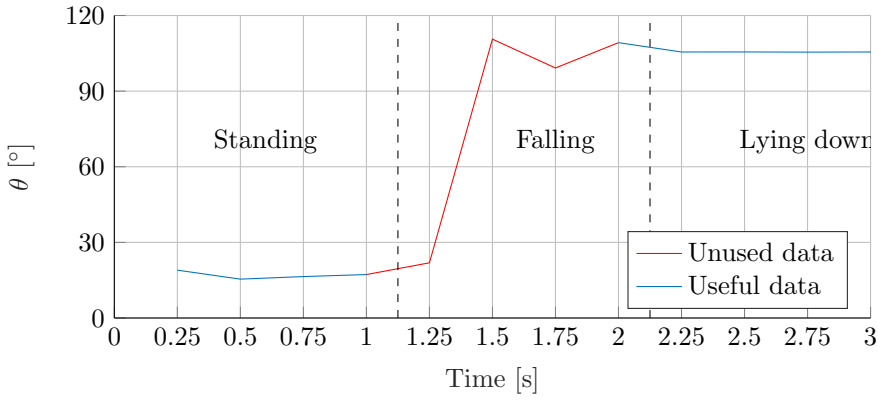

Figure 3.8: Moving average of the calculated θ in a window size of 250 ms. *θ is the angle between the spatial orientation vector of a test person and the gravitational vector, sampled at an interval of* 5 ms. *This Figure illustrates that θ is fluctuating during a fall, but has a stable value before and after a fall occurred.*

3.3.3 Convolutional Neural Network Design

To compare the performance of the proposed rule-based algorithm with ML, we use a CNN, of which the architecture is shown in Figure 3.9. CNN has shown tremendous performance in various classification problems such as image classification [74], modulation classification [75] and wireless technology classification [76–78]. In this work, the CNN is trained with three publicly available fall Datasets presented in [79–81]. These datasets consist of the accelerometer data in the form of X, Y, and Z acceleration values, which were captured on the human body. The proposed rule-based algorithm identifies every event as either 'Fall' or 'Not Fall'. In order to have a fair one-to-one comparison, the CNN is trained with 70 % of each dataset that is categorising the events in a similar way. All the data classes corresponding to falls are combined in the 'Fall' category and all the activities of daily living (ADL) classes are combined in the 'Not Fall' category. Therefore, the CNN also identifies the 'Fall' and 'Not Fall' events in a comparable way.

For the input to the CNN, we consider the SMV values of the raw X, Y, and Z accelerometer data computed according to Formula 3.1. Furthermore, we consider a window size of $20x30 = 600$ SMV values, which represents 3 s in the time domain. The architecture of the CNN is composed of three 2D convolutional layers and four fully connected layers as shown in Figure 3.9. The last fully connected layer of the architecture is the softmax layer with two neurons, representing that the CNN is able to classify the two classes.

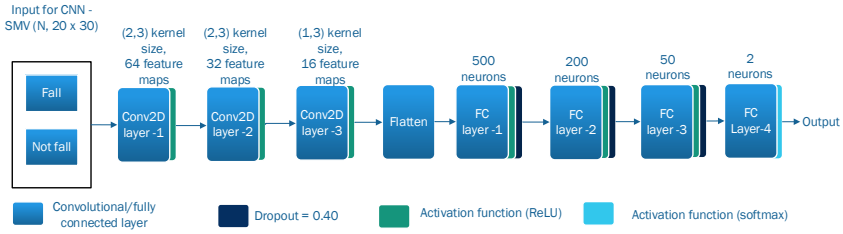

Figure 3.9: Convolutional neural network architecture.

The total number of examples in KFall, SisFall1, SisFall2, and FallAIID are 5036, 4500, 4500 and 1798, respectively. Note that each example is of size (1 x 600), hence containing 600 SMV values computed according to Formula 3.1 from (3 x 600) values of X, Y, and Z. Since we use Conv2D in the CNN architecture, we transformed each example from (1 x 600) to (1,20,30). For training and testing the classifier for each dataset, we divided the data into training, validation, and testing data sets with a split of 70 %/15 %/15 %.

For the optimiser, the Adam optimiser was used as it provided the best accuracy. In addition, *ReduceLROnPlateau* was used from the Tensorflow platform, because it helped in reducing the learning rate from 10^{-3} to 10^{-4} when the validation loss stopped improving. In order to have a fine balance between overfitting and underfitting, a batch size of 512 and a dropout of 0.40 were used. The CNN classifier was trained on a NVIDIA GTX $1080Ti$ Graphics Card, which is available in our in-house Virtual Wall [82]. The classifier was implemented in an abstract level library Keras [83] with Tensorflow [84] as a back-end.

3.4 Measurement and Analysis

3.4.1 Measurement setup

To validate the algorithm, a set of simulations was performed based on the measurement setup in Figure 3.10. A person, approximately 1.8 m tall and wearing the device around his waist, falls on a mattress. Note that when a fall on a mattress is detected, a fall on a hard floor would certainly be detected as the acceleration at the moment of impact is certainly higher. During these measurements, the accelerometer measures negative values along the Y-axis, as shown in Figure 3.10. The MCU reads the accelerometer samples at a sample interval of 200 Hz and continuously transfers them to a PC used for data collection. Note that this is only necessary for the

analysis and is not required in the actual application. The accelerometer was initialised to operate within a range of ± 4 g and the integrated low-pass filtering was selected. Before sampling, inline accelerometer calibration [85] was performed according to the start-up procedure described by the manufacturer.

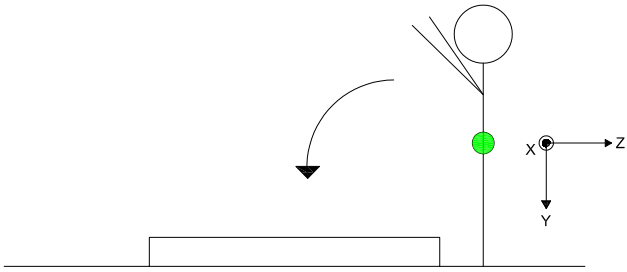

Figure 3.10: Graphical representation of the measurement setup: a person, approximately 1.8 m *tall and wearing the wearable with integrated accelerometer around the waist, is falling forward on a mattress. The orientation of the accelerometer's axes is visualised.*

3.4.2 Fall

Multiple simulations are performed, to obtain the best sample rate for both detection branches, as well as the optimal buffer size and threshold values. The first parameter is the sample rate. Research proposed in [29, 32, 33] suggests a sample interval of 20 ms. However, taking into account that the peak of the fall only exists for approximately 50 ms, we decided to sample at a higher interval of 5 ms.

In Section 3.3.2, Figure 3.7 illustrated the measured fall at a sample interval of 5 ms or a sample rate of 200 Hz. The peak consisted of multiple samples above 3 g, which clearly illustrated that the peak cannot be missed at this sample rate.

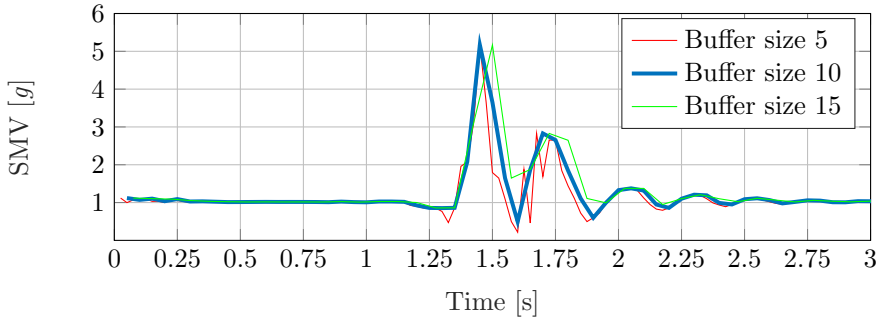

Figure 3.11: Maximum filtered SMV data for a buffer size of 10 *samples of the fall measured in Figure 3.7. The results approach the theoretical fall profile.*

The next parameter is the buffer size of the filter that determines the maximum SMV. A buffer size of 5 will lower the detection time but will increase the noise of the measurement. Utilising a buffer size of 15 will slow down the detection time but has a large influence on the noise filtering. A buffer size of 10 clearly provides the best result, approaching the theoretical fall profile as illustrated earlier in Figure 3.7, preserving the important information while at the same time reducing noise in the measurement. The result of filtering the measurement accordingly is displayed in Figure 3.11.

The last parameter is the threshold value that triggers an alert. From research performed in [70], we know that, while ascending or descending stairs, the SMV will never reach a peak as high as 1.7 *g*. Note that in nursing homes the elderly will generally not even use staircases.

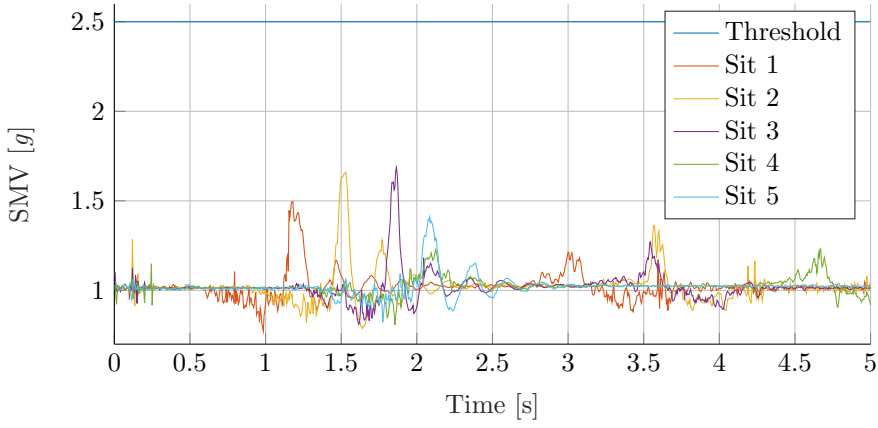

Figure 3.12: Graphical representation of five sit events measured at a sample interval of 5 ms

Measurements were also performed to assess the SMV values when an elderly person falls back in a seat. The measurement setup was as described before, but now the test person was standing in front of a seat, 'fell' into the seat and stood up again. Figure 3.12 illustrates five measured 'sit events' sampled at a rate of 200 Hz. As is shown in the graphs, the sit events did not cause any accelerations above 1.7 g whereas potential harmful fall events easily cause accelerations above a threshold of 2.5 g. This threshold value is chosen at a level that guarantees detection of dangerous fall events, while at the same time avoiding false alerts due to other harmless events.

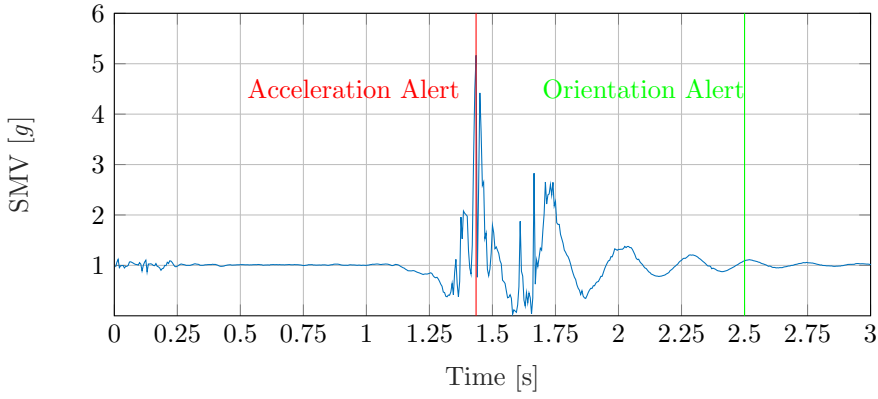

Figure 3.13: Results of the final algorithm applied to the fall from Figure 3.7, which was measured at a sample interval of 5 ms. *The red vertical line represents the acceleration alert and the green vertical line the orientation alert. Since both alerts are set, this is a confirmed fall event.*

After determining the optimal parameter values, we combined the acceleration and orientation branches. Figure 3.13 illustrates the complete algorithm applied to a fall measured at a sample interval of 5 ms. It can be seen that around 1.4 s the acceleration alert flag is set. When taking a closer look, this flag is set at the peak of the fall, which proves the effectiveness of the acceleration detection. After a delay of 1.1 s, this fall is confirmed by the difference in spatial orientation, as can be seen in Figure 3.8. The confirmed fall alert will be sent at 2.5 s.

3.4.3 Validation with open-source dataset

To verify the algorithm, we have selected three online fall detection databases. The first dataset is the SisFall dataset [79]. This dataset was created in 2017 and contains accelerometer data of two different accelerometer and gyroscope data from units mounted at waist level. This dataset was created

with 38 subjects ranging from young to old, the adults/elderly (>60 year) distribution is 23/15. Furthermore, it contains 34 ADL/falls that were repeated 1 or 5 times. In total, this dataset contains two times 4500 ADL/fall events.

Table 3.1: Summary of the test subjects used in three datasets.

	Subjects	**Age [yrs]**	**Weight [kg]**	**Height [cm]**	**Gender [M/F]**
SisFall (2017)	38	[22-70]	[51-142,9]	[152-188]	19/19
FALLAIID (2021)	15	[21-53]	[48-85]	[158-187]	8/7
KFall (2021)	32	[21-29]	[60-79]	[168-180]	32/0

The second dataset is the FallAIID dataset [80], which contains accelerometer, gyroscope, magnetometer, temperature and barometer data measured around the waist, neck and right hand. The 15 test subjects range from young to elderly adults, with 44/35 ADLs/falls at variable times per ADL/Fall. In total, this dataset contains 4760 ADL/Fall events. The third dataset, KFall [81] contains accelerometer, gyroscope and magnetometer data captured also at waist level. It is based on 32 young male test subjects performing 36 ADLs/falls variable times per ADL/fall. In total, this dataset contains 5075 ADL/Fall events. A summary of the test subjects and ADLs/Falls per dataset can be found in Table 3.1 and Table 3.2, respectively.

Table 3.2: Summary of the ADL/falls per dataset.

	Position	**Times repeated**	**ADL/Falls**	**Total events**
SisFall (2017)	Waist	1 or 5	19/15	4500×2
FALLAIID (2021)	Waist, neck, right hand	Variable	44/35	4760
KFall (2021)	waist	Variable	21/15	5075

Since the data in these datasets is captured with different accelerometers and since test subjects are falling in a different way with sometimes less representative falls, some parameter values of the proposed rule based algorithm need to be adjusted. The first adjustment is the amplitude threshold.

Since some measured ADL/Fall datasets contain more noise than others, it is important to set the threshold level above the noise level in order to suppress false alerts. To find the best suitable threshold, the histogram gives the maximum value of an ADL/fall event for each database, as can be seen in Figure 3.14. From this figure, it can be concluded that a threshold between 2 and 3 g suppresses most noise and will result in good performance of the algorithm.

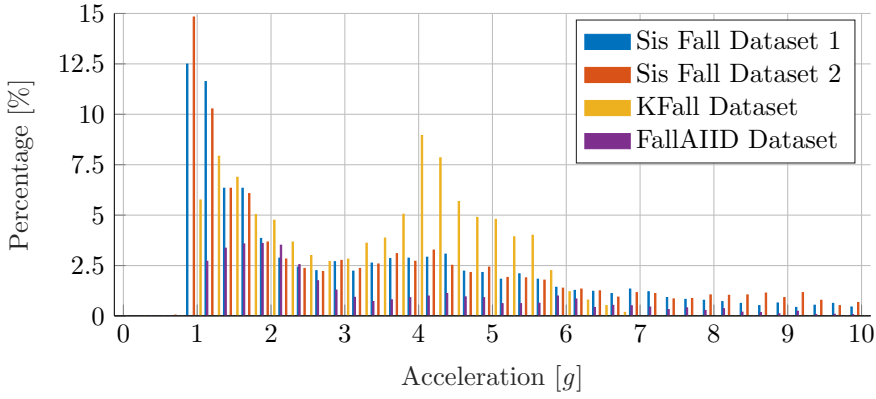

Figure 3.14: Calculated histogram of the maximum values of each event in the dataset.

Figure 3.15 illustrates the results of the proposed algorithm for different amplitude thresholds ranging from 1.75 to 3.5 g in steps of 0.25 g, with a constant timeslot of 1 s and an orientation threshold of 45°. It can be concluded that a threshold of 2.5 g gives the best F_1-score for each dataset, proving that the previously chosen threshold performs well.

Second, we considered the orientation threshold. During extensive testing, it appeared as if some test subjects did not wear the accelerometer unit tight enough to the body. In these situations, where a person fell when trying to sit or stand up from a chair, the recorded orientation differences in the database are smaller than what is realistically possible. In order to compensate for this underestimation, the threshold was lowered to 45° instead of 60°.

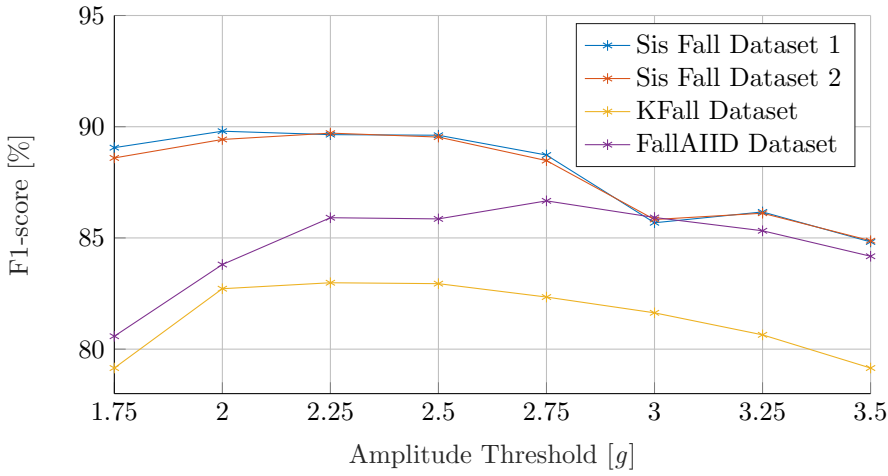

Figure 3.15: Results of the amplitude range simulations of the proposed algorithm.

A final adjustment is the timeslot. To have a clear distinction between a fall and for example a forward jump, the timeslot is increased. In this way, the algorithm is prevented from calculating the orientation difference during the fall or jumping. Table 3.3 gives a short overview of the parameters that were changed for each dataset. The amplitude threshold differs per dataset since this gives us the best result for each dataset. Setting this threshold to the same value results in a minor difference in F_1-score, as can be seen in Figure 3.15.

Table 3.3: Summary of the adjusted parameters for each dataset.

	Paper	**SisFall (2017)**	**FALLAIID (2021)**	**KFall (2021)**
Sample rate	5 ms	5 ms	4.2 ms	10 ms
Amplitude threshold	2.5 g	2 g	2.75 g	2.5 g
Orientation threshold	60°	45°	45°	45°
Timeslot	0.25 s	1 s	1 s	1 s

Table 3.4 represents the accuracy, precision, sensitivity and F_1-score of the developed algorithm applied to all three datasets. It results in an accuracy in the range of 84.89 % to 92.65 %, representing the percentage of

correct decisions. A precision in a range of 81.87 % to 87.01 % is obtained, representing the ratio of true fall detections over all fall detections. A sensitivity in the range of 80.66 % to 92.77 % is observed, corresponding to the ratio of correct fall detections to the number of actual falls events. Based on these values, the F_1-scores are in a range of 82.94 % to 89.8 %, confirming the reliability of the algorithm. One must take into account that these datasets also contain ADLs such as jogging and jumping. These can trigger false alerts in some situations, even though they do not occur often in the lives of the elderly.

Table 3.4: Summary of the obtained accuracy, Precision, sensitivity and F_1-score for the proposed algorithm per datasets.

	SisFall (2017)		**FALLAIID (2021)**	**KFall (2021)**
Accuracy	91.58 %	91.27 %	92.65 %	84.89 %
Precision	87.01 %	86.61 %	81.87 %	85.35 %
Sensitivity	92.77 %	92.44 %	92.06 %	80.66 %
F_1**-score**	89.80 %	89.43 %	86.66 %	82.94 %

Table 3.5 also shows the performance of the CNN algorithm in terms of accuracy, precision, sensitivity and F_1-score. The algorithm was trained on 70 % training data and tested and validated on the 15 % data for each dataset. There can be stated that the results are higher than the results from the proposed rule based algorithm (Table 3.4), but at a much higher power consumption. Furthermore, it can be stated that CNN is very data dependent. When the CNN is trained on both SisFall datasets and KFall, and later validated on FALLAIID, we get an accuracy of 90.32 %, a precision of 73.40 %, a sensitivity of 87.24 % and an F_1-score of 79.72 %.

Table 3.5: Summary of the CNN algorithm for each dataset. The CNN was trained on 70 % data, validated on 15 % and tested on 15 % of each dataset.

	SisFall (2017)		**FALLAIID (2021)**	**KFall (2021)**
Accuracy	95.85 %	96.07 %	94.44 %	93.44 %
Precision	95.38 %	93.28 %	84.48 %	93.43 %
Sensitivity	94.34 %	96.98 %	89.09 %	93.30 %
F_1**-score**	94.86 %	95.09 %	86.72 %	93.36 %

However, CNN also exhibits some drawbacks: a) it requires training and b) it consumes more resources while executing on embedded platforms as compared to the rule-based algorithm. Due to the advancement of ML

on embedded platforms, the second problem can be alleviated, since now procedures exist for generating light weight models including Tensorflow libraries such as Tensorflow Lite and TensorRT. The aim of this system is only to identify 'Fall' and 'No Fall' events and in this case the proposed algorithm performs similar than the CNN algorithm because a) it provides higher accuracy, b) there is no need for training and c) it yields a light weight algorithm. However, if the goal is to identify other 'Fall' and 'No Fall' events such as walking, standing and picking up objects, then developing a rule-based algorithm for such a case would be extremely difficult or rather impossible. In that case, ML would be a nice alternative, because it does not require development of such rules but rather a CNN must be trained by a labelled data set and a similar performance as for a rule-based algorithm can be expected.

3.5 Power management

In a wearable device, the battery lifetime is an important property. When the elderly person is walking around, the MCU and the accelerometer will be in *active mode* and consume power to perform the programmed tasks. Utilising the *no-motion interrupt* of the accelerometer, the MCU is put in a *deep sleep mode*, which dramatically decreases the consumed power. To wake-up the MCU when the person is walking again, the *High-g interrupt* of the accelerometer is used. To lower the power consumption even more, the accelerometer will be put in a *low-power mode*, for example when the elderly person goes to bed and is sleeping for multiple hours. Based on information from a local nursing home for the elderly person, the following scenario is proposed in Table 3.6.

When both MCU and the accelerometer are in active mode, there is an energy consumption corresponding to a hourly charge of 0.45 mAh. Putting the MCU in deep sleep mode decreases the daily required battery charge to 0.13 mAh. When the MCU is in deep sleep mode and the accelerometer is in low-power mode, the total required charge is 7.9 μAh. Taking these consumptions into account, the total required charge for this scenario per day is 2.27 mAh.

Furthermore, the wearable is programmed to send a 'standby' signal every 15 minutes in order to inform the system that the wearable is still active. One such message consists of five subsequent advertisement packets in order to assure proper detection by the system. The 5 packets are sent at a TX-level of 1 mW, which results in a series of peak currents of 9 mA during approximately 20 ms for each message [65]. In a worst-case scenario, the elderly person falls once a day, which results in another five current

Table 3.6: Proposed scenario for a day of an elderly person in a nursing home, based on information from a local home.

Time	**Activity**	**Micro-controller mode**	**Accelero-meter mode**
8:00 - 8:30	Wake-up, get dressed and walking towards the kitchen for breakfast	Active	Active
8:30 - 9:30	Having breakfast and socialising with other residents	Deep Sleep	Active
9:30 - 9:35	Walking towards the garden, room or recreation centre	Active	Active
9:35 - 12:00	Enjoying the moment	Deep Sleep	Active
12:00 - 12:05	Walking towards the kitchen for lunch	Active	Active
12:05 - 13:05	Having lunch and socialising with other residents	Deep Sleep	Active
13:05 - 13:10	Walking towards room	Active	Active
13:10 - 14:30	Sleeping	Deep Sleep	Active
14:30 - 14:35	Walking towards the garden, room or recreation centre	Active	Active
14:35 - 17:30	Enjoying the moment	Deep Sleep	Active
17:30 - 17:35	Walking towards the kitchen for dinner	Active	Active
17:35 - 18:35	Having dinner and socialising with the other residents	Deep Sleep	Active
18:35 - 18:40	Walking back to the room	Active	Active
18:40 - 21:00	Sitting or lying down in bed watching TV	Deep Sleep	Active
21:00 - 22:30	Sleeping (time needed to detect elderly person is sleeping)	Deep Sleep	Active
22:30 - 8:00	Sleeping	Deep Sleep	Low Power

peaks of 9 mA during 20 ms for each message.

Taking all of these parameters into account and using a 3 V CR2032 battery with a capacity of 230 mAh, this results in a battery lifetime of 100 days. The CR2032 was chosen for reasons of compactness and ease of use during development. In this way, we meet the third and fourth design requirement. A larger (rechargeable) cell can always be used if a longer autonomy is preferred. As an example, applying a CR2477N 3 V Lithium Battery with a capacity of 950 mAh would extend the autonomy to more than 414 days maximum. The self-discharge of these lithium-ion batteries is not taken into account, since this is approximately 2 % per year. Therefore, we state that this is neglectable.

3.6 Conclusion

This chapter describes the design of a wearable fall detection sensor for the elderly based on BLE wireless communication, providing excellent room coverage at low energy consumption. The wearable relies on a three-axis accelerometer to find the peak of the fall as well as the change in spatial orientation. This change in spatial orientation is used as a fall confirmation signal. A false detection resulting in a confirmed fall alert is virtually impossible with this approach.

The system is designed, implemented and validated by means of a measurement campaign. In order to assess sensitivity and selectivity, not only fall events were measured but also other harmless conditions causing fairly large accelerations, such as 'falling' into a seat.

Based on the measurement results, realistic parameters were chosen for the algorithms, of which the most important are the threshold values of 2.5 g and 60° for the acceleration and orientation change, respectively. A sample rate of 5 ms was chosen in order to surely capture all relevant details of each fall event.

A validation of the algorithm was performed using three open-source databases containing data for 85 persons, performing 18 835 ADL or fall activities. These fall activities include falling from different starting positions (forward fall, falling while standing up or sitting down, etc.). Based on these data, the algorithm obtained an F_1 score in a range of 82.94 % to 89.8 %, confirming its reliability and illustrating that the first and second design requirements are met. In addition, the proposed rule-based algorithm is compared to ML using CNN. The results show that the CNN algorithm yields an F_1 performance in a range of 86.72 % to 95.09 %, which is comparable to the proposed rule-based algorithm. This way the first and second design requirement are met.

The proposed wearable provides reliable fall detection, without false acceleration alerts (level 1). The orientation confirmation system provides a second, independent variable, making false (level 2) confirmed positives extremely unlikely. The proposed unobtrusive wearable system fits in a $32 \times 23 \times 10\,\text{mm}$ package and autonomously performs measurements as well as communication employing state of the art wireless technology. The system is energy efficient and achieves an autonomy of 100 days on a standard CR2032 coin-cell battery. In this way, the third and fourth design requirement are also met.

3.7 Funding Statement

This work was supported in part by the Research Foundation—Flanders (FWO) through the "MUlti-SErvice WIreless NETwork," FWO/FRS Excellence of Science (EOS) Project and the Erasmus+ programme of the European Union through the "Capacity building for Digital Health Monitoring and Care Systems in Asia (DigiHealth-Asia), 2021-2024" project.

References

[1] World Health Organization. *Number of People over 60 Years set to Double by 2050; Major Societal Changes Required.* https://www.who.int/mediacentre/news/releases/2015/older-persons-day/en/. Accessed on October 18, 2022.

[2] World Health Organization. *World Health Organization Global Report on Falls Prevention in Older Age 2007.* https://extranet.who.int/agefriendlyworld/wp-content/uploads/2014/06/WHo-Global-report-on-falls-prevention-in-older-age.pdf. Accessed on October 18, 2022.

[3] World Health Organization. *Falls Prevention in Older Age.* https://www.who.int/ageing/projects/falls_prevention_older_age/en/. Accessed on October 18, 2022.

[4] S. R. Lord, A. Tiedemann, K. Chapman, B. Munro, S. M. Murray, M. Gerontology, G. R. Ther, and C. Sherrington. *The Effect of an Individualized Fall Prevention Program on Fall Risk and Falls in Older People: A Randomized, Controlled Trial.* Journal of the American Geriatrics Society, 53(8):1296–1304, 8 2005. Available from: https://doi.org/10.1111/j.1532-5415.2005.53425.x, doi:10.1111/j.1532-5415.2005.53425.x.

[5] B. Røyset, B. A. Talseth-Palmer, S. Lydersen, and P. G. Farup. *Effects of a Fall Prevention Program in Elderly: a Pragmatic Observational Study in Two Orthopedic Departments.* Clin Interv Aging, 14:145–154, 1 2019. doi:https://doi.org/10.2147/CIA.S191832.

[6] C. S. Florence, G. Bergen, A. Atherly, E. Burns, J. Stevens, and C. Drake. *Medical Costs of Fatal and Nonfatal Falls in Older Adults.* Journal of the American Geriatrics Society, 66(4):693–698, 3 2018. Available from: https://doi.org/10.1111/jgs.15304, doi:10.1111/jgs.15304.

[7] M. Woolley. *Bluetooth Core Specification v5.1.* Bluetooth Special Interest Group, 2019. Accessed on October 18, 2022.

[8] A. Makhlouf, I. Boudouane, N. Saadia, and A. R. Cherif. *Ambient Assistance Service for Fall and Heart Problem Detection.* Journal of Ambient Intelligence and Humanized Computing, 10(4):1527–1546, 2 2018. Available from: https://doi.org/10.1007/s12652-018-0724-4, doi:10.1007/s12652-018-0724-4.

[9] L. Ren and Y. Peng. *Research of Fall Detection and Fall Prevention Technologies: A Systematic Review.* IEEE Access, 7:77702–77722, 2019. Available from: https://doi.org/10.1109/access.2019.2922708, doi:10.1109/access.2019.2922708.

[10] M. Mubashir, L. Shao, and L. Seed. *A Survey on Fall Detection: Principles and Approaches.* Neurocomputing, 100:144–152, 1 2013. Available from: https://doi.org/10.1016/j.neucom.2011.09.037, doi:10.1016/j.neucom.2011.09.037.

[11] X. Wang, J. Ellul, and G. Azzopardi. *Elderly Fall Detection Systems: A Literature Survey.* Frontiers in Robotics and AI, 7:71, 2020. Available from: https://www.frontiersin.org/article/10.3389/frobt.2020.00071, doi:10.3389/frobt.2020.00071.

[12] G. Koshmak, A. Loutfi, and M. Linden. *Challenges and Issues in Multisensor Fusion Approach for Fall Detection: Review Paper.* Journal of Sensors, 2016:1–12, 2016. Available from: https://doi.org/10.1155/2016/6931789, doi:10.1155/2016/6931789.

[13] T. Xu, Y. Zhou, and J. Zhu. *New Advances and Challenges of Fall Detection Systems: A Survey.* Applied Sciences, 8(3):418, March 2018. Available from: https://doi.org/10.3390/app8030418, doi:10.3390/app8030418.

[14] S. Nooruddin, M. M. Islam, F. A. Sharna, H. Alhetari, and M. N. Kabir. *Sensor-Based Fall Detection Systems: a Review.* Journal of Ambient Intelligence and Humanized Computing, April 2021. Available from: https://doi.org/10.1007/s12652-021-03248-z, doi:10.1007/s12652-021-03248-z.

[15] C. Vishnu, R. Datla, D. Roy, S. Babu, and C. K. Mohan. *Human Fall Detection in Surveillance Videos Using Fall Motion Vector Modeling.* IEEE Sensors Journal, 21(15):17162–17170, August 2021. Available from: https://doi.org/10.1109/jsen.2021.3082180, doi:10.1109/jsen.2021.3082180.

[16] J. Gutiérrez, V. Rodríguez, and S. Martin. *Comprehensive Review of Vision-Based Fall Detection Systems.* Sensors, 21(3):947, February 2021. Available from: https://doi.org/10.3390/s21030947, doi:10.3390/s21030947.

[17] X. Kong, L. Chen, Z. Wang, Y. Chen, L. Meng, and H. Tomiyama. *Robust Self-Adaptation Fall-Detection System Based on Camera Height.*

Sensors, 19(17), 2019. Available from: https://www.mdpi.com/1424-8220/19/17/3768, doi:10.3390/s19173768.

[18] W.-Y. Cai, J.-H. Guo, M.-Y. Zhang, Z.-X. Ruan, X.-C. Zheng, and S.-S. Lv. *GBDT-Based Fall Detection with Comprehensive Data from Posture Sensor and Human Skeleton Extraction.* Journal of Healthcare Engineering, 2020:1–15, June 2020. Available from: https://doi.org/10.1155/2020/8887340, doi:10.1155/2020/8887340.

[19] J. R. T. Neto, G. P. R. Filho, L. Y. Mano, L. A. Villas, and J. Ueyama. *Exploiting Offloading in IoT-Based Microfog: Experiments with Face Recognition and Fall Detection.* Wireless Communications and Mobile Computing, 2019:1–13, May 2019. Available from: https://doi.org/10.1155/2019/2786837, doi:10.1155/2019/2786837.

[20] E. Minguez and M. Faundez-Zanuy. *Low Cost Fall Detection Based on Cortex M4.* In 2019 42nd International Conference on Telecommunications and Signal Processing (TSP). IEEE, 7 2019. Available from: https://doi.org/10.1109/tsp.2019.8769065, doi:10.1109/tsp.2019.8769065.

[21] M. Alwan, P. J. Rajendran, S. Kell, D. Mack, S. Dalal, M. Wolfe, and R. Felder. *A Smart and Passive Floor-Vibration Based Fall Detector for Elderly.* In 2006 2nd International Conference on Information Communication Technologies, volume 1, pages 1003–1007, 2006.

[22] G. Feng, J. Mai, Z. Ban, X. Guo, and G. Wang. *Floor Pressure Imaging for Fall Detection with Fiber-Optic Sensors.* IEEE Pervasive Computing, 15(2):40–47, 2016. doi:10.1109/MPRV.2016.27.

[23] A. M. Tabar, A. Keshavarz, and H. Aghajan. *Smart Home Care Network Using Sensor Fusion and Distributed Vision-Based Reasoning.* In Proceedings of the 4th ACM International Workshop on Video Surveillance and Sensor Networks, VSSN '06, page 145–154, New York, NY, USA, 2006. Association for Computing Machinery. Available from: https://doi.org/10.1145/1178782.1178804, doi:10.1145/1178782.1178804.

[24] D. Martelli, F. Artoni, V. Monaco, A. M. Sabatini, and S. Micera. *Pre-Impact Fall Detection: Optimal Sensor Positioning Based on a Machine Learning Paradigm.* PLoS ONE, 9(3):e92037, 3 2014. Available from: https://doi.org/10.1371/journal.pone.0092037, doi:10.1371/journal.pone.0092037.

[25] T. Mauldin, M. Canby, V. Metsis, A. Ngu, and C. Rivera. *SmartFall: A Smartwatch-Based Fall Detection System Using Deep Learning.* Sensors, 18(10):3363, October 2018. Available from: https://doi.org/10.3390/s18103363, doi:10.3390/s18103363.

[26] A. Shahzad and K. Kim. *FallDroid: An Automated Smart-Phone-Based Fall Detection System Using Multiple Kernel Learning.* IEEE Transactions on Industrial Informatics, 15(1):35–44, 1 2019. Available from: https://doi.org/10.1109/tii.2018.2839749, doi:10.1109/tii.2018.2839749.

[27] P. Kostopoulos., T. Nunes., K. Salvi., M. Deriaz., and J. Torrent. *Increased Fall Detection Accuracy in an Accelerometer-based Algorithm Considering Residual Movement.* In Proceedings of the International Conference on Pattern Recognition Applications and Methods - Volume 2: ICPRAM,, pages 30–36. INSTICC, SciTePress, 2015. doi:10.5220/0005179100300036.

[28] G. B. Huq, J. Basilakis, and A. Maeder. *Evaluation of Tri-Axial Accelerometery Data of Falls for Elderly through Smart Phone.* In Proceedings of the Australasian Computer Science Week Multiconference, ACSW '16, Canberra, Australia, 2016. Association for Computing Machinery. Available from: https://doi.org/10.1145/2843043.2843385, doi:10.1145/2843043.2843385.

[29] S. Khojasteh, J. Villar, C. Chira, V. González, and E. de la Cal. *Improving Fall Detection Using an On-Wrist Wearable Accelerometer.* Sensors, 18(5):1350, April 2018. Available from: https://doi.org/10.3390/s18051350, doi:10.3390/s18051350.

[30] Y. Su, D. Liu, and Y. Wu. *A Multi-Sensor based Pre-Impact Fall Detection System with a Hierarchical Classifier.* In 2016 9th International Congress on Image and Signal Processing, BioMedical Engineering and Informatics (CISP-BMEI). IEEE, 10 2016. Available from: https://doi.org/10.1109/cisp-bmei.2016.7852995, doi:10.1109/cisp-bmei.2016.7852995.

[31] D. Ajerla, S. Mahfuz, and F. Zulkernine. *A Real-Time Patient Monitoring Framework for Fall Detection.* Wireless Communications and Mobile Computing, 2019:1–13, 9 2019. Available from: https://doi.org/10.1155/2019/9507938, doi:10.1155/2019/9507938.

[32] A. Shahzad, S. Ko, S. Lee, J.-A. Lee, and K. Kim. *Quantitative Assessment of Balance Impairment for Fall-Risk Estimation Using Wearable Triaxial Accelerometer.* IEEE Sensors Journal, 17(20):6743–6751,

10 2017. Available from: https://doi.org/10.1109/jsen.2017.2749446, doi:10.1109/jsen.2017.2749446.

[33] Y. Liu, S. J. Redmond, T. Shany, J. Woolgar, M. R. Narayanan, S. R. Lord, and N. H. Lovell. *Validation of an Accelerometer-Based Fall Prediction Model.* In 2014 36th Annual International Conference of the IEEE Engineering in Medicine and Biology Society. IEEE, 8 2014. Available from: https://doi.org/10.1109/embc.2014.6944631, doi:10.1109/embc.2014.6944631.

[34] F. Luna-Perejón, M. J. Domínguez-Morales, and A. Civit-Balcells. *Wearable Fall Detector Using Recurrent Neural Networks.* Sensors, 19(22):4885, 11 2019. Available from: https://doi.org/10.3390/s19224885, doi:10.3390/s19224885.

[35] E. Casilari, R. Lora-Rivera, and F. García-Lagos. *A Study on the Application of Convolutional Neural Networks to Fall Detection Evaluated with Multiple Public Datasets.* Sensors, 20(5):1466, 3 2020. Available from: https://doi.org/10.3390/s20051466, doi:10.3390/s20051466.

[36] L. Palmerini, J. Klenk, C. Becker, and L. Chiari. *Accelerometer-Based Fall Detection Using Machine Learning: Training and Testing on Real-World Falls.* Sensors, 20(22), 2020. Available from: https://www.mdpi.com/1424-8220/20/22/6479, doi:10.3390/s20226479.

[37] G. Santos, P. Endo, K. Monteiro, E. Rocha, I. Silva, and T. Lynn. *Accelerometer-Based Human Fall Detection Using Convolutional Neural Networks.* Sensors, 19(7):1644, April 2019. Available from: https://doi.org/10.3390/s19071644, doi:10.3390/s19071644.

[38] N. Liu, D. Zhang, Z. Su, and T. Wang. *Preimpact Fall Detection for Elderly Based on Fractional Domain.* Mathematical Problems in Engineering, 2021:1–17, February 2021. Available from: https://doi.org/10.1155/2021/6661034, doi:10.1155/2021/6661034.

[39] S. B. Kwon, J.-H. Park, C. Kwon, H. J. Kong, J. Y. Hwang, and H. C. Kim. *An Energy-Efficient Algorithm for Classification of Fall Types Using a Wearable Sensor.* IEEE Access, 7:31321–31329, 2019. Available from: https://doi.org/10.1109/access.2019.2902718, doi:10.1109/access.2019.2902718.

[40] M. C. Gilly and V. A. Zeithaml. *The Elderly Consumer and Adoption of Technologies.* Journal of Consumer Research, 12(3):353, 12 1985. Available from: https://doi.org/10.1086/208521, doi:10.1086/208521.

[41] K.-C. Yang and P.-H. Shih. *Cognitive Age in Technology Acceptance: at What Age are People Ready to Adopt and Continuously Use Fashionable Products?* Telematics and Informatics, 51:101400, 8 2020. Available from: https://doi.org/10.1016/j.tele.2020.101400, doi:10.1016/j.tele.2020.101400.

[42] A. Ramachandran and A. Karuppiah. *A Survey on Recent Advances in Wearable Fall Detection Systems.* BioMed Research International, 2020:1–17, January 2020. Available from: https://doi.org/10.1155/2020/2167160, doi:10.1155/2020/2167160.

[43] T. Tamura, T. Yoshimura, M. Sekine, M. Uchida, and O. Tanaka. *A Wearable Airbag to Prevent Fall Injuries.* IEEE Transactions on Information Technology in Biomedicine, 13(6):910–914, 2009.

[44] J. Chen, K. Kwong, D. Chang, J. Luk, and R. Bajcsy. *Wearable Sensors for Reliable Fall Detection.* In 2005 IEEE Engineering in Medicine and Biology 27th Annual Conference, pages 3551–3554, 2005.

[45] F. Wu, H. Zhao, Y. Zhao, and H. Zhong. *Development of a Wearable-Sensor-Based Fall Detection System.* International Journal of Telemedicine and Applications, 2015:1–11, 2015. Available from: https://doi.org/10.1155/2015/576364, doi:10.1155/2015/576364.

[46] T. N. Gia, V. K. Sarker, I. Tcarenko, A. M. Rahmani, T. Westerlund, P. Liljeberg, and H. Tenhunen. *Energy Efficient Wearable Sensor Node for IoT-Based Fall Detection Systems.* Microprocessors and Microsystems, 56:34–46, February 2018. Available from: https://doi.org/10.1016/j.micpro.2017.10.014, doi:10.1016/j.micpro.2017.10.014.

[47] P. Fino, C. Frames, and T. Lockhart. *Classifying Step and Spin Turns Using Wireless Gyroscopes and Implications for Fall Risk Assessments.* Sensors, 15(5):10676–10685, 5 2015. Available from: https://doi.org/10.3390/s150510676, doi:10.3390/s150510676.

[48] A. Bourke and G. Lyons. *A Threshold-Based Fall-Detection Algorithm Using a Bi-Axial Gyroscope Sensor.* Medical Engineering & Physics, 30(1):84–90, 1 2008. Available from: https://doi.org/10.1016/j.medengphy.2006.12.001, doi:10.1016/j.medengphy.2006.12.001.

[49] O. Almeida, M. Zhang, and J.-C. Liu. *Dynamic Fall Detection and Pace Measurement in Walking Sticks.* In 2007 Joint Workshop on High Confidence Medical Devices, Software, and Systems and Medical Device Plug-and-Play Interoperability (HCMDSS-MDPnP 2007). IEEE,

6 2007. Available from: https://doi.org/10.1109/hcmdss-mdpnp.2007.28, doi:10.1109/hcmdss-mdpnp.2007.28.

[50] E. Casilari, M. Álvarez-Marco, and F. García-Lagos. *A Study of the Use of Gyroscope Measurements in Wearable Fall Detection Systems.* Symmetry, 12(4):649, April 2020. Available from: https://doi.org/10.3390/sym12040649, doi:10.3390/sym12040649.

[51] S.-L. Hsieh, C.-C. Chen, S.-H. Wu, and T.-W. Yue. *A Wrist -Worn Fall Detection System using Accelerometers and Gyroscopes.* In Proceedings of the 11th IEEE International Conference on Networking, Sensing and Control, pages 518–523, 2014. doi:10.1109/ICNSC.2014.6819680.

[52] F.-T. Wang, H.-L. Chan, M.-H. Hsu, C.-K. Lin, P.-K. Chao, and Y.-J. Chang. *Threshold-Based Fall Detection using a Hybrid of Tri-Axial Accelerometer and Gyroscope.* Physiological Measurement, 39(10):105002, October 2018. Available from: https://doi.org/10.1088/1361-6579/aae0eb, doi:10.1088/1361-6579/aae0eb.

[53] Lifeline. *Medical Alert Systems for Seniors With Fall Detection.* https://www.lifeline.ca/en/about-us/fall-detection-technology-autoalert/. Accessed on October 18, 2022.

[54] Apple. *Use fall detection with Apple Watch.* https://support.apple.com/en-us/HT208944. Accessed on October 18, 2022.

[55] Owlytics Healthcare. https://www.owlytics.com/. Accessed onOctober 18, 2022.

[56] Vayyar Home. *Vayyar Home sensors.* https://vayyarhome.com/. Accessed on October 18, 2022.

[57] J. G. Argañarás, Y. T. Wong, R. Begg, and N. C. Karmakar. *State-of-the-Art Wearable Sensors and Possibilities for Radar in Fall Prevention.* Sensors, 21(20):6836, October 2021. Available from: https://doi.org/10.3390/s21206836, doi:10.3390/s21206836.

[58] HipHope Technologies. https://www.hip-hope.com/. Accessed on October 18, 2022.

[59] Bluetooth Special Interest Group. *Bluetooth Mesh Glossary of Terms.* https://www.bluetooth.com/learn-about-bluetooth/bluetooth-technology/topology-options/le-mesh/mesh-glossary/#proxy. Accessed on October 18, 2022.

[60] Bluetooth Special Interest Group. *An Introduction to the Bluetooth Mesh Proxy Function.* https://www.bluetooth.com/bluetooth-resources/bluetooth-mesh-proxy-kit/. Accessed on October 18, 2022.

[61] N. S. Suriani, F. A. N. Rashid, and N. Y. Yunos. *Optimal Accelerometer Placement for Fall Detection of Rehabilitation Patients.* Journal of Telecommunication, Electronic and Computer Engineering, 10:25–29, 2018.

[62] A. Özdemir. *An Analysis on Sensor Locations of the Human Body for Wearable Fall Detection Devices: Principles and Practice.* Sensors, 16(8):1161, 7 2016. Available from: https://doi.org/10.3390/s16081161, doi:10.3390/s16081161.

[63] P. Bulić, G. Kojek, and A. Biasizzo. *Data Transmission Efficiency in Bluetooth Low Energy Versions.* Sensors, 19(17):3746, 8 2019. Available from: https://doi.org/10.3390/s19173746, doi:10.3390/s19173746.

[64] Bluetooth Special Interest Group. *Bluetooth Generic Attributes.* https://www.bluetooth.com/specifications/gatt/. Accessed on October 18, 2022.

[65] Silicon Laboratories. *BGM13P Blue Gecko Bluetooth Module Data Sheet.* https://www.silabs.com/documents/public/data-sheets/bgm13p-datasheet.pdf, 2019. Accessed on October 18, 2022.

[66] ARM. https://www.arm.com/products/silicon-ip-cpu. Accessed on October 18, 2022.

[67] TAG Connect. *TAG Connect.* http://www.tag-connect.com/. Accessed on October 18, 2022.

[68] Silicon Laboratories. *Programming Internal Flash Over the Serial Wire Debug Interface.* https://www.silabs.com/documents/public/application-notes/an0062.pdf. Accessed on October 18, 2022.

[69] Bosch. *Accelerometer sensor BMA280.* https://www.bosch-sensortec.com/products/motion-sensors/accelerometers/bma280.html. Accessed on October 18, 2022.

[70] T. Xu, W. Sun, S. Lu, K. ming Ma, and X. Wang. *The Real-Time Elderly Fall Posture Identifying Scheme with Wearable Sensors.* International Journal of Distributed Sensor Networks, 15(11):155014771988561, 11 2019. Available from: https://doi.org/10.1177/1550147719885616, doi:10.1177/1550147719885616.

[71] E. C. Ifeachor and B. W. Jervis. *Digital Signal Processing: A Practical Approach.* Pearson Education, 2nd edition, 2002.

[72] M. H. Hayes. *Schaum's Outline of Digital Signal Processing.* McGraw-Hill, Inc., USA, 1st edition, 1998.

[73] C. L. Karmaker. *Determination of Optimum Smoothing Constant of Single Exponential Smoothing Method: A Case Study.* International Journal of Research in Industrial Engineering, 6(3):184–192, 2017. doi:10.22105/riej.2017.49603.

[74] D. Ciregan, U. Meier, and J. Schmidhuber. *Multi-Column Deep Neural Networks for Image Classification.* In 2012 IEEE Conference on Computer Vision and Pattern Recognition, pages 3642–3649. IEEE, 2012.

[75] T. J. O'Shea, J. Corgan, and T. C. Clancy. *Convolutional Radio Modulation Recognition Networks.* In C. Jayne and L. Iliadis, editors, Engineering Applications of Neural Networks, pages 213–226, Cham, 2016. Springer International Publishing.

[76] J. Fontaine, E. Fonseca, A. Shahid, M. Kist, L. A. DaSilva, I. Moerman, and E. De Poorter. *Towards Low-Complexity Wireless Technology Classification across Multiple Environments.* Ad Hoc Networks, 91:101881, 2019.

[77] A. Shahid, J. Fontaine, M. Camelo, J. Haxhibeqiri, M. Saelens, Z. Khan, I. Moerman, and E. De Poorter. *A Convolutional Neural Network Approach for Classification of LPWAN Technologies: Sigfox, LoRa and IEEE 802.15. 4G.* In 2019 16th Annual IEEE International Conference on Sensing, Communication, and Networking (SECON), pages 1–8. IEEE, 2019.

[78] M. Camelo, A. Shahid, J. Fontaine, F. A. P. de Figueiredo, E. De Poorter, I. Moerman, and S. Latre. *A Semi-Supervised Learning Approach Towards Automatic Wireless Technology Recognition.* In 2019 IEEE International Symposium on Dynamic Spectrum Access Networks (DySPAN), pages 1–10. IEEE, 2019.

[79] A. Sucerquia, J. D. López, and J. F. Vargas-Bonilla. *SisFall: A Fall and Movement Dataset.* Sensors, 17(1), 2017. Available from: https://www.mdpi.com/1424-8220/17/1/198, doi:10.3390/s17010198.

[80] M. Saleh, M. Abbas, and R. B. Le Jeannès. *FallAllD: An Open Dataset of Human Falls and Activities of Daily Living for Classical and Deep*

Learning Applications. IEEE Sensors Journal, 21(2):1849–1858, 2021. doi:10.1109/JSEN.2020.3018335.

[81] X. Yu, J. Jang, and S. Xiong. *A Large-Scale Open Motion Dataset (KFall) and Benchmark Algorithms for Detecting Pre-impact Fall of the Elderly Using Wearable Inertial Sensors*. Frontiers in Aging Neuroscience, 13:399, 2021. Available from: https://www.frontiersin.org/article/10.3389/fnagi.2021.692865, doi:10.3389/fnagi.2021.692865.

[82] imec. *imec testbed*. https://doc.ilabt.imec.be/ilabt/virtualwall/. Accessed on October 18, 2022.

[83] Keras. *Keras*. https://keras.io/. Accessed on October 18, 2022.

[84] Tensorflow. *Tensorflow*. https://www.tensorflow.org/. Accessed on October 18, 2022.

[85] Bosch. *Multiple Acceleration Sensors - Inline calibration*. https://www.bosch-sensortec.com/media/boschsensortec/downloads/application_notes_1/bst-mas-an030.pdf. Accessed on October 18, 2022.

4

Bluetooth Low Energy based Power Efficient WSN for Industrial IoT Train Integrity Monitoring

Nick De Raeve, Jo Verhaevert, Patrick Van Torre, Frederick Ronse and Hendrik Rogier

Accepted by IEEE 2022 7th International Conference on Smart and Sustainable Technologies (SpliTech), Jul 2022.

⋆⋆⋆

Monitoring train integrity is a very important topic for economical, management and safety reasons. Knowing the localization, volume and other parameters is very valuable for most train and large industry companies. Current literature focuses on placing many sensors in a Wireless Sensor Network (WSN) around the train wagons, but do not take battery lifetime into perspective. With the increasing interest in industrial Internet of Things (IoT) applications, the connectivity and battery lifetime are very important parameters. In this chapter, the vibrations measured on train wagons are analysed in order to find the most optimal trigger point to wake up or to put the WSN in a deep sleep mode. This way, a large amount of power can be saved and extend the battery lifetime significantly. Fur-

thermore, several Received Signal Strength Indicator (RSSI) measurements were performed to find the optimal Tx level and antenna topology for communication between different wireless sensor nodes on the train wagon. The proposed measurements show that an inexpensive accelerometer and a prefabricated antenna are perfectly usable in the WSN. RF measurements on the brakes results in an average Package Receive Rate (PRR) of approximately 92 % *and an Average Received Power (ARP) of around* −83 dBm *starting from a Tx level of* 4 dBm*.*

4.1 Introduction

Monitoring Train Integrity (TI) is a very important topic for economical, management and safety reasons. Knowing where a train and/or train wagons are located, how much freight they are carrying, the condition of the brakes, etc. can save the company a lot of money. Furthermore, having a real-time track and trace of these trains and train wagon parameters will increase the ease of use and maintenance significantly.

In literature, extensive research is performed in developing Wireless Sensor Network (WSN) inside [1] and outside [2, 3] train wagons [4], based on different communication protocols [5]. A typical WSN consists of several Sensor Nodes (SNs) spread across a train wagon and transfer their data to the Central Node (CN), some of these sensors have an integrated energy harvester [6], [7]. In a later step, these WSN can be connected in an industrial Internet of Things (IoT) network. This paper describes acceleration and RF measurements performed on train wagons in an industrial environment based on Bluetooth Low Energy (BLE) [8]. The acceleration measurements are key in order to make the different SNs in the WSN more power-efficient. It is important to know when a train is moving and when it has stopped. Based on these two physical parameters, the WSN can be placed in a deep sleep mode or the SNs can be woken up and data can be transferred to a CN. RF measurements illustrate what type of antenna is ideal to deploy in this harsh RF environment, but also what Tx level is ideal to transfer the data in a power efficient way.

In Section 4.2 the different measurement setups are elaborated followed by the hardware used for these measurements. Next, in Section 4.3, measurements are described combined with a brief discussion of these results. Finally, there is a conclusion (Section 4.4) which acceleration measures can be taken and which antenna can be used at what Tx level.

4.2 Measurement Setup

4.2.1 Used hardware

All measurements were performed with the BLE development boards from Silicon Laboratories (SiLabs) containing the multiprotocol ERF32MG13 chip [9]. This System-on-Chip (SoC) contains a radio with a maximum Tx level of 19 dBm at the frequency of 2.45 GHz, consists of an on-board 32-bit, 38.4 MHz ARM Cortex M4 microcontroller (MCU) with DSP instruction set. Furthermore, this board has an integrated F-antenna and an U.FL connector. This way, other antennas can easily be connected.

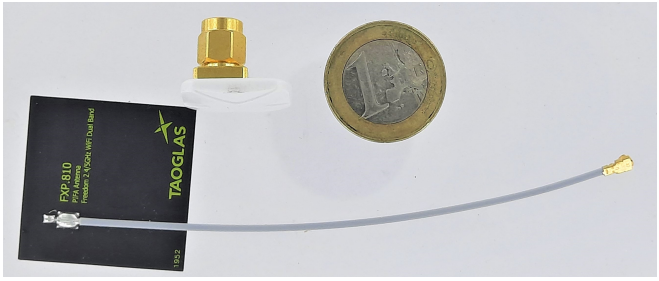

Figure 4.1: Picture of the selected antennas with on the left the patch antenna and on the top the button antenna.

For the RF measurements proposed in subsection 4.2.3, the following two antennas were selected. The first investigated antenna is a dual-band planar inverted-F antenna (PIFA) [10] with a frequency range of 2.4 GHz to 2.5 GHz and 4.9 GHz to 6 GHz, with a radiation efficiency of 76 % and 84 % and a maximum gain of 2.4 dBi and 5 dBi, respectively. This antenna is linearly polarized with an almost omnidirectional radiation pattern at 2.45 GHz, which makes it an excellent antenna for BLE. This polymer antenna has an overall size of $31 \times 31 \times 0.1$ mm, as can be seen in Figure 4.1 on the left side. We further refer to this as the *'patch'* antenna.

The second investigated antenna is also a PIFA [11] with a frequency range of 2.4 GHz to 2.5 GHz, a radiation efficiency of 30.6 % and a maximum gain of 0.4 dBi in free space. This antenna is also linear polarized with an almost omnidirectional radiation pattern at 2.45 GHz. This Acrylonitrile Butadiene Styrene (ABS) antenna has an overall size of $19.8 \times 14.3 \times 16.4$ mm, as can be seen in Figure 4.1 on the top side. We further refer to this as the *'button'* antenna. Two PIFAs where selected since this topology is easy to fabricate, they are small and have a large platform tolerance.

To perform the acceleration measurements of subsection 4.2.2, the ultra-small, low-power, triaxial accelerometer BMA280 [12] was selected. Fur-

thermore, this accelerometer has already been soldered on the development board of SiLabs. This sensor features an integrated low-pass filter with an output data rate up to 500 Hz for an unfiltered input data rate of 2 kHz. Moreover, it possesses a resolution of 4096 LSB/g in the ± 2 g range, can be used in ± 2 g, ± 4 g, ± 8 g and ± 16 g range, communicates via an SPI 3-wire communication link. Moreover, it contains an integrated temperature sensor and multiple interrupts that can be configured to respond on motion events as well as on prolonged motionless conditions. These properties make the accelerometer excellent to detect when a train wagon is moving or not.

4.2.2 Acceleration measurement setup

The first setup proposed in this chapter is used for acceleration measurements. Here, an accelerometer will be attached to a train wagon and will measure the vibrations of a train wagon that is starting and stopping with or without air brakes.

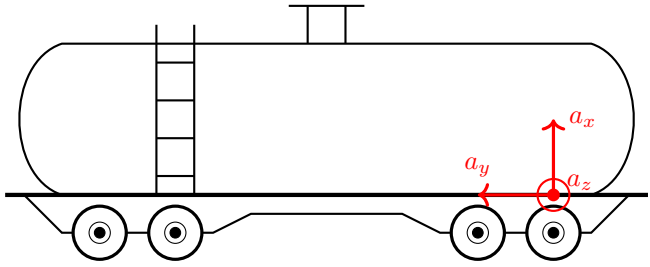

Figure 4.2: Acceleration measurement set up. The train wagon is equipped with an accelerometer attached via a 3D-printed polylactic acid (PLA) mount to the frame above the outermost wheel axle.

The accelerometer is mounted on a 3D-printed PLA support and is attached via neodymium magnets to the wagon above the most outer wheel axle, as can be seen in Figure 4.2 and Figure 4.3. PLA is a hard plastic so in combination with the large neodymium magnets, the accelerometer will measure the train vibrations and the damping effect can be neglected. This way, the X-axis (a_x) of the accelerometer is perpendicular towards the wheel axle of the train wagon, for measuring the gravitational force. The Y-axis (a_y) is alongside the train wagon, for measuring the movement of the wagon. The Z-axis (a_z) is in line with the wheel axle of the train wagon, for measuring left or right movements. The accelerometer will continuously measure the vibrations of the train wagon and transfer the data to a personal computer (PC) at a sample rate of 200 Hz or 5 ms. In this way, a clear view of the measured vibrations on the train wagon is illustrated.

(a) Container wagon

(b) Tank wagon

Figure 4.3: Accelerometer attached to the container and tank wagon above the most outer wheel axle.

4.2.3 RF measurement setup

The second proposed setup consists of Received Signal Strength Indicator (RSSI) measurements. The main purpose of these measurements is to find the optimal Tx level of a BLE node that is sending sensor data towards an CN also mounted on the train wagon.

Figure 4.4 illustrates the measurement setup, where a top view of a train wagon can be seen. A Tx node is placed at position 0 and a RX node is placed at positions 1, 2 and 3, respectively. From position 0 to 1, there is a clear Line-of-Sight (LoS) link, although with a lot of metal in the vicinity. From position 0 to 2, there is no LoS, and a large empty or full metal tank can shadow the communication link. From position 0 to 3, there is no LoS, but due to the position of the transmitter and receiver, there can be less obstruction when compared to the link from position 0 to 2.

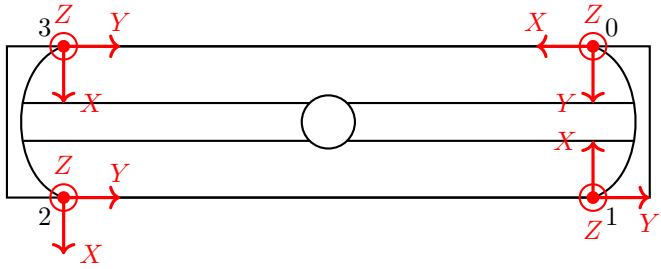

Figure 4.4: Top view representation of the RF measurement set-up on the tank wagon. The four corners are labelled from 0 to 3. At 0 a Tx node is placed, while at 1, 2 and 3 an Rx node is placed.

The Tx node is programmed to send 300 coded advertisement packages with an interval of 20 ms at a certain Tx level ranging from 0 dBm to 10 dBm in steps of 1 dBm. Due to battery management reasons, a Tx level of more than 10 dBm is not measured. The advertisement packages are labelled in the data, in order to prevent erroneous data capturing of other nodes. The Rx node was programmed to continuously scan for these coded advertisement packets, but also to log the RSSI level and to count the amount of received packages at a certain Tx level. Both nodes were mounted on a 3D-printed PLA support with an integrated neodymium magnet. Figure 4.5 illustrates the Rx node attached on the wagon at position 2.

Figure 4.5: Rx node attached at position 2 on the tank wagon.

4.3 Measurements & Discussion

4.3.1 Acceleration measurements

With the acceleration, the vibration of the train wagon in the moving direction is measured. These measurements are used to calculate the Signal Magnitude Vector (SMV) as follows.

$$SMV = \sqrt{a_X^2 + a_Y^2 + a_Z^2} \tag{4.1}$$

The measurements are performed on a train, composed of a small locomotive and two different wagons. The first one was a container and the second one a tank, both empty.

4.3.1.1 Wagon stopped

Efficiently employing the low-power and sleep modes of the WSN can drastically extend the battery lifetime. Instead of a battery-intensive continuous scan by the MCU, the system is mostly placed into a deep sleep mode and is only woken up by accelerometer events, if a train movement is detected. As mentioned earlier, the BMA280 has several built-in interrupts which are very useful.

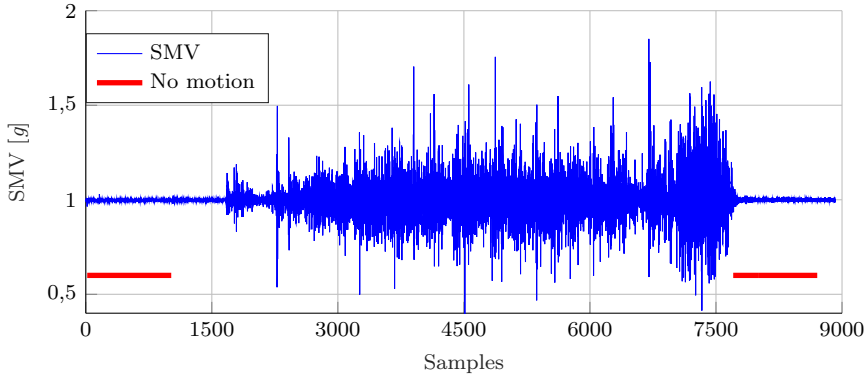

Figure 4.6: No motion interrupt result based on vibrations measured on the first wagon, with air brakes.

Figure 4.6 illustrates the vibration of the container wagon measured at a sample rate of 4 ms. To find out if the train has stopped, the *no motion interrupt* is selected. An interrupt is triggered when the slope of all selected axes is smaller than the predefined threshold for a certain time slot or a consecutive amount of samples. The red lines in Figure 4.6 show the result of the *no motion interrupt*. The parameters of this interrupt are a time

slot of 4 s or 1000 consecutive samples and a slope difference of 100 *mg*. It can be stated that this interrupt performs as desired. A larger time slot will prevent the MCU from waking up too fast in case the wagon stopped without air brakes.

4.3.1.2 Is the train moving?

Secondly, knowing when the train is moving, is important to put the WSN in a deep sleep mode until the train stopped and a *no motion interrupt* is triggered. The BMA280 has two built-in interrupts that can be utilized.

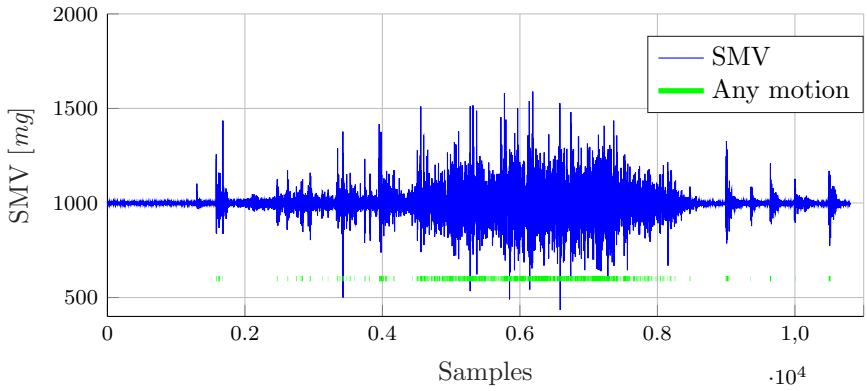

Figure 4.7: Any motion interrupt result based on vibrations measured on the first wagon, no air brakes.

The *any motion interrupt* is triggered if the slope difference of the selected axes for a certain amount of consecutive samples is larger than a predefined threshold. Figure 4.7 illustrates the 473 alerts that are triggered on the measured vibration of the container wagon not utilizing air brakes, sampled at a rate of 4 ms. The parameters of this interrupt are a time slot of 16 ms or 4 consecutive samples and a slope difference of 50 *mg* is used.

A second possible interrupt is called *High-g interrupt*. This interrupt is triggered if the absolute value of one of the selected axis ('or' relation) is higher than a predefined threshold for at least the defined time slot. The interrupt is cleared when the absolute value of all axis ('and' relation) is lower than the threshold minus the lower hysteresis level for the defined time slot.

Figure 4.8 illustrates the vibrations measured on the second wagon sampled at a sample rate of 4 ms and when braking with air brakes. The parameters of the interrupt are a time slot of 80 ms or 20 consecutive samples, a threshold on 1150 *mg* (purple line) and a lower hysteresis level of 250 *mg*

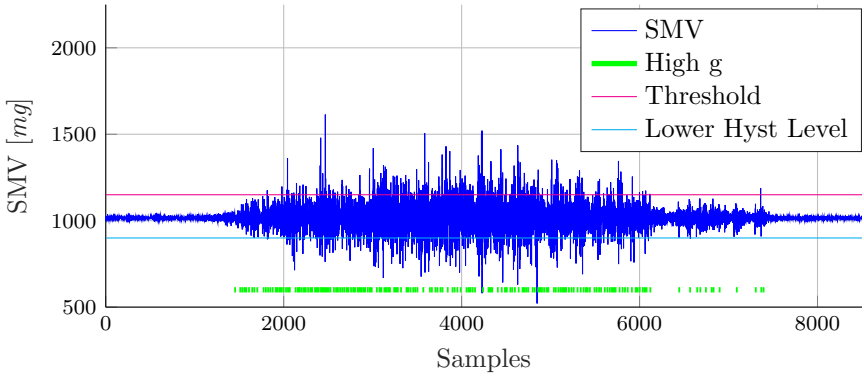

Figure 4.8: High-g interrupt result based on vibrations measured on the second wagon, with air brakes.

(cyan line). This results in 168 triggered interrupts. This clearly illustrates that both interrupts can be used to place the WSN in a deep sleep mode very efficiently. Since the accelerometer has a current consumption of 130 µA in normal mode, the influence on the battery lifetime is minimal. Furthermore, it can be noticed that the measured peaks are smaller on the second wagon, but still measurable.

4.3.1.3 Air brakes

Based on measurements, braking with or without air has less influence on the measured SMV. Figure 4.6 and Figure 4.7 illustrate the vibrations measured from the container wagon that is braking with and without air brakes, respectively. One can clearly see that after the wagon stops without air brakes, it results in decreasing repetitive shocks from the hydraulic absorbers. Most of these are perfectly measurable and do not have an influence on the WSN or the measurements these sensors make. With air brakes, it results in a smooth full stop. However, as soon as the brakes were released, some small aftershocks were noticed.

4.3.2 RF Measurement

The RF measurements consist of logging the RSSI level and the amount of received packages at a certain Tx level. In post-processing, the Average Received Power (ARP) and the Package Receive Rate (PRR) are calculated, as follows.

$$ARP_{TX}\,[\text{dBm}] = 10.\log_{10}\left(\frac{1}{m}.\sum_{n=1}^{m} 10^{\frac{RSSI_n\,[\text{dBm}]}{10}}\right) \tag{4.2}$$

$$PRR_{TX}\,[\%] = \frac{m}{300} \tag{4.3}$$

m = number of received packets

4.3.2.1 Reference measurements

As reference measurement, the Rx and Tx node were placed in the anechoic chamber with a distance of approximately 3.5 m between both nodes. Figure 4.9 illustrates the ARP for three different situations: two patch antennas as Tx and Rx node, a button antenna as Tx node and a patch antenna as Rx node and two button antennas as Tx and Rx node. This result clearly proves that the patch-patch combination gives the highest ARP and hence has the best reception. The combinations with the button antenna results in weaker signals down to sometimes unusable reception. For the button-button link no values were received between 0 dBm to 5 dBm, because the corresponding ARPs are lower than the minimal Rx sensitivity of the MCU. Figure 4.10 shows the PRR, where the same conclusion can be drawn. Based on these results, the button-patch link results in a good quality reception although with very low received power levels. Therefore, the link margin is limited.

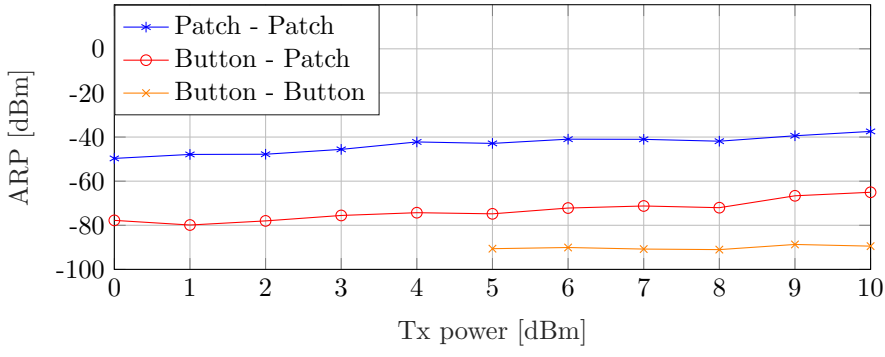

Figure 4.9: ARP: reference measurement in the anechoic chamber.

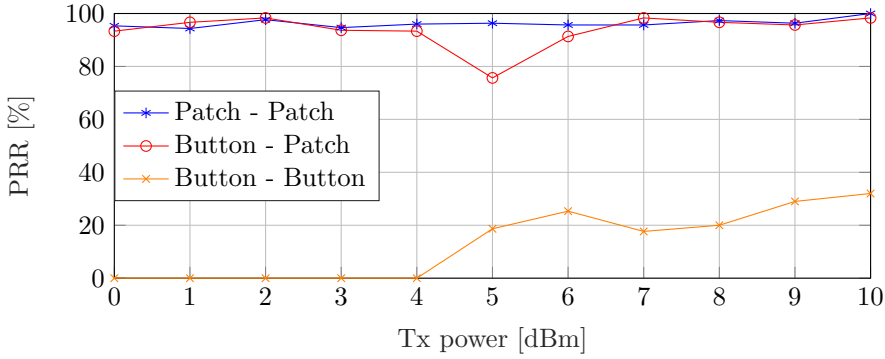

Figure 4.10: PRR: reference measurement in the anechoic chamber.

4.3.2.2 Real-life measurements

Based on the measurements performed in the anechoic chamber, it can be stated that the button antenna has a worse performance. To confirm this statement, the measurements were repeated in real-life. Figure 4.11 and Figure 4.12 illustrate the ARP and PRR on a full tank wagon. In order to see how the antenna link performs in the worse condition, the Tx node was placed at position 0 and the Rx node was placed on position 2. Figure 4.11 illustrates that the ARP level of the button-button and button-patch link are lower than the minimum Rx sensitivity level of -94.6 dBm from the radio integrated in the MCU. Figure 4.12 proves that no packets were received for those links. Therefore, the patch-patch antenna link was selected to perform the other measurements.

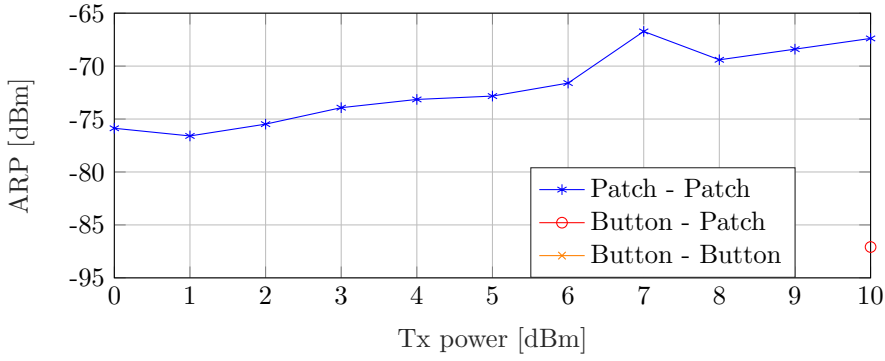

Figure 4.11: ARP: full tank wagon for the different antenna links.

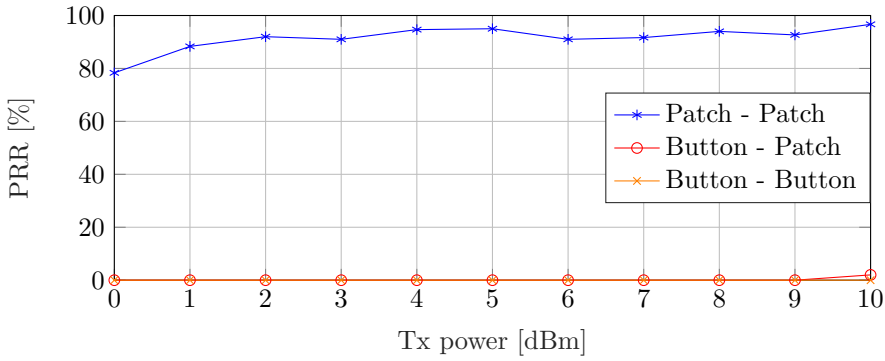

Figure 4.12: PRR: full tank wagon for the different antenna links.

Figure 4.13 illustrates the ARP on an empty tank wagon. From position 0 to 1, we have a better performance compared to the reference measurement because the measurement distance between the nodes is smaller. From position 0 to 2 or 3, there is a serious decrease in received power, but still enough to have a good communication between both nodes. Figure 4.14 illustrates the PRR for the empty tank wagon. The same conclusion can be drawn for the position 0 to 1 link. From position 0 to 2, there is a good reception, although metal structures of the train wagon need to be taken into account. Starting from 2 dBm transmit power, an ARP of around -82 dBm and a PRR of approximately 65 % are measured. From position 0 to 3, there is some fluctuation, probably due to multipath effects. Based on the performed measurements, we can conclude that the patch-patch link performs well even when a large metal structure is in close proximity. This is due to the properties of the employed antenna, more importantly the omnidirectional radiation at a frequency of 2.45 GHz of the patch antenna.

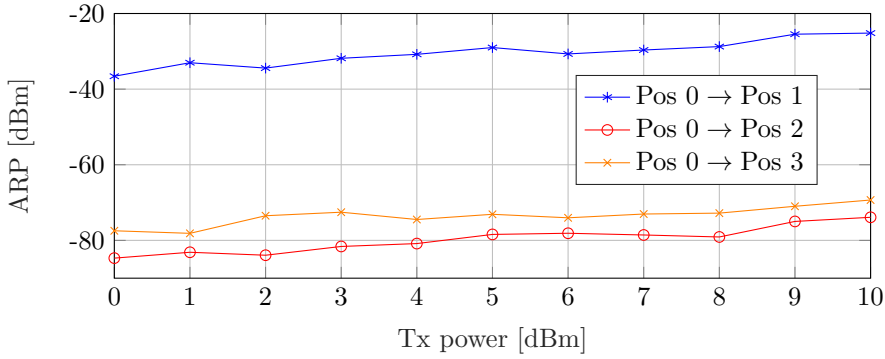

Figure 4.13: ARP: patch-patch link on an empty tank wagon.

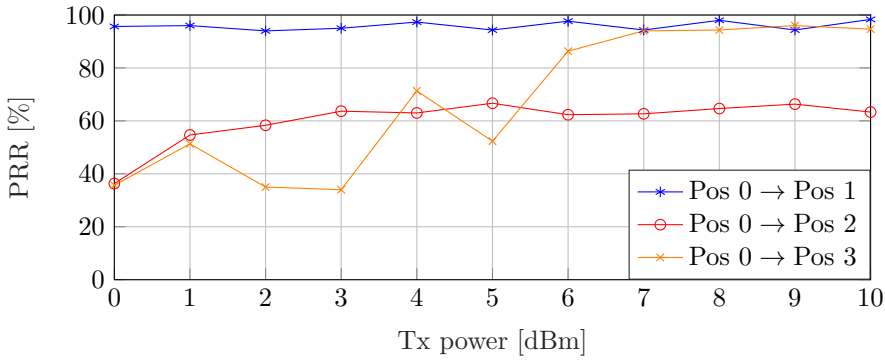

Figure 4.14: PRR: patch-patch link on an empty tank wagon.

Figure 4.15 presents the measured results for the ARP and Figure 4.16 for the PRR on another tank wagon, completely filled. The same conclusion can be drawn, but with a better performance. For the worst communication link 0 to 2, starting from a Tx power level of 2 dBm, there is a PRR of 90 % and an ARP of approximately −75 dBm. From position 0 to 2, an increase of approximately 5 dBm ARP level and 50 % PRR is observed. When the measurements on the full and empty tank wagon are compared, the statement can be made that the buildings surrounding these train wagons have a positive influence on the ARP and PRR. Since most of the communication will happen during the rest period at the factory or train stations, this will positively influence the communication between de nodes.

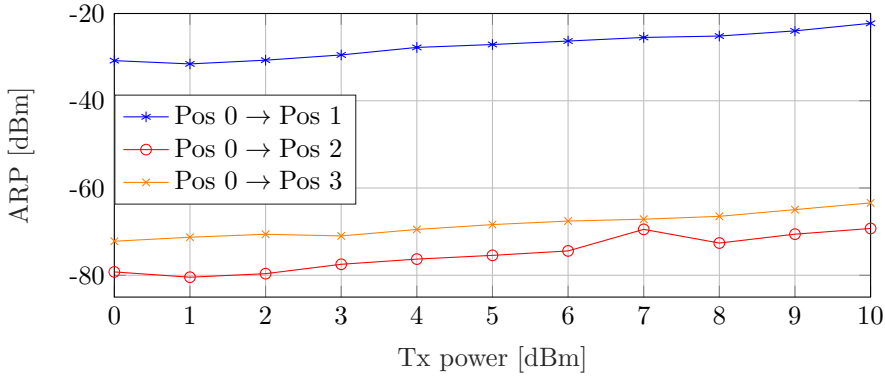

Figure 4.15: ARP: patch-patch link on a full tank wagon.

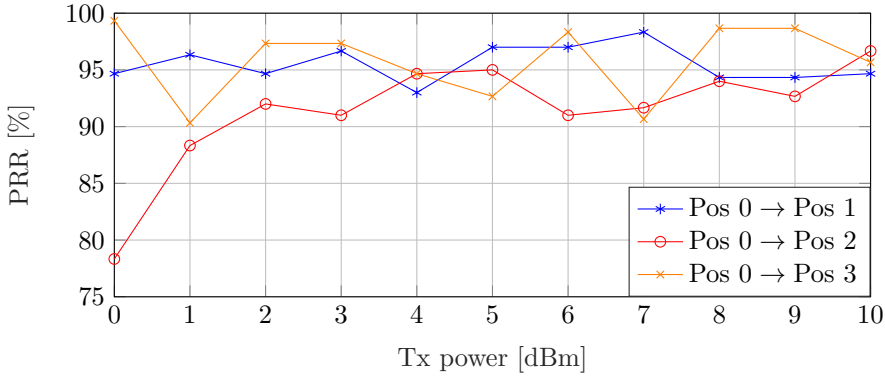

Figure 4.16: PRR: patch-patch link on a full tank wagon.

4.3.2.3 Brakes

In a next step, the nodes were placed on the outside of the brakes of the tank wagon. At each side, the wagon has four steel wheels, each having their own brake pair. The node was always placed on the most outer wheel brake, as can be seen in Figure 4.17. Figure 4.18 and Figure 4.19 show the results for the ARP and PRR on an empty tank wagon brakes, respectively. From brake 1 to 2, there is an ARP level ranging from −75 dBm to −65 dBm and a PRR of 95 %. This illustrates that reliable communication is possible.

From brake position 0 to 2, similar results were measured, so the same conclusion can be drawn. It is important to mention that during these measurements, the nodes were attached in front of the big steel wheels. Therefore, from position brake 0 to 2, the RF signals encounter at least two large metal structures. Final measurement, a Tx node is placed on the CN

(a) Brake position 2 *(b) CN in position 0*

Figure 4.17: Nodes placed on the brake and CN on the train wagon.

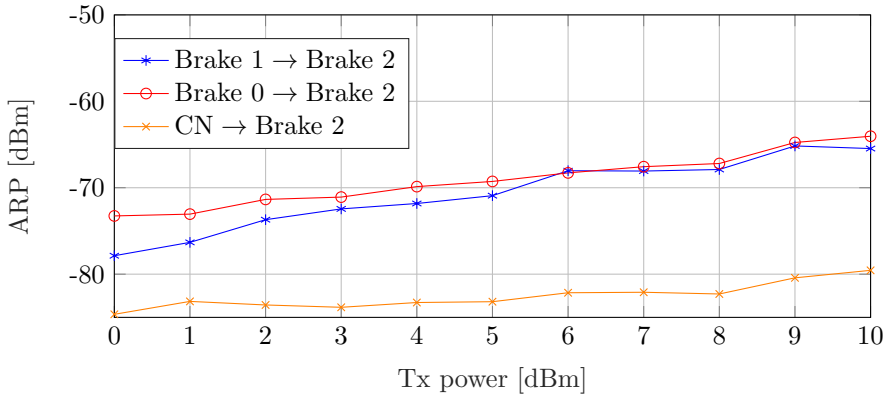

Figure 4.18: ARP: from the outer brake on an empty wagon.

that is mounted above the train platform in position 0 and the Rx node is placed on the brake in position 2. The CN is the grey box mounted on the train wagon in Figure 4.17b. From the CN to 2, the received signal levels decrease. This is because the signals are close to the big metal plate underneath the tank wagon as well as the steel wheels. As conclusion, starting from a Tx level of 4 dBm an average PRR of approximately 92 % is measured and an ARP of around −83 dBm is measured.

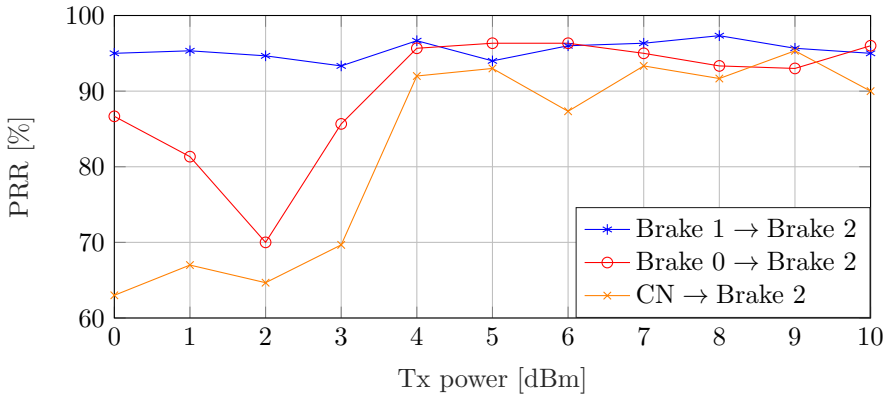

Figure 4.19: PRR: from the outer brake on an empty wagon.

4.4 Conclusion

This paper presents the possibilities to use an accelerometer to put a WSN in a deep sleep mode or to wake up the system when connected to an industrial IoT network. Furthermore, it proposes a low cost, easy producible and commercially available PIFA antenna that works perfectly in these harsh metal environments train wagon are.

The first set measurements introduced in this paper were acceleration measurements. These were obtained on different train wagon types, braking with or without air brakes. Based on these measurements and the built-in interrupts from the BMA280, a WSN on the train wagon can easily be put to sleep or wake up. Employing the no motion, any motion and high-g built-in interrupts of the accelerometer, the movements of the train can be easily monitored and the WSN can be put to sleep or wake up. This will have a large impact on the battery lifetime of each SN. Furthermore, it can be concluded that there is a small difference between braking with or without air brakes, but no large impact on the measured vibrations or selected interrupt have been observed.

The second set of measurements introduced, were the RF measurements. Two prefabricated PIFAs were placed on a train wagon, to measure the RSSI levels at different Tx levels. Afterwards, the PRR and ARP were calculated. This illustrated that the first selected patch antenna performs best in every position on the train wagon. In a final step, the patch antenna was placed on the outer brakes and outer wheels of the wagon. Despite the large amount of metal structures, the antenna kept performing in a desirable way.

These measurements also illustrate that there are limited differences between a full or empty tank wagon. Starting from a Tx level of 2 dBm,

there is an PRR and an ARP of approximately 90 % and −75 dBm on a full tank wagon, respectively. On an empty tank wagon, less favourable, but still usable results were registered. The measurement on the brakes of the empty train wagon clearly illustrated that reliable communication is possible. Starting from a Tx level of 4 dBm an average PRR and ARP of roughly 92 % and −83 dBm is measured.

References

[1] U. Biaou, S. Iben Jellal, M. Bocquet, S. Baranowski, A. Rivenq, and P. Mariage. *Study of the Positioning of Wireless Sensors for Communication at* 2.4 GHz *Inside the Train.* In 2017 International Conference on Wireless Technologies, Embedded and Intelligent Systems (WITS), pages 1–5, 2017. doi:10.1109/WITS.2017.7934612.

[2] N. Barkovskis, A. Salmins, K. Ozols, M. A. Moreno García, and F. P. Ayuso. *WSN Based on Accelerometer, GPS and RSSI Measurements for Train Integrity Monitoring.* In 2017 4th International Conference on Control, Decision and Information Technologies (CoDIT), pages 0662–0667, 2017. doi:10.1109/CoDIT.2017.8102670.

[3] A. Lo Schiavo. *Fully Autonomous Wireless Sensor Network for Freight Wagon Monitoring.* IEEE Sensors Journal, 16(24):9053–9063, 2016. doi:10.1109/JSEN.2016.2620149.

[4] M. T. Lazarescu and P. Poolad. *Asynchronous Resilient Wireless Sensor Network for Train Integrity Monitoring.* IEEE Internet of Things Journal, 8(5):3939–3954, 2021. doi:10.1109/JIOT.2020.3026243.

[5] M. Soliman, Y. Dawoud, E. Staudinger, S. Sand, A. Schuetz, and A. Dekorsy. *Influences of Train Wagon Vibrations on the MmWave Wagon-to-Wagon Channel.* In 12th European Conference on Antennas and Propagation (EuCAP 2018), pages 1–5, 2018. doi:10.1049/cp.2018.0962.

[6] Y. Gong, S. Wang, Z. Xie, T. Zhang, W. Chen, X. Lu, Q. Zeng, Y. Gao, and W. Huang. *Self-Powered Wireless Sensor Node for Smart Railway Axle Box Bearing via a Variable Reluctance Energy Harvesting System.* IEEE Transactions on Instrumentation and Measurement, 70:1–11, 2021. doi:10.1109/TIM.2021.3076857.

[7] L. Wang, T. He, Z. Zhang, L. Zhao, C. Lee, G. Luo, Q. Mao, P. Yang, Q. Lin, X. Li, R. Maeda, and Z. Jiang. *Self-Sustained Autonomous Wireless Sensing Based on a Hybridized Teng And PEG Vibration Mechanism.* Nano Energy, 80:105555, 2021. Available from: https://www.sciencedirect.com/science/article/pii/S2211285520311290, doi:https://doi.org/10.1016/j.nanoen.2020.105555.

[8] S. L. Oliva, A. Palmieri, L. Invidia, L. Patrono, and P. Rametta. *Rapid Prototyping of a Star Topology Network based on Bluetooth Low Energy Technology.* In 2018 3rd International Conference on Smart and Sustainable Technologies (SpliTech), pages 1–6, 2018.

[9] Silicon Laboratories. *EFR32MG13 Series 1 Modules*. www.silabs.com. Accessed on October 18, 2022.

[10] Taoglas. *Freedom FXP810 2.4/*4.9 GHz *to* 6.0 GHz *Flex PCB Antenna,* 100 mm*, I-PEX MHF® I (U.FL)*. www.taoglas.com. Accessed on October 18, 2022.

[11] Taoglas. *WCM.01.0151W* 2.4 GHz *Button Antenna*. www.taoglas.com. Accessed on October 18, 2022.

[12] Bosch Sensortech. *Acceleration Sensor BMA280*. www.bosch-sensortec.com. Accessed on October 18, 2022.

5 Conclusion

"If this does not appeal to you sufficiently to recognize in me a discoverer of principles, do me, at least, the justice of calling me an "inventor of some beautiful pieces of electrical apparatus""

– Nikola Tesla, 1907

This dissertation has focused on the development of sensor nodes for Wireless Sensor Network (WSN) based on Bluetooth Low Energy (BLE) for on-body and industrial Internet of Things (IoT) applications. The research was applied to three different topics where small low-power, low-cost sensor nodes were required.

The first topic treats detecting vulnerable road user (VRU) in the blind spot of vehicles. A complete low-power and low-cost detection system was developed utilizing three types of nodes. First, Detection Nodes (DNs) are mounted alongside the right side of a truck and trailer. These nodes will continuously advertise their presence. The VRUs are wearing a small, unobtrusive band around their arm that continuously scan for advertisement packages from the DN. When VRU and truck are too close to each other, the Received Signal Strength Indicator (RSSI) levels are too high, and a self-developed rule based algorithm will trigger an alert on the wearable, but also in the Central Node (CN) inside the cabin of the truck driver. Thereby, there is a shared responsibility between VRU and truck driver. Based on some extensive simulations, the different parameters for the rule based algorithm were retrieved. The full system was tested in real life. This

resulted in a detection range of approximately 8 m. Moreover, research was presented on the development of a miniaturized DN that fits inside the sidelight of a trailer. By utilizing a multilayer Printed Circuit Board (PCB) with limited peripherals and specific developed planar inverted-F antenna (PIFA) antenna topology.

The second topic is about detecting elderly after a fall. The detection of such an event happens with a low-power, low-cost and unobtrusive patient wearable that can be worn around the waist. It is based on a simple rule-based algorithm that is continuously monitoring the acceleration and the orientation towards the gravitational vector. When both thresholds are crossed by the measured values, an alert is set. Based on extensive simulations on real-life measurements and open-source databases, an acceleration threshold of 2.5 g and an orientation threshold of 45° were found as the best fitted parameters. Validating the algorithm on these open-source databases, containing data for 85 persons, performing 18 835 activities of daily living (ADL) or fall activities, resulted in an F_1-score in a range of 82.94 % to 89.8 %, confirming its reliability. The proposed convolutional neural network (CNN) algorithm results in an F_1-score of a range of 86.72 % to 95.09 %, which is comparable to the proposed rule-based algorithm. The combination of the developed PCB and rule-based algorithm results in a battery autonomy of 100 days on a CR2032 battery. In further research, the other part of the system was developed. When the patient wearable detects and sends an alert, a fixed DN mounted inside the room will receive this. The DN will add the necessary information such as room number and floor to the alert package and forward the message to the Network Nodes (NNs) that are scattered in the hallways of the nursing home. These nodes will look for the closest care taker that is wearing the Caretaker Node (CTN) and pass on the alert. Upon receiving, the caretaker will know the personal details of the elderly (from the patient wearable) and the location were the elderly fell (from the DN). Based on measurements performed with developed PCBs and basic prefabricated antennas, perfect wireless communication was achieved at the lowest Tx level possible. An Average Received Power (ARP) of −64.78 dBm and a Package Receive Rate (PRR) of approximately 90.5 % was retrieved over a distance of 40 m. Furthermore, it takes 3 s to transfer an alert with one NN and 3.5 s with two NNs over a maximum distance of 50 m and 84 m in a hallway environment, respectively. This results in an energy efficient, low-cost fall detection system.

Third and final topic deals with train integrity. Modern trains are equipped with multiple sensors that are combined in a WSN. Measurements were performed to find the best suited antenna topology to perform wireless communication between sensor nodes on locomotives and train wag-

ons. Furthermore, some acceleration measurements were performed to determine the best fitted built-in interrupt to make a WSN on a train energy efficient. Basic Radio Frequency (RF) measurements inside an anechoic chamber demonstrated that a basic prefabricated patch PIFA performed best. The real-life measurements, where the Tx nodes was placed on the brakes, resulted in a PRR of approximately 92 % and an ARP of approximately −83 dBm at a Tx level of 2 dBm. The acceleration measurements illustrated that the built-in interrupts of the selected accelerometer work perfectly to detect whether a train is moving or standing still. Based on these measurements, a WSN with a small and inexpensive accelerometer and antenna may be implemented.

These three topics clearly illustrates that BLE is a perfect communication protocol for WSNs in different fields. Since Bluetooth was developed to be energy efficient and always had a decent data throughput compared to its energy consumption, it can be used in all sorts of IoT applications. In literature, much research is performed to make BLE even more energy efficient by utilizing advertisement packages as data throughput, since this consumes less power compared to data throughput via a connection between nodes.

Future Work

Although for most of these topics excellent results were obtained, some extras could be added to have an overall increase in performance of the proposed systems. For the blind spot detection and warning system, the developed wearable could be realized on a flex or flex-rigid PCB. This would make it more easy to wear the wearable and extra peripherals could be added. Furthermore, by utilizing the same System-on-Chip (SoC), as mentioned in Appendix A, the overall design will be smaller and easier to implement in other pedestrian of cyclist equipment and clothing. Depending on this equipment, some energy harvesters (EHs) could be implemented. This way, the battery life time will be extended in an efficient way. From a commercial point of view, a smartphone application could be developed in order to replace the dedicated wearable. Even though, more research needs to be performed in order to develop an application that performs with the same accuracy and efficiency. Next, the DNs could be upgraded to BLE Mesh. In this way, sending the alert messages to the CN would be easier, and the complete system would be more scalable in DN amount. Still, this will have an influence on the battery lifetime. Implementing a direction finding technique by Angle of Arrival (AoA) estimation, which is featured in BLE 5, would make the detection more accurate.

For the topic of fall detection, future steps would consist in making the system easier in usability. By implementing Near-Field Communication (NFC) and/or Radio-frequency identification (RFID), the caretaker could easily clear an alert by pushing there CTN tag against the wall where the DN is mounted. This is a small and inexpensive measure that has a huge influence in the performance and ease of use for the caretakers. Furthermore, the wearable and CTN could be extended with EHs. Since the care taker is moving a lot while working, a micro generator system (MGS) could be implemented. The DNs could be extended with AoA estimation. This will enable, the system to tell the nursing personnel where exactly the elderly fell inside his room. Finally, the patient's wearable could be extended with other sensors. This will allow the caretaker to see more vital parameters of the fallen elderly and alert a doctor if necessary. Finally, by developing a suitable antenna for each node, the performance will be increased.

Appendix

A

Wearable Bluetooth Low Energy Based Miniaturized Detection Node for Blind Spot Detection and Warning System on Vehicles

Nick De Raeve, Quinten Van den Brande, Matthias de Schepper, Jo Verhaevert, Patrick Van Torre and Hendrik Rogier

Published in IEEE 2021 6th International Conference on Smart and Sustainable Technologies (SpliTech), 2021, pp. 1-5, Oct 2021.

⋆⋆⋆

Annually, approximately 10 *people are involved in a lethal blind spot accident on Belgian roads, even though a lot of money is invested in the development of blind spot detection systems and in raising the awareness of this phenomenon. In previous research, we developed a blind spot detection and warning system based on Bluetooth Low Energy (BLE) and Received Signal Strength Indicator (RSSI) measurements. In this chapter, the miniaturization of the Detection Node (DN) and wearable is presented. There will be*

a closer look at the development of the Printed Circuit Board (PCB) and the folded Shorted Patch (S-P) antenna that will be integrated into the sidelights of trailers. In a future step, the wearable design will be updated with the same miniaturization steps taken in this chapter.

A.1 Introduction

In 2020, approximately 100 people were killed on Belgium roads [1]. 10 % of the killed are due to a blind spot accident. Annually, a lot of money is invested by government and traffic safety organizations to raise awareness of this problem. However, the danger still exists. The main problem lies in the lack of reliable communication between the truck driver and the vulnerable road user (VRU). To eliminate or possibly solve this problem, we proposed a blind spot detection and warning system based on Bluetooth Low Energy (BLE) in a previous work [2]. In this chapter, there will be a closer look at the miniaturization of the Detection Node (DN), so it can be fitted inside the small lights alongside a truck trailer.

Industries provide multiple solutions, each with their disadvantages [3, 4]. In literature, multiple research is conducted in the placing of cameras [5] and the optimization of different algorithm types [6, 7] to detect VRUs in the blind spot. It is a known fact that camera systems suffer from some known problems. Most of them have a limited coverage area, have a bad performance when dirty and are hindered by privacy regulations. Combined with a high implementation cost, cameras are not the most ideal solution. Furthermore, some research is performed in detection based on radar [8]. Both systems will detect VRUs, but suffer from several false positives and true negatives [3, 4]. Besides camera and radar, there are also the systems that use wearables [2, 9]. These utilize an on-body wearable to detect how close they are to a truck. Once too close they will trigger an alert so the VRU and truck driver are notified about a potential blind spot accident.

This chapter presents the miniaturization of the DN. First, there will be a closer look at the design of the Printed Circuit Board (PCB) and the folded Shorted Patch (S-P) antenna. It is followed by the measurements and discussion of the PCB and the antenna. Finally, the conclusion and future work are presented.

A.2 Design

The proposed system from [2] consists of five DNs placed alongside a truck with a trailer. A Central Node (CN) is positioned inside the cabin of the truck. The DNs are continuously advertising the presence of the truck.

A VRU is wearing the wearable, also proposed in [2] and can be seen in Figure A.1, and receives all these advertisement packages. Based on the Received Signal Strength Indicator (RSSI) values, the possibility of an accident is calculated. When both parties are too close, an alert is triggered on the wearable device, but the wearable also connects to the closest DN. Based on this connection, another alert is triggered in the cabin of the truck. From this moment, there is a shared responsibility between both parties and important lifesaving safety measures can be taken. The wearable worn by the VRU contains leds, buzzer and vibration motor to alarm the person in every possible method.

Figure A.1: Student wearing the designed wearable next to a truck, that is equipped with the designed system.

The communication between the different nodes of the proposed system relies on BLE. Therefore, we utilize the BGM111 module from Silicon Laboratories (SiLabs) [10] is utilized. These modules use the BLE4.2 stack [11] and contain an on-board 32-bit, 38.4 MHz Advanced RISC Machines (ARM) Cortex M4 [12] microcontroller (MCU) with Digital Signal Processing (DSP) instruction set, combined with an integrated antenna. The PCB of the DN, integrated in an in-house constructed plastic 3D-printed box, is shown in Figure A.2. Besides the electronic components, this PCB contains also the chip antenna and has a size of 45×30 mm, necessary as ground plane for the chip antenna.

This system is upgraded by a miniaturization of the DN. Due to the required ground plane size for the chip antenna, these DNs cannot be built inside a sidelight of a trailer, as can be seen in Figure A.3. Therefore, a miniaturization of the DN is required, taking into account the following constraints. First of all, the PCB has to fit inside the housing of the sidelight, resulting in dimensions smaller than 30×20 mm. Further, the module in the detection has to run on Bluetooth Mesh [13] to facilitate more convenient

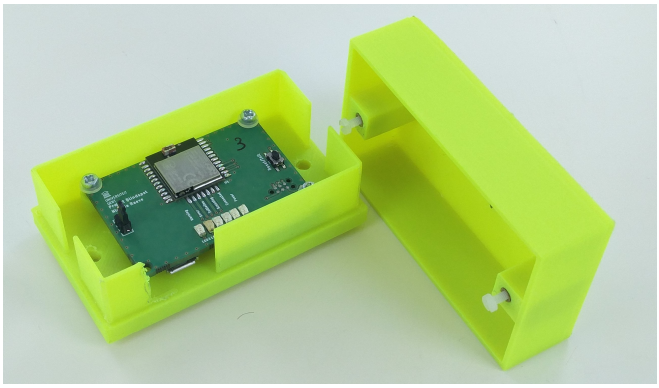

Figure A.2: Designed DN presented in [2].

data transfer between the DNs and the CN. Finally, since the node will be implemented inside the metal chassis of the trailer, a dedicated and adapted antenna has to be developed, satisfying the aforementioned dimension restrictions.

Figure A.3: Picture of a sidelight on European Truck.

A.2.1 Printed Circuit Board

The design of the miniaturized PCB relies on the Silicon Laboratories EFR32MG13 [14] System-on-Chip (SoC). It contains a 32-bit ARM [12] Cortex-M4 core with 40 MHz maximum operating frequency, 512 kB of flash and 64 kB of Random Access Memory (RAM), an integrated power amplifier with up to 19 dBm and an integrated balun for 2.4 GHz. Furthermore, this SoC also supports the use of Bluetooth Mesh [13]. This all is combined in a package of 5×5 mm, which results in a serious downsize compared to the earlier mentioned BGM111.

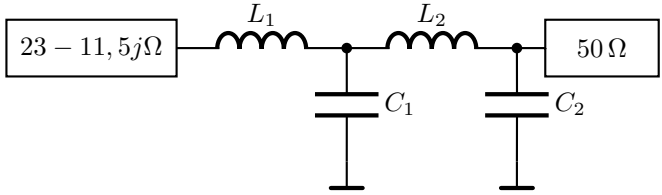

Figure A.4: Applied matching network.

Table A.1: Calculated LC values.

Inductor	**Value** [nH]	**Capacitor**	**Value** [pF]
L_1	1.3	C_1	5.3
L_2	1.5	C_2	3.2

An SubMiniature version A (SMA) connector has been added to the PCB for easier testing of multiple antenna topologies. To provide maximal power transfer towards the antenna, a fourth order LC-matching network is designed in order to conjugate match the $50\,\Omega$ SMA connector interface to the $(23 - j11.5)\,\Omega$ impedance of the EFR32MG13P MCU, as can be seen in Figure A.4. The matching network, described further, determines the values for L and C, as is given in Table A.1. Furthermore, by implementing Grounded Co-Planar Waveguide (GCPW) [15], the traces are minimized even further. Taking all these steps into account, a new PCB is designed and is visualized in Figure A.5. This PCB has an overall size of 30×20 mm, which is a serious reduction in size compared with the previous design.

A.2.2 Miniaturized BLE antenna

As the antenna is required to support the Institute of Electrical and Electronics Engineers (IEEE) 802.15.1 standard (Bluetooth mesh), a reflection coefficient with respect to $50\,\Omega$, $|S_{11}|$, below -10 dB is imposed in the

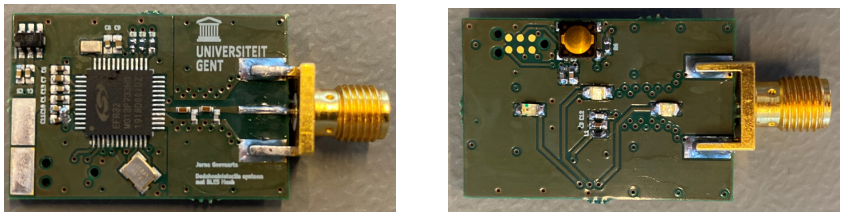

(a) Top *(b) Bottom*

Figure A.5: Designed miniaturized PCB for the DN.

2.400 GHz to 2.4835 GHz frequency band. In addition a 3 dB-beamwidth greater than 70° in the azimuth-plane is imposed in order to ensure sufficient coverage in a large area next to the truck. Finally, maximum dimensions for the antenna are set at 35 × 25 mm to fit the antenna inside the sidelight of the truck. Note that special care is required when integrating the antenna inside the light, as the large metallic structures can severely influence the antenna performance.

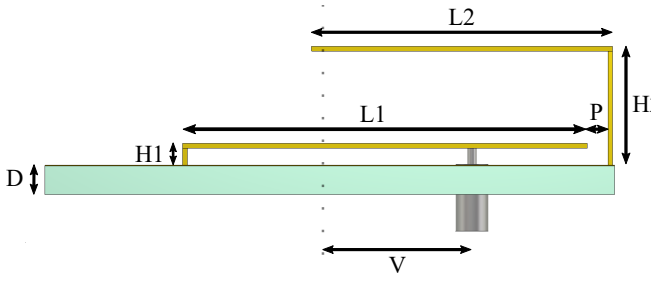

Figure A.6: Annotated representation of the folded Shorted-Patch (S-P) antenna constructed out of 0.25 mm *brass sheets in yz-plane view.*

To realize the imposed requirements a folded Shorted-Patch antenna, based on [16], is proposed. The antenna essentially consists of two planar inverted-F antenna (PIFA) implemented on an air substrate constructed out of 0.25 mm brass sheets, as depicted also in Figure A.6 and Figure A.7. By stacking both PIFA elements on top of each other and, hence, creating a tight coupling between them, mode bifurcation is achieved [17]. By judiciously optimizing the respective resonance frequencies of the antenna, a strong miniaturization of the antenna structure is obtained, meanwhile taking into account the above described design criteria. The final antenna dimensions after optimization are depicted in Table A.2.

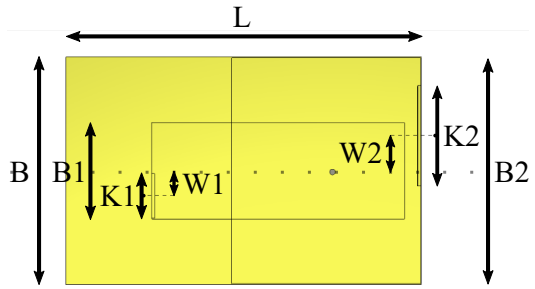

Figure A.7: Annotated representation of the folded Shorted-Patch (S-P) antenna constructed out of 0.25 mm *brass sheets in xy-plane view.*

Table A.2: Dimensions after optimization of the folded Shorted-Patch (S-P) antenna.

Dimension	**Value [mm]**	**Dimension**	**Value [mm]**
L	31.26	$L2$	16.53
B	20.00	$B2$	19.72
D	1.60	$H2$	6.50
$L1$	22.20	$W2$	3.06
$B1$	8.45	$K2$	8.80
$H1$	1.19	P	1.39
$W1$	2.20	V	4.77
$K1$	3.94		

A.3 Simulations & discussion

After designing the PCB, the matching network as well as the proposed antenna topology is simulated.

A.3.1 Matching network

In subsection A.2.1, the fourth order LC-matching network is discussed. It is used to match the MCU with the SMA connector. GCPWs further minimize the necessary PCB traces. The values for the matching can be found in Table A.1, whereas all the different sizes of the waveguide can be extracted from Figure A.9.

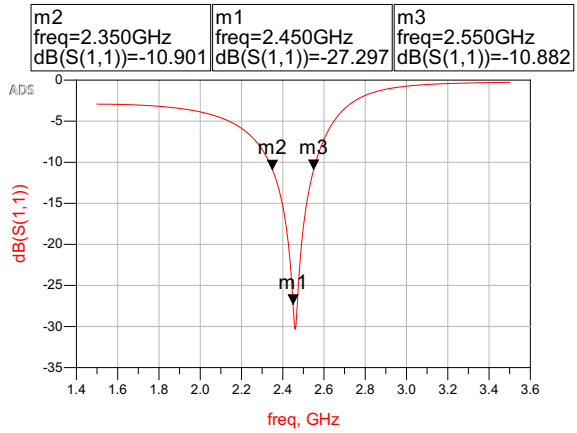

Figure A.8: Simulated S_{11} of the designed matching network.

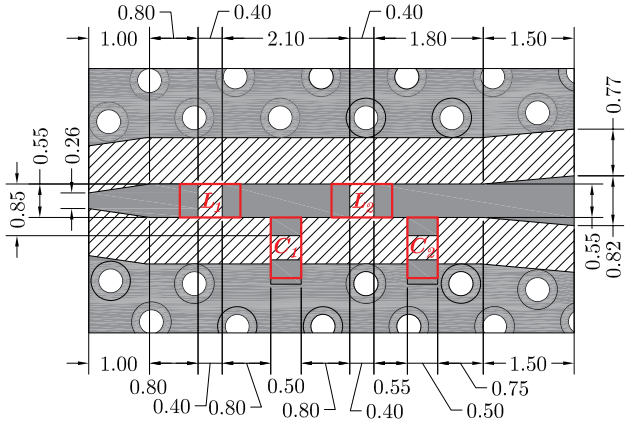

Figure A.9: Designed matching network with implemented GCPW.

The S_{11} of the designed matching network is visualized in Figure A.8. At the centre frequency of 2.45 GHz, there is a S_{11} of -27.3 dB. The S_{11} is smaller than -10 dB in the entire frequency band 2.34 GHz to 2.56 GHz. This results in an impedance bandwidth of approximately 200 MHz.

A.3.2 Folded Shorted-Patch antenna results

The simulated S-parameters of the optimized antenna, depicted in Figure A.11, show a $|S_{11}| < -10\,\text{dB}$ from 2.35 GHz to 2.55 GHz. The simulated gain pattern in the azimuth and elevation plane is shown in Figure A.12a and Figure A.12b, showing a peak gain of 2.1 dBi and 2.4 dBi, respectively. A 3 dB-beamwidth of 360° and 103.6° can be observed in the azimuth and elevation plane, respectively.

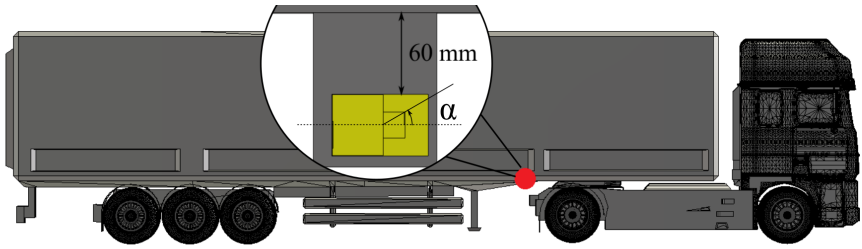

Figure A.10: Truck with antenna integration orientation $\alpha = 0°$.

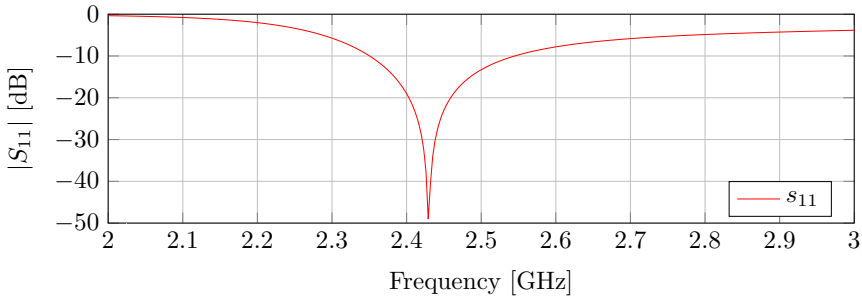

Figure A.11: Simulated S_{11} of folded S-P antenna constructed out of 0.25 mm *brass sheets.*

In order to validate the antenna performance in realistic deployment scenarios, the folded S-P antenna is also simulated when integrated into a sidelight on the trailer of a truck, as depicted in Figure A.10. A full metal truck was included in the simulation program. In real life, the truck is not completely full metal, but this gives us a worst case scenario. Here, the red dot indicates the location of the antenna on the trailer, behind the last wheel of the truck. The antenna is placed 60 mm below the container frame of the trailer.

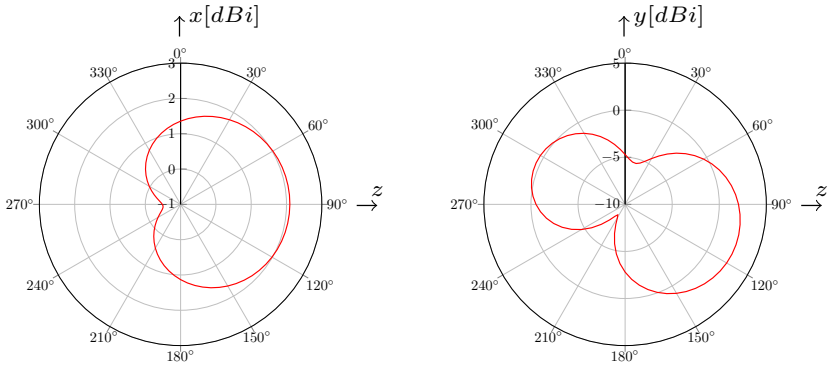

(a) Azimuth. *(b) Elevation.*

Figure A.12: Simulated gain of the standalone folded S-P antenna constructed out of 0.25 mm *brass sheets.*

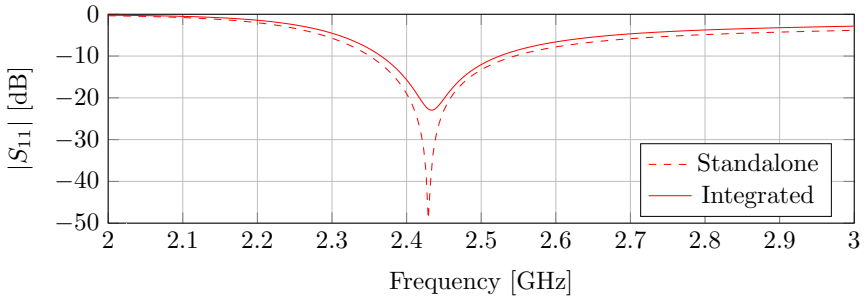

Figure A.13: Simulated S_{11} of folded S-P antenna constructed out of 0.25 mm *brass sheets integrated on a truck.*

Figure A.13 shows that the effect of the integration platform is negligible on the antenna impedance and, as such, on the reflection coefficient. To analyse the impact of the truck on the radiation performance, the radiation pattern is simulated for different antenna integration orientations, defined by the angle α. Again, the integration platform has negligible influence on the radiation pattern when $\alpha = 0°$ or $\alpha = 180°$, as can be seen in Figure A.14. However in contrast, when $\alpha = 90°$ the integration platform lowers the main beam direction in the elevation platform, thereby decreasing the overall gain in the azimuth plane. As the PIFA antenna has a sufficiently large ground plane and there are no objects in the reactive near field of the antenna, perpendicular to the antenna ground plane, it can be stated that the integration platform will have a negligible impact on the antenna polarisation. Furthermore, the radiation pattern contains both strong horizontal

and vertical polarisation components, which will guarantee the polarisation mismatch will never cancel the full link budget as the orientation of the antenna on the wearable is continuously changing. A further optimization of the wearable antenna could positively influence the polarisation mismatch.

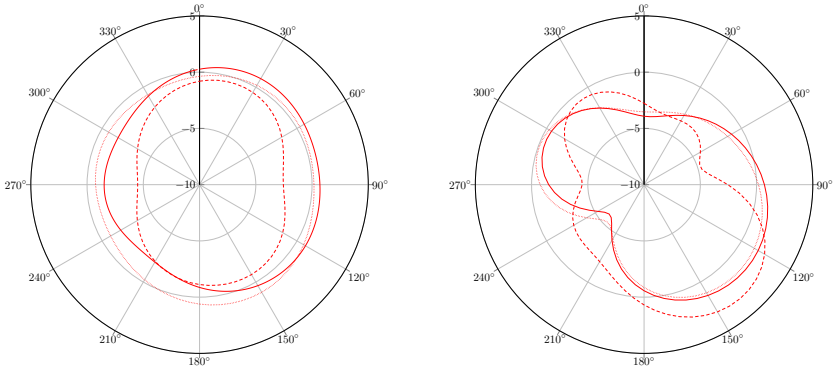

(a) Azimuth. *(b) Elevation.*

Figure A.14: Simulated gain of the integrated folded S-P antenna constructed out of 0.25 mm *brass sheets for different integration orientations. The solid line represents* $\alpha = 0^\circ$*, the dashed line* $\alpha = 90^\circ$ *and the dotted line* $\alpha = 180^\circ$*.*

A.4 Conclusion

This chapter describes the upgrading and miniaturization of a previously developed DN for blind spot detection and warning system for vehicles based on BLE. The entire system consists of five DNs placed alongside a truck, continuously transmitting advertising packets to potential wearable nodes in its vicinity. In order to integrate the DNs into the trailer sidelights, a miniaturized and highly integrated design is proposed.

To this end, both the PCB and antenna have been redesigned: a smaller PCB footprint is obtained and a miniaturized folded S-P antenna is designed to fit within this footprint. A fourth order matching network is added to convert the transceiver output impedance from $(23 - j11.5)\,\Omega$ to the required $50\,\Omega$. All these measures result in a perfect integrable design.

A.5 Future work

In a future work, there will be more optimizations of the entire system. For the DN, the following measures will be implemented. First of all, to decrease the overall size, the antenna will be matched to the impedance of

the MCU. In that way, the matching network can be reduced and both the PCB and the antenna can be integrated on one PCB.

Further, by implementing Bluetooth Mesh [13], it will be more convenient to transfer data between different DNs, but also towards the CN. Replacing a DN will be cheaper and less complicated due to the provisioning process [18] of Bluetooth Mesh.

Finally, by implementing Angle of Arrival (AoA) [19], the system will be able to provide more accurate detection.

By utilizing the same SoC and PCB design, the wearable can be reduced in size as well. This will also improve the possibility to redevelop the solid PCB wearable to a flex or flex-rigid design, making the wearable more unobtrusive. Additionally, the PCB could be integrated in other equipment that is used for walking, cycling or daily carrying.

References

[1] VIAS Institute. *Road Safety Barometer*. https://www.vias.be/en/research/road-safety-monitoring-survey/. Accessed on October 18, 2022.

[2] N. De Raeve, M. de Schepper, J. Verhaevert, P. Van Torre, and H. Rogier. *A Bluetooth-Low-Energy-Based Detection and Warning System for Vulnerable Road Users in the Blind Spot of Vehicles*. Sensors, 20(9), 2020. doi:10.3390/s20092727.

[3] VIAS Institute. *Accidents involving Trucks - Phase 1*. https://www.vias.be/en/onderzoek/onze-publicaties/ongevallen-met-vrachtwagens-fase-1/. Accessed on October 18, 2022.

[4] VIAS Institute. *In-Depth Investigation of Crashes Involving Heavy Goods Vehicles*. https://www.vias.be/en/onderzoek/onze-publicaties/ongevallen-met-vrachtwagens-fase-2/. Accessed on October 18, 2022.

[5] N. Stojanovic, I. Grujic, J. Glisovic, O. I. Abdullah, and S. Vasiljevic. *Application of New Technologies to Improve the Visual Field of Heavy Duty Vehicles' Drivers*. In New Technologies, Development and Application II, pages 411–421. Springer International Publishing, April 2019.

[6] H. Lee, M. Ra, and W.-Y. Kim. *Nighttime Data Augmentation Using GAN for Improving Blind-Spot Detection*. IEEE Access, 8:48049–48059, 2020. doi:10.1109/ACCESS.2020.2979239.

[7] D. Kwon, R. Malaiya, G. Yoon, J.-T. Ryu, and S.-Y. Pi. *A Study on Development of the Camera-Based Blind Spot Detection System Using the Deep Learning Methodology*. Applied Sciences, 9(14), 2019. Available from: https://www.mdpi.com/2076-3417/9/14/2941, doi:10.3390/app9142941.

[8] G. Liu, L. Wang, and S. Zou. *A Radar-Based Blind Spot Detection and Warning System for Driver Assistance*. In 2017 IEEE Second Advanced Information Technology, Electronic and Automation Control Conference (IAEAC), pages 2204–2208, March 2017. doi:10.1109/IAEAC.2017.8054409.

[9] J. Verhaevert. *Detection of vulnerable road users in blind spots through Bluetooth Low Energy*. In 2017 Progress in Electromagnetics Research

Symposium - Spring (PIERS), pages 227–231, St.-Petersburg, Russia, 2017.

[10] Silicon Laboratories. *BGM111 Blue Gecko Bluetooth module data sheet.* https://www.silabs.com/documents/public/data-sheets. Accessed on October 18, 2022.

[11] Bluetooth Special Interest Group. *Specification of the Bluetooth System, covered Core Package Version 4.2.* https://www.bluetooth.com/specifications/archived-specifications/. Accessed on October 18, 2022.

[12] ARM. https://www.arm.com/products/silicon-ip-cpu. Accessed on October 18, 2022.

[13] Bluetooth Special Interest Group. *Mesh networking is blue.* https://www.bluetooth.com/learn-about-bluetooth/recent-enhancements/mesh/. Accessed on October 18, 2022.

[14] Silicon Laboratories. *EFR32MG13 Series 1 Modules.* https://www.silabs.com/wireless/zigbee/efr32mg13-series-1-modules. Accessed on October 18, 2022.

[15] M. Bozzi, A. Georgiadis, and K. Wu. *Review of Substrate-Integrated Waveguide Circuits and Antennas.* Microwaves, Antennas & Propagation, IET, 5:909 – 920, 07 2011. doi:10.1049/iet-map.2010.0463.

[16] R. Li, G. DeJean, M. Tentzeris, and J. Laskar. *Development and Analysis of a Folded Shorted-Patch Antenna with Reduced Size.* IEEE Transactions on Antennas and Propagation, 52(2):555–562, 2004. doi:10.1109/TAP.2004.823884.

[17] Q. Van den Brande, S. Lemey, J. Vanfleteren, and H. Rogier. *Highly Efficient Impulse-Radio Ultra-Wideband Cavity-Backed Slot Antenna in Stacked Air-Filled Substrate Integrated Waveguide Technology.* IEEE Transactions on Antennas and Propagation, 66(5):2199–2209, 2018. doi:10.1109/TAP.2018.2809626.

[18] Bluetooth Special Interest Group. *Provisioning a Bluetooth Mesh Network.* https://www.bluetooth.com/blog/provisioning-a-bluetooth-mesh-network-part-1/. Accessed on October 18, 2022.

[19] Bluetooth Special Interest Group. *How AoA & AoD Changed the Direction of Bluetooth Location Services.* https://www.bluetooth.com/blog/new-aoa-aod-bluetooth-capabilities/. Accessed on October 18, 2022.

B

Fall Detection and Warning System for Nursing Homes based on Bluetooth Low Energy

Nick De Raeve, Cédric Nzamuye, Nicolas Claus, Jo Verhaevert, Patrick Van Torre and Hendrik Rogier

Accepted by IEEE 2022 7th International Conference on Smart and Sustainable Technologies (SpliTech), Jul 2022.

⋆⋆⋆

Fall accidents are a frequent problem with the elderly and lead to severe injuries and/or could have a lethal ending. To prevent these potential deaths the nursing personnel visits the elderly on a regular basis. This has an enormous influence on the mental and physical capabilities of the nursing personnel. In combination with the ever-growing presence of Internet of Things (IoT) applications, this chapter proposes a low-power wireless fall detection and warning system based on Bluetooth Low Energy (BLE). The aim of the system is to lower the workload of the nursing personnel and prevent elderly from dying from hypothermia. The system consists of a patient wearable (P) monitoring the movement of the elderly, a Detection Node (DN) scanning the room of the elderly to pinpoint the position of the

fallen elderly, multiple Network Nodes (NNs) in the hallways sending the alert messages to the closest caretaker wearing a Caretaker Node (CTN). This node visualizes all vital parameters, so the nursing personnel can help in the fastest way possible. A proof-of-concept is proposed in this paper, together with measurements and power analysis.

B.1 Introduction

About 40 % of elderly people over 65 year old, pass away due to fall accidents [1], [2], [3]. To prevent these falls from happening, much effort is performed in personal training for the elderly [4]. These fall accidents have a large financial impact on the medical system [5] since the nursing personnel has to manually check if a fall occurred. The consequence of this action, is an extra physical and mental stress added to the baseline stress level of the nursing personnel.

In current literature, much research is performed in developing algorithms based on cameras [6], wearables [7], RF based [8] detection or a fusion of different data streams [9, 10]. Many of these algorithms are based on a type of machine learning (ML). A disadvantage of this system is the need for representative training data [11] which can be difficult to achieve. Most wearables proposed in literature are large and have the sole purpose to obtain data, but cannot be used in real life. Furthermore, it is a known fact that elderly people do not like the use of large or too complicated wearables [12], [13]. Next, the care taking personnel is never part of the proposed solutions, so no effort in lowering their stress levels is proposed.

To prevent the elderly from suffering serious injuries and trying to lower the stress level from the nursing personnel, a small unobtrusive fall detection and warning wearable was proposed in a previous publication [14]. Here, a proof-of-concept for a low-cost fall detection and warning system based on Bluetooth Low Energy (BLE) [15] is proposed. This system has to send the alert messages from the wearable to the closest nursing personnel in a fast and low-power way.

This chapter is further structured as follows. First, the design of the system and the development of the different nodes is elaborated in Section B.2. It is followed by the executed measurements in Section B.3 and by a small conclusion in Section B.4. In Section B.5, some extra future features are summarized.

B.2 Design

B.2.1 Design requirements

Based on the advantages and disadvantages of the current system presented in literature, multiple design requirements were adopted:

1. A low-cost and low-power system
2. Easy to implement system
3. Compact and unobtrusive wearable for patient and care taker
4. Fast reception of an alert package at the care taker

B.2.2 System design

Taking the previously called design requirements into account, a system with four different types of nodes is proposed. The first node is the patient wearable P_1, which is depicted as a green dot in Figure B.1. This wearable contains an accelerometer to monitor the movements of the elderly and was developed in an earlier publication [14]. It utilizes a rule based algorithm based on the retrieved accelerometer data. The algorithm consists of two thresholds. First, the Signal Magnitude Vector (SMV) is calculated. When this value is higher than a predefined threshold of 2.5 g, the peak of the fall is found. Second, the orientation towards the gravitational vector before the peak and after the peak is calculated. When the difference between these two angles is larger than 45°, a fall occurred and the wearable will send an alert. This alert will be picked up by the Detection Node (DN), which is depicted as a red dot in Figure B.1. This node will not only forward the alert package, but will also include the necessary data (like room number and floor), so the nursing personnel can find the elderly efficiently. In this way, the system can detect other elderly who fall in a room different from theirs, and the nursing personnel does not go to the wrong room or floor. In Subsection B.5, some extra features that could be added are summarized.

The DN sends this updated alert package to the NNs, which are depicted as blue dots in Figure B.1. For illustrative purpose, these nodes are drawn close to each other, in reality the distance is larger. These nodes have the sole purpose to look for the closest nursing personnel or forward it the surrounding NNs. When a CTN, depicted as a purple dot in Figure B.1, is in proximity of a NN, the alert will be picked up. The nurse will get an alert and see the important parameters like temperature, patient name, patient room, floor number, etc. To achieve this, a custom-made advertisement package is made and sent to the required nodes.

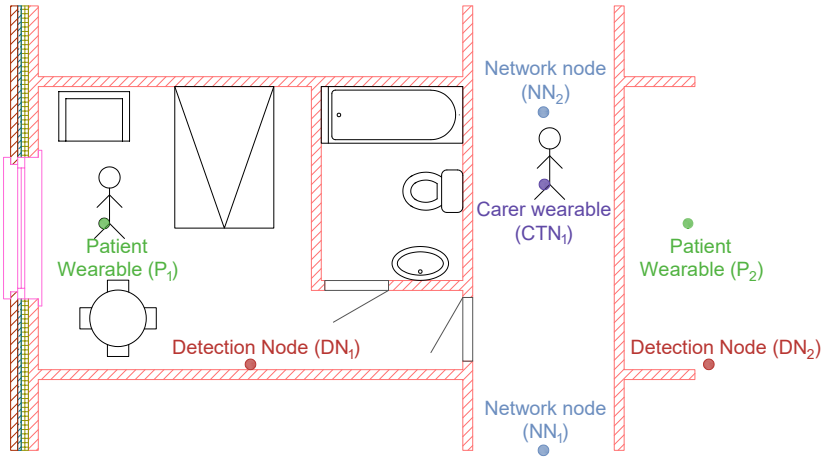

Figure B.1: Top view of a typical nursing room with a part of the hallway. The patient is wearing the wearable P_1 (green dot) and the Detection Node (DN) is placed in a central position of the room (red dot). Furthermore, the Network Nodes (NNs) (blue dot) are mounted on the ceiling of the hallway while the nursing personnel is wearing the Caretaker Node (CTN) (purple dot).

When an alert is handled, the nursing personnel pushes a button on the CTN and the complete system knows the alert is handled. To handle multiple fall accidents at the same time, the NN is equipped with an alert stack function, so the first in first out (FIFO) principal is used.

B.2.3 Communication steps

Figure B.2 gives a graphical representation of the communication steps that are taken when a fall is detected by one of the patient's wearable P_x. It triggers an alert and sends an alert package to the DN_x inside the room where the elderly fell. This node adds the necessary data to the alert package and sends it to the closest NN_x. This node sends the message to the other NNs when there is no CTN is in the proximity. When the CTN receives the alert message, the NNs marks this alert stack entity as *'Being Handled'*. When the nursing personnel helped the elderly, the handled button on the CN_x or DN_x is pushed. This sends a package to the closest NN_x and the alert stack entity is cleared. Next, the NN forwards the message to all other NNs where the same entity is cleared.

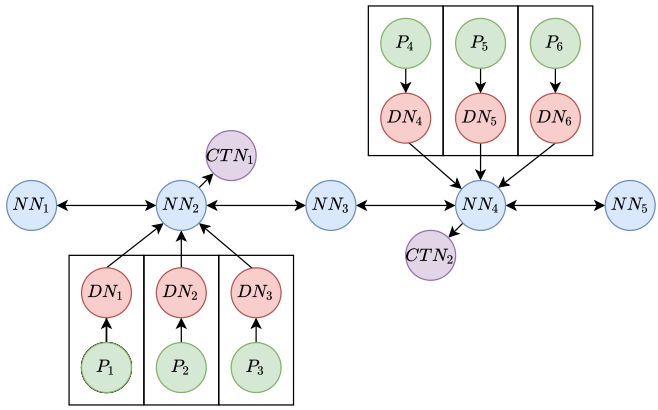

Figure B.2: Graphical representation of the different communication steps of the proposed system.

B.2.4 PCB Design

To test the proposed system, some hardware was designed. Since most of the nodes contain the same hardware and peripherals, only one Printed Circuit Board (PCB) is designed. Figure B.3 displays the layout of the PCB for the designed nodes. The design relies on the EFR32MG13P632F512GM48-CR wireless System-on-Chip (SoC) from Silicon Laboratories (SiLabs) [16]. This multiprotocol SoC uses the BLE5.1 stack and contains an on-board 32-bit 38.4 MHz ARM [17] Cortex-M4 microcontroller (MCU) with DSP instruction set. This ARM Cortex-M4 is a modern general-purpose MCU and makes it ideal for employment in many low-power systems.

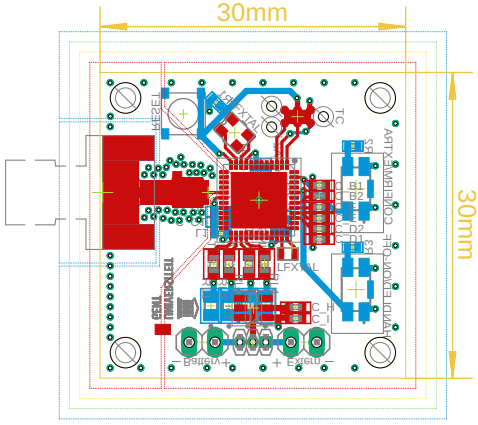

Figure B.3: Graphical representation of the developed CTN PCB.

The complete module has an overall size of 30 × 30 mm. It contains two pushbuttons, four LEDs and the other peripherals, required by the SoC. Furthermore, a TAG-connect [18] connector is used to program the nodes via the Serial Wire Debug (SWD) protocol [19]. The Power Supply Unit (PSU) is a standard small battery of 3.3 V or can be switched to a standard lab PSU. Since this is a proof-of-concept, an SMA connector is added so multiple antennas could be tested. The pushbuttons and LEDs have a specific purpose for each node. For the CTN, the pushbutton have a "alert handled" or "require more help" function. For the NN they are not necessary and hence not soldered.

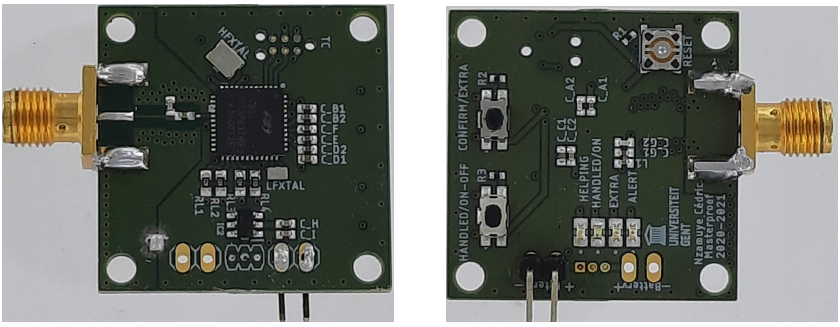

(a) Top. *(b) Bottom.*

Figure B.4: Picture of the developed PCB.

Figure B.5 illustrates the Delta 7A hinged mount WiFi/ISM antenna of Siretta is selected to perform the measurements proposed in subsection B.3. This is a dual-band $\lambda/4$ omnidirectional dipole antenna tuned at the 2.4 GHz and 5.8 GHz range, with a radiation efficiency of 63.6 % and 66.2 %, respectively. This antenna is vertically polarized with an almost omnidirectional radiation pattern at 2.45 GHz, which makes it an appropriate antenna for BLE. This cylindrical hinged mount antenna has an overall length of 108 mm and the bottom diameter is 9.3 mm. The integrated SMA connector, makes this an ideal and low-cost antenna to perform these measurements. In the future, the antenna will be co-optimized with the fall detection circuit for optimal performance.

Figure B.5: The soldered PCB with the hinged dual-band Delta 7A from Siretta connected.

B.3 Measurement & Discussion

To test this proof-of-concept, some measurements were performed.

B.3.1 Range Measurement

First, the range of the system is determined based on a series of Received Signal Strength Indicator (RSSI) measurements over different distances. One of the design requirements of this system (Section B.2.1) is a low-cost and low-power solution. To meet this requirement, BLE is used as main communication protocol. This makes the system easily scalable and uses minimal power to transfer large amounts of data. Furthermore, the amount of NNs should be limited to keep the production and installation cost low.

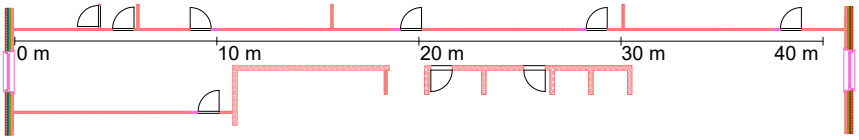

Figure B.6: Graphical representation of range measurement setup in the hallway at a Ghent University building.

To get a general idea of the range the system covers, RSSI measurements are performed. The first NN is placed on the left side of the hallway and is set to a fixed Tx level of 0 dBm. This node sends 2000 labelled advertisement packages. In this way, no other packages can be received and influence the measurements. The second NN is placed at a distance of 10 m, 20 m, 30 m and 40 m and continuously scans for advertisement packages. A graphical representation of the measurement setup is visible in Figure B.6. Afterwards, the RSSI values are used to calculate the Average Received Power (ARP) and the Package Receive Rate (PRR) based on equation 4.2 and 4.3, respectively.

$$ARP_{TX}\,[\text{dBm}] = 10.\log_{10}\left(\frac{1}{m}.\sum_{n=1}^{m} 10^{\frac{RSSI_n\,[\text{dBm}]}{10}}\right) \tag{B.1}$$

$$PRR_{TX}\,[\%] = \frac{m}{2000} \tag{B.2}$$

m = number of received packets

The results of the range measurements are visible in Figure B.7 and Figure B.8. Figure B.7 illustrates the calculated ARP of 2000 RSSI values received at the NN. An ARP of −48.61 dBm, −58.12 dBm, −60.04 dBm and −64.78 dBm at a distance of 10 m, 20 m, 30 m and 40 m result in a perfect communication possibility. Taking into account that the minimum Rx sensitivity level of the used MCU is −94.6 dBm. These result also illustrates that at a distance of 40 m, communication is still perfectly possible and could be extended even further.

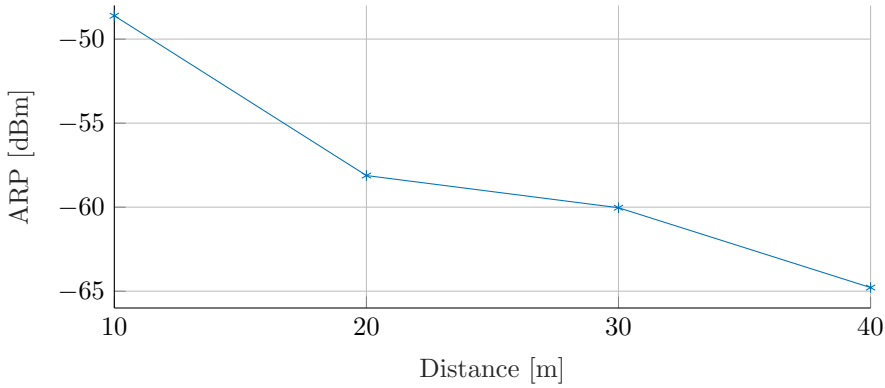

Figure B.7: Measured ARP at a distance of 10 m, 20 m, 30 m *and* 40 m *from a NN sending* 2000 *advertisement packages at a Tx level of* 0 dBm.

Figure B.8 illustrates the calculated PRR of 2000 RSSI values received at the NN. This graph, just like the previous, illustrates reliable communication with an average PRR of approximately 90 % over all measured distances. Both graphs clearly illustrate that the hallway has a positive effect on the range and performance of the system. Furthermore, placing an NN about every 40 m in a hallway of a nursing home keeps the system low-cost. The low-power requirement is also achieved, since a Tx level of 0 dBm has minimal influence on the battery lifetime or power consumption.

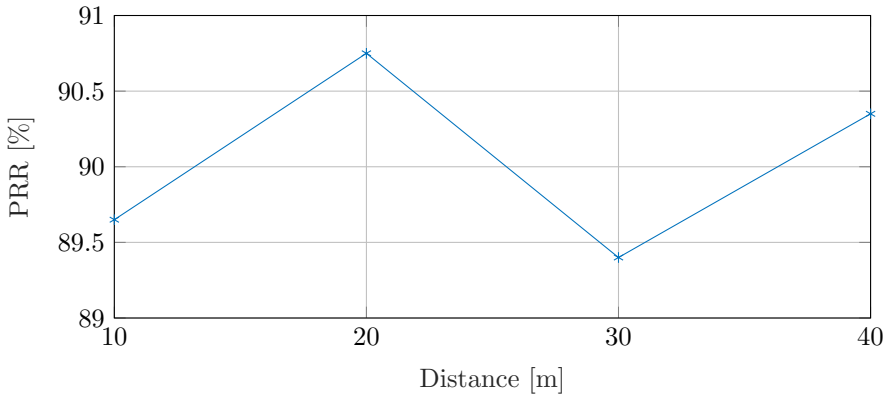

Figure B.8: Measured PRR at a distance of 10 m, 20 m, 30 m *and* 40 m *from a NN sending* 2000 *advertisement packages at a Tx level of* 0 dBm.

B.3.2 Latency Measurement

Latency is the second important factor that is measured. Since the system has to send alert messages to the CTN, it is important to know how long it takes to receive an alert. For this setup, the hallway from another Ghent University building is used, as can be seen in Figure B.9. The P and DN are placed at position *A*. The NN and CTN are placed at a certain position, ranging from 22 m to 84 m (labelled from *B* to *I* in Figure B.9). The positions were chosen based on obstacles in the hallway that could hinder the communication signals. During these measurements, the time between registering a fall and receiving it on the CTN is logged. The nodes transmit at a fixed Tx level of 0 dBm to keep the energy consumption as low as possible.

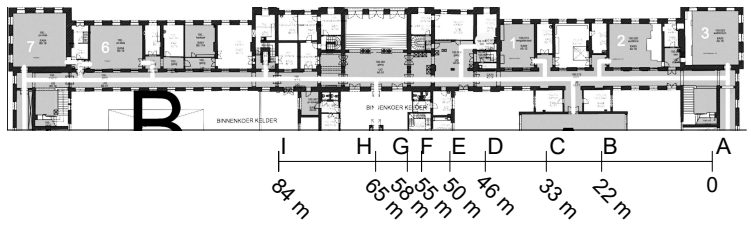

Figure B.9: Graphical representation of the latency measurements in the hallway at the Ghent University building.

The latency between sending an alert on the wearable P and receiving this on a CTN, passing a DN and one NN, resulted in an overall latency of approximately 3 s. Adding an extra NN to this chain has a serious influence

on the extension of the range, but a limited influence on the latency. The overall latency is increased to roughly 3.5 s. This measurement provides the required proof for the fourth design requirement in Section B.2.

B.4 Conclusion

This paper proposes a proof-of-concept for a low-cost fall detection and warning system based on BLE for nursing homes. The proposed system consists of four nodes. The first node is worn on the patient and triggers an alert in case of a fall event. Inside each room, a DN is mounted that will scan the room for alert messages. In the hallway of the nursing home a network of NNs is deployed. On arrival of an alert package, these nodes scans for the closest CTN and sends the alert. When no CTN is in proximity, the alert is forwarded to the next NN.

This paper covers the high-level communication steps of the complete system, as well as the hardware that is developed. Some extra peripherals are added to these PCBs, so each node could be used in a real-life test. Furthermore, some measurements were performed. First, RSSI levels are measured to calculate the ARP and PRR. An ARP of -64.78 dBm and a PRR of approximately 90.5 % were measured at a distance of 40 m. This proves the low-cost and low-power property of the proposed proof-of-concept. Furthermore, the numbers prove that the system can cover more than 40 m. In the latency measurements, over a distance of 50 m the systems takes more or less 3 s with one NNs to transfer an alert from patient wearable to CTN. When an NN is added, a distance of 84 m is achieved with a latency of roughly 3.5 s, proving the fourth design requirement of fast reception of an alert package at the care taker. In conclusion, based on the communication protocol of BLE and the performed measurements, all design requirements are fulfilled.

B.5 Future Work

In a next step, multiple modifications can be made for each node. The DN could be extended with Angle of Arrival (AoA). Since the MCU is utilizing BLE5.1, AoA is a good extension to the detection range. When a fall occurs, the wearable detects the fall, but the DN is able to pinpoint at with position the fall happened. This way, the nursing personnel can determine how dangerous the fall was. If an elderly person falls in the bathroom for instance, there is a greater risk of serious injuries.

The CTN can be extended with a small LCD screen. The LCD screen makes it more convenient to read the data from the wearable and replaces

the LEDs efficiently. Next, a vibration motor and buzzer can be added to make the receiving alert more noticeable for the nursing personnel wearing the CTN. Of course, the power management is an important parameter in this design. In an addition, a wireless charging coil is a nice feature to charge the integrated battery.

Both nodes can be extended with Near-Field Communication (NFC) and/or Radio-frequency identification (RFID). When the nursing personnel enters a room, they can cancel or handle the alert by simply touching the NFC and/or RFID reader with their tag integrated in the CTN. This small and inexpensive adaptation has a large influence on the ease of use. Furthermore, a suitable antenna topology is needed for both nodes since they are placed on the ceiling of the hallway or against the wall of the room. Therefore, a hemispherical radiation pattern is preferred.

References

[1] S. E. Carter, E. M. Campbell, R. W. Sanson-Fisher, and W. J. Gillespie. *Accidents in Older People Living at Home: a Community-Based Study Assessing Prevalence, Type, Location and Injuries.* Australian and New Zealand Journal of Public Health, 24(6):633–636, December 2000. Available from: https://doi.org/10.1111/j.1467-842x.2000.tb00532.x, doi:10.1111/j.1467-842x.2000.tb00532.x.

[2] World Health Organization. *World Health Organization Global Report on Falls Prevention in Older Age 2007.* https://extranet.who.int/agefriendlyworld/wp-content/uploads/2014/06/WHo-Global-report-on-falls-prevention-in-older-age.pdf. Accessed on October 18, 2022.

[3] World Health Organization. *Number of People over 60 Years set to Double by 2050; Major Societal Changes Required.* https://www.who.int/news/item/30-09-2015-who-number-of-people-over-60-years-set-to-double-by-\2050-major-societal-changes-required. Accessed on October 18, 2022.

[4] World Health Organization. *Falls.* https://www.who.int/news-room/fact-sheets/detail/falls. Accessed on October 18, 2022.

[5] C. S. Florence, G. Bergen, A. Atherly, E. Burns, J. Stevens, and C. Drake. *Medical Costs of Fatal and Nonfatal Falls in Older Adults.* Journal of the American Geriatrics Society, 66(4):693–698, 3 2018. Available from: https://doi.org/10.1111/jgs.15304, doi:10.1111/jgs.15304.

[6] C. Vishnu, R. Datla, D. Roy, S. Babu, and C. K. Mohan. *Human Fall Detection in Surveillance Videos Using Fall Motion Vector Modeling.* IEEE Sensors Journal, 21(15):17162–17170, August 2021. Available from: https://doi.org/10.1109/jsen.2021.3082180, doi:10.1109/jsen.2021.3082180.

[7] S. Nooruddin, M. M. Islam, F. A. Sharna, H. Alhetari, and M. N. Kabir. *Sensor-Based Fall Detection Systems: a Review.* Journal of Ambient Intelligence and Humanized Computing, April 2021. Available from: https://doi.org/10.1007/s12652-021-03248-z, doi:10.1007/s12652-021-03248-z.

[8] J. G. Argañarás, Y. T. Wong, R. Begg, and N. C. Karmakar. *State-of-the-Art Wearable Sensors and Possibilities for Radar in Fall Pre-*

vention. Sensors, 21(20):6836, October 2021. Available from: https://doi.org/10.3390/s21206836, doi:10.3390/s21206836.

[9] L. Ren and Y. Peng. *Research of Fall Detection and Fall Prevention Technologies: A Systematic Review*. IEEE Access, 7:77702–77722, 2019. Available from: https://doi.org/10.1109/access.2019.2922708, doi:10.1109/access.2019.2922708.

[10] X. Wang, J. Ellul, and G. Azzopardi. *Elderly Fall Detection Systems: A Literature Survey*. Frontiers in Robotics and AI, 7:71, 2020. Available from: https://www.frontiersin.org/article/10.3389/frobt.2020.00071, doi:10.3389/frobt.2020.00071.

[11] X. Yu, J. Jang, and S. Xiong. *A Large-Scale Open Motion Dataset (KFall) and Benchmark Algorithms for Detecting Pre-impact Fall of the Elderly Using Wearable Inertial Sensors*. Frontiers in Aging Neuroscience, 13:399, 2021. Available from: https://www.frontiersin.org/article/10.3389/fnagi.2021.692865, doi:10.3389/fnagi.2021.692865.

[12] M. C. Gilly and V. A. Zeithaml. *The Elderly Consumer and Adoption of Technologies*. Journal of Consumer Research, 12(3):353, 12 1985. Available from: https://doi.org/10.1086/208521, doi:10.1086/208521.

[13] K.-C. Yang and P.-H. Shih. *Cognitive Age in Technology Acceptance: at What Age are People Ready to Adopt and Continuously Use Fashionable Products?* Telematics and Informatics, 51:101400, 8 2020. Available from: https://doi.org/10.1016/j.tele.2020.101400, doi:10.1016/j.tele.2020.101400.

[14] N. De Raeve, A. Shahid, M. de Schepper, E. De Poorter, I. Moerman, J. Verhaevert, P. Van Torre, and H. Rogier. *Bluetooth-Low-Energy-Based Fall Detection and Warning System for Elderly People in Nursing Homes*. Journal of Sensors, 2022:1–14, January 2022. Available from: https://doi.org/10.1155/2022/9930681, doi:10.1155/2022/9930681.

[15] R. Colella, L. Spedicato, V. Molinaro, A. Ranavolo, L. Patrono, C. Leo, M. Tumolo, S. Sabina, and L. Catarinucci. *2.4 GHz BLE-based Smart Sensing System for Remote Monitoring of Health, Safety and Comfort at Workplace*. In 2021 6th International Conference on Smart and Sustainable Technologies (SpliTech), pages 01–05, 2021. doi:10.23919/SpliTech52315.2021.9566398.

[16] Silicon Labratories. *EFR32MG13 Mighty Gecko Multi-Protocol Wireless SoC Family Data Sheet*, 2020. Accessed on October 18, 2022.

[17] ARM. https://www.arm.com/products/silicon-ip-cpu. Accessed on October 18, 2022.

[18] *TAG Connect*. http://www.tag-connect.com/. Accessed on October 18, 2022.

[19] Silicon Laboratories. *Programming Internal Flash Over the Serial Wire Debug Interface*. https://www.silabs.com/documents/public/application-notes/an0062.pdf. Accessed on October 18, 2022.